UNIVERSITY OF CALIFORNIA, SAN DIEGO

A Fundamental Approach for Storage Commodity Classification

A thesis submitted in partial satisfaction of the
requirements for the degree
Master of Science

in

Engineering Sciences (Mechanical Engineering)

by

Michael J. Gollner

Committee in charge:

Forman A. Williams, Chair
Jonathan Perricone
Kalyanasundaram Seshadri
Stefan G. Llewellyn-Smith

2010

The thesis of Michael J. Gollner is approved, and it is acceptable in quality and form for publication on microfilm and electronically:

_____

_____

_____

_____

Chair

University of California, San Diego

2010

TABLE OF CONTENTS

LIST OF FIGURES

LIST OF TABLES

NOMENCLATURE

Symbols

B	B-number (Spalding Mass Transfer Number) (-)
C_p	Specific Heat at Constant Pressure (J/kg K)
g	Acceleration Due to Gravity (m/s^2)
h	Heat Transfer Coefficient (W/m^2 K)
ΔH_c	Heat of Combustion (J/kg)
ΔH_g	Heat of Gasification (J/kg)
k	Thermal Conductivity (W/m K)
L	Latent Heat of Vaporization (J/kg)
$\dot{m}_f{}''$	Mass-Loss Rate per Unit Area (Mass Flux) (kg/m^{2}s)
Nu	Nusselt Number (-)
Pr	Prandtl Number (-)
$\dot{q}''$	Heat Flux per Unit Area (W/m^2)
r	Mass Consumption Number (-)
Ra	Rayleigh Number (-)
T	Temperature (K)
t	Time (s)
X_f	Flame Length (Height) (m)
X_p	Pyrolysis Length (Height) (m)
Y_{O_2}	Oxygen Mass Fraction (-)

y_f Flame Standoff Distance (cm)

δ Thickness (cm)

Greek Symbols

α Thermal Diffusivity (m^2/s)

χ Radiation Fraction (-)

ϵ Emissivity of a Material (-)

ν Kinematic Viscosity (m^2/s)

ν_s Stoichiometric Oxygen/Fuel Mass Ratio (-)

β Flame to Pyrolysis Height Ratio (-)

ρ Density (kg/m^3)

σ Stefan Boltzmann Constant (W/m^2K^4)

τ Characteristic Time for Flame Spread (s)

Subscripts

g Gas

∞ Ambient

f Flame

p Pyrolysis Region

Abbreviations

NFPA National Fire Protection Association

HRR Heat-Release Rate

NIST National Institute of Standards and Technology

FM Factory Mutual (Renamed FM Global)

ACKNOWLEDGEMENTS

I am grateful to have had a mentor who sparked my interest in fire protection engineering. Jonathan Perricone showed me how combustion and fire science can be applied to practical engineering problems, and suggested this research project while I was an intern at Schirmer Engineering. My experience as an intern was a fun, knowledge-building experience thanks to the support of my colleagues there.

I am also fortunate to have found two of the most energetic, inspiring, knowledgeable advisers any student could ask for, Professors Ali Rangwala and Forman Williams. Ali Rangwala became my inspiration to continue my studies, and his energy and support has helped me within and beyond the laboratory. Forman Williams has been there to provide the deep understanding of combustion thoery that can come from no one else, and is always there to support me. I am also grateful to the Department of Fire Protection Engineering at the Worcester Polytechnic Institute for extending me a warm welcome and support while performing experiments there. Todd Hetrick, Kris Overholt, Scott Rockwell, Cecilia Florit, and Randall Harris all helped to make these laboratory experiments possible.

My classmates at UCSD have helped me in many ways over the past year, Kevin Peng and Karl Olney have been the best groupmates in numerous projects, Javier Urzay has always offered his support and so many others have made my experience here enjoyable.

Without great roomates like Karl Olney and Diana Krivosheya I would never have been able to get so much work done or maintain my sanity. Above all I must thank my parents for their constant support and motivation to my continued schooling, and Agnieszka Cieplak for her loving support and attempts to add much needed adventure into my life.

I would also like to acknowledge financial support from Garner Palenske of Schirmer Engineering and donations of tested commodity from David LeBlanc of Tyco.

The text of Chapters 3, 4, and 5 has partially included the following publication: "Controlling Parameters Involved in the Burning of Standard Storage Commodities: A Fundamental Approach Towards Fire Hazard Classification," at the *6th*

U.S. National Combustion Meeting, (Ann Arbor, Michigan), 2009. M. J. Gollner, T. Hetrick, A. S. Rangwala, J. Perricone, and F. A. Williams. The thesis author is the primary researcher in this publication.

VITA

2006-2008	Fire Protection Engineering Intern, Schirmer Engineering, an AON Global Company
2007	Undergraduate Researcher, Combustion Diagnostics and Environmental Sensing Laboratory, University of California, San Diego
2008	Bachelor of Science, Mechanical Engineering, University of California, San Diego
2009	Graduate Teaching Assistant, University of California, San Diego
2010	Master of Science, Mechanical Engineering, University of California, San Diego

PUBLICATIONS

Gollner, M. J., Hetrick, T., Rangwala, A. S., Perricone, J., Williams, F. A., *Controlling Parameters Involved in the Burning of Standard Storage Commodities: A fundamental approach towards fire hazard classification.* Sixth U.S. National Combustion Meeting of the Combustion Institute. May, 2009.

Overholt, K., Gollner, M. J., Rangwala, A. S., *Characterizing the Flammability of Corrugated Cardboard Using a Cone Calorimeter.* Sixth U.S. National Combustion Meeting of the Combustion Institute. May, 2009.

ABSTRACT OF THE THESIS

A Fundamental Approach for Storage Commodity Classification

by

Michael J. Gollner

Master of Science in Engineering Sciences (Mechanical Engineering)

University of California, San Diego, 2010

Forman A. Williams, Chair

Experimental tests were conducted on a single cartoned, unexpanded Group A plastic commodity to evaluate an approach to commodity classification in complex fuel geometries. The approach is based on comparing the chemical energy released during the combustion process with the energy required to vaporize the fuel. The ratio of these two quantities is often called the mass transfer number, B-number or Spalding number.

The Group A commodity tested was essentially a three-dimensional cardboard box subdivided by cardboard placeholders for individual unexpanded polystyrene cups. Experiments consisted of burning the front face of a single box with all remaining faces uniformly insulated. Measurements of gas temperatures, mass-loss rate and heat flux from the flame were used to calculate a modified B-number, which includes consideration of the role of radiant heat transfer. Results from experiments have produced time-averaged B-numbers for stages of burning. Comparison to a concurrent study using a cone calorimeter on smaller-scale material samples shows good agreement between these methods. Future use of the results to improve commodity classification for better assessment of fire danger is discussed.

Chapter 1

Introduction

1.1 Problem

Imagine a design method that affords engineers the ability to predict the full-scale performance of a proposed sprinkler protection strategy in terms of a measurable parameter that universally defines fire suppression and control for any commodity. Such a method could infuse limitless creativity into the design process by providing engineers with the tools that they need to accurately evaluate full-scale performance during the design phase. This is the ultimate goal of engineers dedicated to fire-suppression research and development. However, the current state of the art falls well short of this idealization.

In engineering, there are two limits of acceptable ways of generating a solution to a problem. The first, and most preferable, method is to extract a solution directly from the set of equations that govern the physical and/or chemical process under investigation. The major strength of this approach lies in the known validation of the source. The most significant weakness of this approach, however, is that the complexity introduced by real-world applications is often so computationally expensive that the approach becomes impractical, even when the underlying set of equations is known, which often it is not.

The second approach consists of experimentation within the parameters of the scientific method. Such experimentation may be used in conjunction with the first approach to provide validation, or as a standalone method to draw correlations

between significant parameters. The strength of this method lies in the ability to focus on isolated cause-and-effect relationships; however, it is often the case that many experiments are necessary to produce only narrowly applicable solutions.

To date, the field of fire-protection engineering has invested heavily in the latter of these two approaches for the development of fire-suppression strategies. As a result, engineers have been able to produce solutions to many unique design challenges; yet these results lack cohesion within the global research framework. Consequently, the National Fire Protection Association's (NFPA) standard *NFPA 13: Standard for the Installation of Sprinkler Systems* has evolved into a nearly 350-page document including several appendices with detailed qualifications of the narrow applicability of various experimental efforts [1]. This complicates its application to the fire protection of commodities in warehouses.

Given this characterization, engineers must question the validity of the basic design principles espoused by NFPA 13 in an effort to merge such data into the more widely applicable design methods necessary for practitioners to function. This introduces questions focused on the input and output of the experimental process. For instance, if the general performance of sprinkler protection is to be evaluated, commodity classification may be viewed as the primary input, with the level of fire control and/or suppression designated as the output. Other required inputs to this model would include sprinkler characteristics, ignition location and initial fire size. This is seen in figure 1.1 where commodity and storage description is used as an input to determine the free burn heat-release rate (HRR) [2]. The current standard contains a significant level of subjectivity with respect to these parameters.

A report recently published by the Fire Protection Research Foundation, a non-profit research organization dedicated to the communication of research for the development of codes and standards, found an absence of any credible basis for multiple commodity classifications in NFPA 13 [3]. Additional research has, not surprisingly, confirmed a lack of repeatability for the data in question [2] (see pages 149-153 of this reference). In light of these discoveries, there is a need for research engineers to rectify the situation by creating a solid and broad foundation for the way forward. Such a foundation will never truly be found without a focus on the complex physical and chemical processes that characterize fire suppression.

Figure 1.1: Conceptual sprinklered warehouse fire model flowchart proposed by Zalosh.

The purpose of fire safety standards is to establish uniform specifications for a material, product, process or procedure that will yield a desired minimum level of protection. The broader problem in fire protection is that such standards and associated performance targets were created and have evolved separately from a fundamental knowledge of fire. The result is a product with wide variation in quality and effectiveness due to ill-defined objectives. The aim of this project is to begin resolving such objectives by clarifying the role of basic parameters.

1.2 Warehouse Fire Risk

Storage of commodities in large warehouses poses a unique hazard to occupants, fire fighters, and surrounding communities due to the concentration of

flammable, often toxic materials commonly stored to heights of up to 16 meters (50 ft). A key aspect of the protection strategy for these large warehouses is resolving the thermal load presented by a given set of materials in a known configuration. Despite strong advances in the fire sciences, over the last three decades this area of fire protection has been overlooked. Protection strategies in these facilities are deficient, evident from the series of large loss fires that have occurred over the last two decades as shown in table 1. A long history of destruction has resulted from warehouse fires, including fire fighter deaths and environmental catastrophe. These large structures present a unique fire fighting situation; fire fighters investigating fires enter a maze-like inferno where the seat of a fire may occur deep and high above the floor within a space where visibility quickly decays. Lives have been risked and in come cases lost in such situations where firefighters are tasked with augmenting the performance of an automatic sprinkler system (table 1.1).

The environmental damage occurring from these warehouse fires can also be disastrous, as seen by the classic example of the Sandoz Chemical Plant and Storage Facility fire that occurred near Basle, Switzerland in 1986. Pesticides from the chemical plant were washed into the Rhine River in the course of fire-fighting efforts killing fish populations for over a year and threatening the water supplies of residents in several countries downstream [12]. Similar detrimental effects occurred during similar chemical warehouse fires in Nantes, France in 1987 resulting in the evacuation of over 25,000 people because of a toxic smoke plume [13]. Fire departments are faced with difficult situations when combating large warehouse fires balancing the protection of their fire fighters, potential victims within the building, and environmental impacts to the surrounding community. Out-of-control warehouse fires that become a risk to the local environment leave fire departments few options to respond to such threats. Fighting a fire with water for days may cause environmental damage to local water supplies, and allowing a fire to burn unabated may create a large toxic plume - more knowledge of the fire hazard of commodities within a warehouse must be obtained to effectively make such decisions. This includes knowledge of the capability limits of the suppression system. A logical response from the engineering community is to reduce such risks by optimizing the automated suppression system.

1.3 Proposed Solution

The goal of commodity classification is to characterize the thermal loading presented by a particular set of materials in a known configuration. Knowledge of the thermal load in turn facilitates the design of effective fire protection systems. The burning rate, fire-spread rate, time to ignition, and fuel vaporization temperature are all factors that govern the burning of a fuel, but for a fire in a warehouse setting, an adequate means of suppression might well be determined solely from the burning rate of the commodity in the warehouse. While the critical heat flux and time to ignition are relevant in determining whether a fire will start, since the function of sprinklers protecting a facility is to control and suppress fires that occur, their requirements are influenced more strongly by the burning rate and spread rate, and spread rates may correlate with burning rates. This premise motivated the present investigations. Currently there exists no elegant and straightforward method for calculating the burning rate of a three-dimensional fuel, such as occurs in a warehouse commodity. Unless existing two-dimensional models of combustion can be adapted to characterize three-dimensional burning, engineers are left with only computationally expensive numerical methods for evaluating complex combustion processes.

A solution is proposed to use a model for two-dimensional burning that may be well suited for the purposes of determining measurable commodity classification and fire suppression sought by NFPA 13. The basic premise of this method consists of classifying commodities in terms of a time-varying parameter known as the mass transfer number (also known as the B-number or the Spalding number). This dimensionless parameter is quite simply a ratio that compares a summation of the various impetuses (i.e. heat of combustion) for burning to a summation of the various resistances (i.e. heat of vaporization) to the process. For any given system, the B-number may be derived directly from the set of governing equations for combustion (i.e. first principles). The parameter therefore has inherent universal meaning and validation. The B-number has been shown to describe both the burning rate and upward spread rate of a solid burning fuel [14, 15], which makes it ideally suited for this application.

The B-number is a dimensionless ratio, and therefore independent of scale. This gives the possibility of comparing systems of fuel on a natural scale that defines

fire severity. The B-number can also be used to deduce valuable information related to fire spread and smoke generation. This could be a meaningful basis for measurable commodity classification. Determination of this parameter is accomplished by small-scale experimentation, resulting in highly decreased costs for fire testing and an increase in the global database of fire protection engineering information.

Prior work classified material flammability using a B-number specific to homogeneous materials [14, 15]. A warehouse commodity, however, consists of collections of different materials and a practical flammability ranking scheme should take into account the flammability of basic product, its packaging, and its container. Experimental determination of a B-number for a group of different materials packaged together has never been attempted before. Successful completion of this study will allow a fire protection engineer to classify warehouse commodities based on a fundamental non-dimensional number, thereby facilitating estimation of parameters such as mass burning rate, heat-release rate, and flame-spread rate. All these parameters are crucial when selecting sprinkler locations and characteristics.

By definition, there exists a critical B-number for any given fuel system below which fire extinction occurs [16]. This could enable engineers to make suppression and extinction a measurable quantity, as well as allowing the exploration of extinction and suppression by means other than sprinklers.

1.4 Experimental Approach

For this study, a Group A plastic commodity was chosen to be carefully studied at the small-scale level for a number of reasons. Because this commodity group represents the greatest hazard and because its large-scale behavior has been extensively studied, more data on its small-scale burning behavior may be useful for connecting large-scale and small-scale phenomena. The commodity is essentially a three-dimensional cardboard box subdivided by cardboard placeholders for individual polystyrene cups. Experiments consisted of burning the front face of a single box with all other sides uniformly sealed and insulated. Measurements of gas temperatures, mass-loss rate and heat flux from the flame were used to calculate a modified B-number, which includes consideration of the role of radiant heat transfer. Smaller-

scale tests have been conducted using a cone calorimeter in a concurrent study [17]. Data collected in that study matches well with observations on the Group A plastic commodity.

Table 1.1: Recent fire losses in large warehouse storage facilities.

05/22/09	Furniture Warehouse– Houston, TX	4,600 m^2 warehouse, filled with furniture and electronics. An Inventory of $5 million was lost. 120 Fire Fighters were involved in putting the fire out [4].
12/11/07	Warehouse Fire– Hemingway, SC	15,329 m^2 warehouse storing plastic Tupperware. Warehouse was protected by sprinklers to code, 78 firefighters responded but fire burned out of control for a 35-hour period [5].
6/19/07	Furniture Warehouse Fire– Charleston, SC	9 firefighters died. Furniture presented a much larger fire hazard than protection system could handle. Flashover occurred while firefighters were attempting to find the seat of the fire after one employee was rescued. [6].
12/16/03	Furniture Warehouse Fire– NY	1 firefighter died while searching for the seat of a fire in a furniture and mattress warehouse [7].
3/14/01	Supermarket Fire– Phoenix, AZ	1 firefighter died. Fire began in storage pile in the rear of the store, spreading throughout the store rapidly via attic and duct space [8].
12/18/99	Paper Warehouse Fire– MS	1 firefighter died after becoming lost in a paper warehouse fire. The structure was equipped with a sprinkler system [9].
12/3/99	Cold-Storage and Warehouse Building Fire– MA	6 firefighters died after becoming lost in a six-floor, maze-like building searching for two victims. The building was abandoned at the time of the fire [10].
4/16/96	Lowes Store– Albany, GA	Fire grew so rapidly it penetrated the roof and filled the building with smoke down to the 1.5 m (5 ft) level, all within about 5 minutes. The fire took over 2 days to extinguish, destroying the 8,000 m^2 warehouse. Deficient protection resulted from commodities stored in racks not matched to the fire hazard [11].

Chapter 2

Literature Review

In order to improve upon the process of commodity classification, an extensive review of current and past classification schemes is necessary. The issue of material flammability is first investigated. An overview of methods that have been important for classifying commodities in the past will be included, with a comparison to methods in use today. A history of the B-number and why it may serve as a superior flammability criterion will finish the literature review.

2.1 Fundamental Flammability

Depending on the application, factors controlling flammability and fire hazard vary [18, 19]. In general, for both plastics and cellulosic materials five major components adequately express flammability: ignition, fire growth, burning intensity, generation of smoke and toxic compounds, and extinction/suppression [20]. Each of these components has been the subject of flammability and hazard testing methods on materials yet no known method has succeeded in expressing flammability as a cohesive unit comprised of these various elements. The methodology to classify materials being developed here is intended to express the "fire hazard" of an item, in an effort to specify adequate protection. To that end, flammability will be defined as a material's ability to begin and sustain combustion. Extinction, suppression and control are often interchanged in literature, but their definitions must be distinct in this application. Throughout this paper extinction will be defined as the point

where a material ceases to combust, suppression as controlling a fire so that it no longer spreads laterally or vertically to ignite new material, and control as the act of preventing the spread of fire beyond a designated control point during a defined test period. With respect to a ranking parameter, four quantities will be evaluated: ignition, heat-release rate, flame spread and extinction.

Williams describes ignition as "the process whereby a material capable of reacting exothermically is brought to a state of rapid combustion," [21]. A material may be ignited by either spontaneous ignition or piloted ignition. The process of a material heating by a convective or radiative source from a distance is a basic example of spontaneous ignition, where the material has an external heat flux initiating combustion but no spark or flame. Piloted ignition can occur at a much lower temperature than spontaneous ignition, but requires an external spark or flame to 'pilot' ignition. Ignition is an integral part of measuring flammability because it defines the point where a material will begin to combust. Flame spread is a measurement of how easily a flame spreads across a solid combustible material, emanating from a point of ignition [22]. It is important to quantify flame spread for flammability in order to determine how quickly a fire will spread over a material or through an enclosure, yet doing so can be difficult. The rate of flame spread may vary depending on the shape and orientation of a sample.

Both radiant and convective heat fluxes are emitted during burning, but radiant heating dominates during many fire phenomena [23]. The HRR of a fire is an estimation of the rate at which heat is generated. It is often described as the product of the mass-loss rate ($\dot{m}_f''$) and effective heat of combustion, ΔH_c [24]. The HRR is not unique to a material, but varies with the arrangement and size of the burning material. It is also a time-dependent parameter, as the mass-loss rate of a material varies over stages of burning. Reducing the supply of flammable vapors to below a critical level in a combustion reaction can cause control of flaming combustion. However, re-introduction of this limiting parameter to the system can yield re-ignition if adequate heat and fuel remain. The same level of control may be exerted by manipulation of heat and fuel. Determining the conditions that constitute such control is critical for designing means of fire protection.

2.2 Applied Flammability

Two approaches exist to reduce the flammability of a storage commodity: preventing fire ignition or providing adequate fire suppression. A great deal of work has been done, thoroughly summarized for plastics by Hilado, to reduce the flammability of plastics by adding fire suppressants to or modifying the makeup of the materials [19]. The general approach taken in warehouse storage configurations is that of suppression, and commodity classification is used to design the parameters of suppression necessary to contain or extinguish fires.

2.3 Basis of Warehouse Storage Classification Methods

In the United States commodity classification for fire prevention purposes is outlined by FM Global, a research-based risk-insurance company, and the NFPA, whose standards are adopted in most states to determine minimum protection requirements for buildings. Both methods utilize a similar outline with some minor differences in which commodities are classified into categories. Tables 2.1 and 2.2 show the general classification scheme in use today for both NFPA and FM Global [1, 25]. The distinction between Group A and Group B plastics is different in NFPA 13 than in FM Global Property Loss Data Sheet 8-1 [25]. Table 2.3 lists some examples of plastics in different categories and their properties from NFPA 13. Several of the NFPA 13 Group A plastics are considered to be good examples of Group B plastics in FM Global Property Loss Data Sheet 8-1, including polycarbonate, polyethylene, polyproylene, and thermosetting polyesters [2]. These differences are a product of subjectivity in the approach.

Table 2.1: Generic commodity classification in NFPA 13

Class	**Product**	**Packaging**	**Plastic Content**
I	Noncombustible	None; on pallets. Single wall carton, or paper wrap.	Negligible
II	Noncombustible	Multi-wall carton, or wood crate or wood box.	Negligible
III	Wood, paper, leather, natural fiber textile, or Group C plastic.	None or ordinary combustible.	Negligible ($\leq$ 5%) Group A or Group B
IV	Class I, II, or III with 5-15 weight % or 5-25 vol % of Group A plastic.	Anything except Group A plastic.	Either Group B or an appreciable amount of Group A as defined for product.

Commodities in tables 2.1 and 2.2 are listed in order of severity, Class I being mostly non-combustible material stored within combustible packaging, while Group A plastics are plastic materials with a high heat of combustion (Btu/lb or kJ/kg) and burning rate (lb/min or kg/min) greater than all other classes [25]. The classifications are based mainly on results of large-scale fire testing in models of warehouses with sprinklers. A ranking scheme based upon comparison of the heat of combustion (ΔH_c) to the heat of gasification (ΔH_g) shown in table 2.3 was proposed by Zalosh, but the inability for the ratio to distinguish differences between similar plastics of varying densities was reasoned to illustrate the inability of a rigid parameter scale to accurately classify materials [2]. This ratio, although similar to the B-number, does not include loss terms that can be accounted for in experimental measurements.

To perform large-scale testing of the severity of these commodities engineering researchers at FM Global created "prototype" or "standard" commodities which are used in large-scale research and testing of sprinkler systems, shown in table 2.4. Test commodities that were used in original benchmark testing in the 1970's as well as the standard commodities still used in benchmark rack-storage testing today are shown. Specifications for standard commodities were chosen based upon common stored goods at the time initial testing was done. The standard Class II commodity consists of a metal lined double tri-wall cardboard carton, with the metal lining

Table 2.2: Plastic commodity classification in FM Global Datasheet 8-1

Group	**Description**	**Examples**
C	Plastics with a heat of combustion and burning rate similar to those of ordinary combustibles. (Protected at Class III)	Phenolics, silicone, etc.
B	Plastics that have heat-release rates higher than ordinary combustibles, but lower than Group A plastics.	Polypropylene, polycarbonate, nylon, etc.
A	Plastics that have a heat of combustion much higher than ordinary combustibles and burning rate higher than Group B plastics.	Polyurethane, polystyrene, etc.

Table 2.3: Summary of plastic commodity classification in NFPA 13, where ΔH_c is the material's heat of combustion and ΔH_g is its heat of gasification.

Polymer	$\boldsymbol{\Delta H_c}$ **(kJ/g)**	$\boldsymbol{\Delta H_g}$ **(kJ/g)**
Group A Plastics		
Polycarbonate	29.7	2.1
Polyethylene	43.6	1.8(LD), 2.3(HD)
Polymethylmethacrylate (PMMA)	25.2	1.6
Polypropylene	43.4	2.0
Polystyrene	39.9	1.3-1.9
Group B Plastics		
Cellulose Acetate	17.7	-
Nylon	30.8	2.4
Silicone Rubber	21.7	-
Group C Plastics		
Phenolic	10-36.4	1.6-3
Polytetraflouroethylene (PTFE)	5.3	-
Polyvinyl Chloride (PVC, rigid)	16.4	2.5
Urea Formaldehyde	14.6	-

Table 2.4: Commodity ranking applied from NFPA 231 and FM Global Datasheets

Class/Group	**Original test commodity(1970's testing)**	**Benchmark/standard test commodity (used in modern testing)**
Class I	No testing performed, assumed density required 12% < Class II	Glass jars in compartmentalized cardboard carton
Class II	Metal-lined double tri-wall cardboard cartons	Metal-lined double tri-wall cardboard cartons
Class III	Hallmark paper products	Paper cups in compartmented cardboard cartons
Class IV	3M paper + plastic products	25 wt% PS Cups + paper cups in compartmented cardboard cartons
Group C Plastic	Not tested	Not tested
Group B Plastic	Not tested	Not tested
Group A Plastic	PS cups in compartmented cardboard carton	PS cups in compartmented cardboard carton

designed to hold the structure of the box in place lowering the peak heat release rate of the overall commodity [2]. Standard commodities for Class I, III and IV commodities consist of eight compartmented, single-wall, corrugated paper cartons consisting of 125 16oz cups inside. The Class I standard commodity consists of glass cups, Class II consists of paper cups, and Class IV a mix of polystyrene and paper cups [2]. Dean, as part of the Factory Mutual Research Corporations's (now FM Global) research program in plastics, developed what has become the standard commodity for Group A plastics, the same compartmented corrugated paper carton with 125 unexpanded polystyrene cups [26]. Polystyrene was chosen as the plastic because it represented the most severe fire in all small and large-scale tests conducted, and the arrangement in cartons created a very repeatable fire test.

2.4 Area-Density Curves

The 1972 Edition of *NFPA 13: Standard for the Installation of Sprinkler Systems* contains the first area-density curves used to design hydraulically calculated

sprinkler systems shown in figure 2.1 [3]. These curves give the required amount of sprinkler coverage depending on the occupancy of a building, which is determined by the group of commodities contained in that building, as classified into 7 distinct groups, Class I-IV and Group C-A in order of increasing severity. The curves themselves were developed from full-scale testing of several of these commodities. The testing however did not include any plastics because they were not yet stored in large quantities at many facilities, and only one type of sprinkler was used because it was the most commonly available protection [3]. There were no "stages" of burning in these initial tests, which did not involve plastics, because the importance of packaging was not yet well captured.

The tests involved starting a fire in a given storage commodity at a position in a sprinklered area simulating a large warehouse and determining whether the sprinklers "control" the fire, that is, prevent it from spreading significantly beyond the initial ignition area. The design area of sprinkler operation is the area in which sprinklers would open in a fire with a given ceiling sprinkler density. At a given sprinkler density, the design area of sprinkler operation thus is proportional to the number of sprinklers that were activated by the fire prior to "control." The fact that the area decreases with increasing density in these curves therefore can be understood because at higher density water is deposited onto a rack storage fire at a higher rate, so that the size to which the fire grows before sprinklers "control" the spread of the fire will be less, leading to a smaller area of sprinkler activation. Ceiling sprinkler density can be increased by either increasing the number of sprinklers within a given area or increasing the water pressure of the sprinkler system. The curves do not imply that a larger initial area of fire involvement at the time of ignition or that a warehouse of larger area requires less sprinkler density for "control", as might generally be surmised in the absence of knowledge of the test protocol; on the contrary, a large initial fire requires at least as high a sprinkler density as a smaller one.

The original sprinkler area-density curves were developed as the result of a series of full-scale tests from 1969-72 to determine the amount of suppression coverage required for different stored commodities, as shown in figure 2.2. These sprinkler area-density curves (which ironically are no longer curves but straight lines in the most current edition of NFPA 13) determine the flow rate of water required from sprinklers

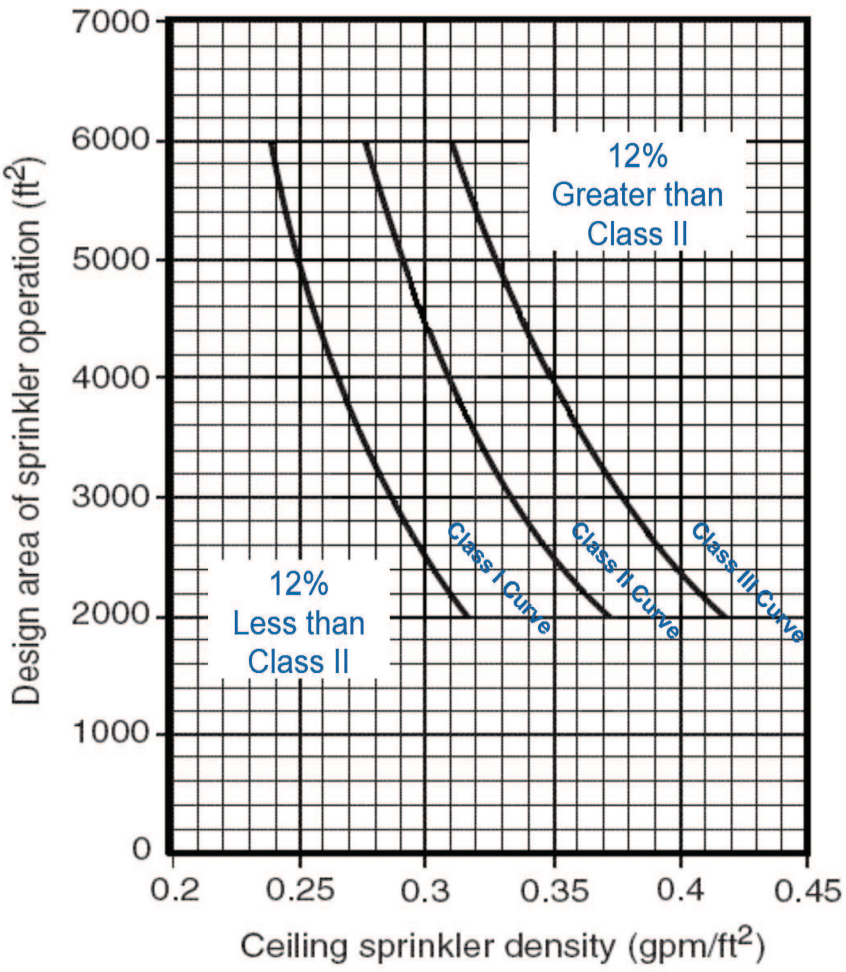

Figure 2.1: Area-density curves first used to determine the required amount of sprinkler coverage based on occupancy in the 1972 edition of NFPA 13. The class III curve was set 12% greater than the class II curve based on one test and the Class I curve was assumed to lie 12% lower than the Class II curve without any testing. All three curves have identical slopes even though the slope was only measured by tests for the class II curve. The identical setting of slopes was justified by an unverified concept called parallelism [27].

to combat a fire of a given size. Sprinkler designers today must design their sprinkler systems to meet the density requirements of these curves for the specific commodity stored in the designed warehouse. A long series of large and small-scale rack storage tests were conducted on a range of different commodities until it was decided upon that the "standard" commodity used to set a baseline of testing was to be a Class II commodity (double tri-wall corrugated cardboard carton with metal liner) [2].

Varying the ceiling sprinkler density by means of increasing water pressure, a full-scale rack storage setup was then burned to determine the number of sprinklers that operated during the test to contain the fire. The design area of sprinkler operation was then determined by the area of the grid of sprinklers that operated during the test. Six tests were used to set the "baseline" curve for Class II commodities, of which only one test was repeated at the same sprinkler density due to cost and time limitations. Serious discrepancies lead one to question the validity of the tests, including the fact that the pass/fail criteria for tests was changed throughout the test series, and generally only required that the fire not go beyond the confines of the mock facility.

Figure 2.2 shows the tests used to set design-area curves for NFPA 13 [27]. The baseline Class II curve has only 3 tests, 65, 66, and 68 that fall onto the curve used in the original standard. Two tests conducted with high-hazard commodities, tests 64 and 78, were used to "set" curves for class III and IV commodities, even though these tests did not actually fall onto these curves. It was decided that the Class I commodity, with little hazardous material should require less coverage, so it was set 12% lower than the class II curve without additional testing. The seemingly overlooked step in the process is the assumption of parallel curves delineating separate hazard classes in an arbitrary manner [3]. No testing was performed to verify this concept. A similar series of tests were later performed on plastics to develop similar curves for Group A-C plastics [26]. The fact remains that little, if any scientific basis has been applied to either the selection of commodities or the standards created to protect configurations of such commodities. Millions have been spent on additional large-scale testing to address issues for a multitude of specific warehouse configurations, without regard to developing a widely-applicable protection scheme with verified and validated levels of protection.

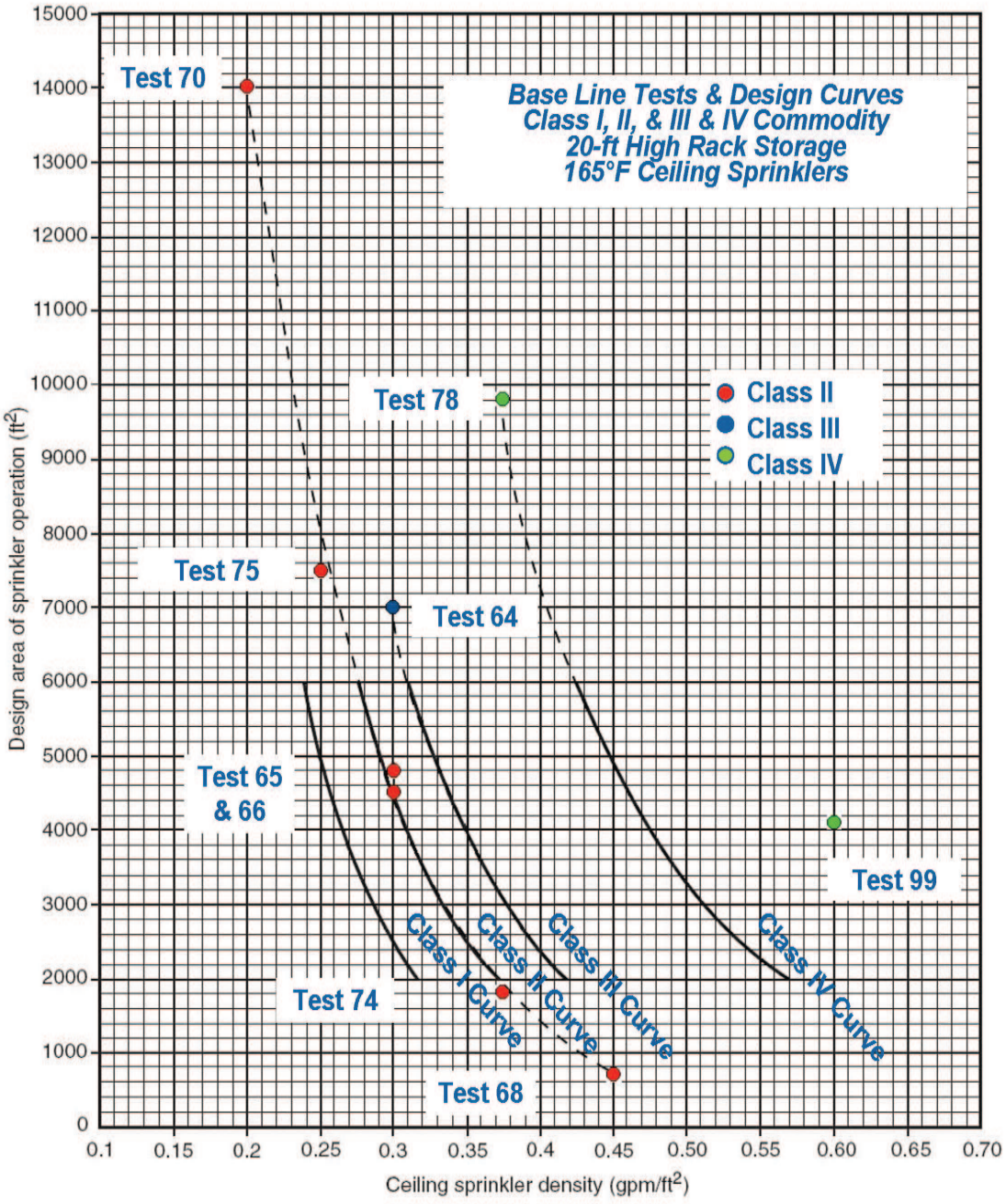

Figure 2.2: Large-scale rack storage tests were carried out to generate area-density curves for Class I–IV commodities. The Class II curve was set by 6 tests, and the slope of that curve was duplicated for Class I, III, and IV commodities. Test 64 and 78 were used to designate the location of the Class III and Class IV curves respectively. No tests were conducted on Class I commodities, and the curve was set 12% lower than the Class II curve [27].

2.5 Test Methods for Classification

Tewarson conducted extensive work at FM Global creating a classification methodology that uses four experimentally measured parameters to classify the flammability hazard of a material or a commodity [18]. These parameters address different aspects of flammability: the Critical Heat Flux (CHF) and Thermal Response Parameter (TRP) are associated with ignition, the Heat Release Parameter (HRP) is associated with combustion, and the Fire Propagation Index (FPI) is associated with fire propagation. A fundamental shortfall of these parameters is their dimensionality, which prohibits scaling analyses. The FPI, for example, has units of $((\mathrm{m/s^{1/2}})/(\mathrm{kW/m})^{2/3})$, revealing no clear fundamental definition because the parameter is based upon correlations of experimental data and not fundamental physics. There is also no method to tie these parameters together in a comprehensive manner for fire hazard assessment. Each of these parameters is determined for a material based on measurements conducted on commonly used apparatuses: The Ohio State University (OSU) Heat Release Apparatus, the Factory Mutual Research Corporation (FMRC) Flammability Apparatus, The National Institute of Standards and Technology (NIST) Flame Spread Apparatus (LIFT) and a Cone Calorimeter. All of these will be referred to as bench-scale calorimeters below. A summary of flammability parameters and testing apparatus are shown in figure 2.3.

Bench-scale calorimeters are used primarily in fire protection engineering to determine the HRR of a combustible material. The most common bench-scale calorimeter in use today is the Cone Calorimeter, shown in figure 2.4 [24]. The Cone Calorimeter measures the HRR of a burning sample via the oxygen consumption method: the mass fractions of combustion products and the flow rate are measured from the exhaust to calculate heat release [28]. A small sample is placed into the apparatus, mounted either horizontally or vertically, and a 5-kW heating element heats the sample with radiant, heat while an electric spark is used as the ignition pilot [29]. The portion of the apparatus holding the test sample is mounted on a load cell to measure the specimen mass-loss rate over time. Measurements vary depending on the area, thickness, and orientation of samples tested, and great care must be taken to test samples properly. This apparatus was used in a study of smaller-scale tests of

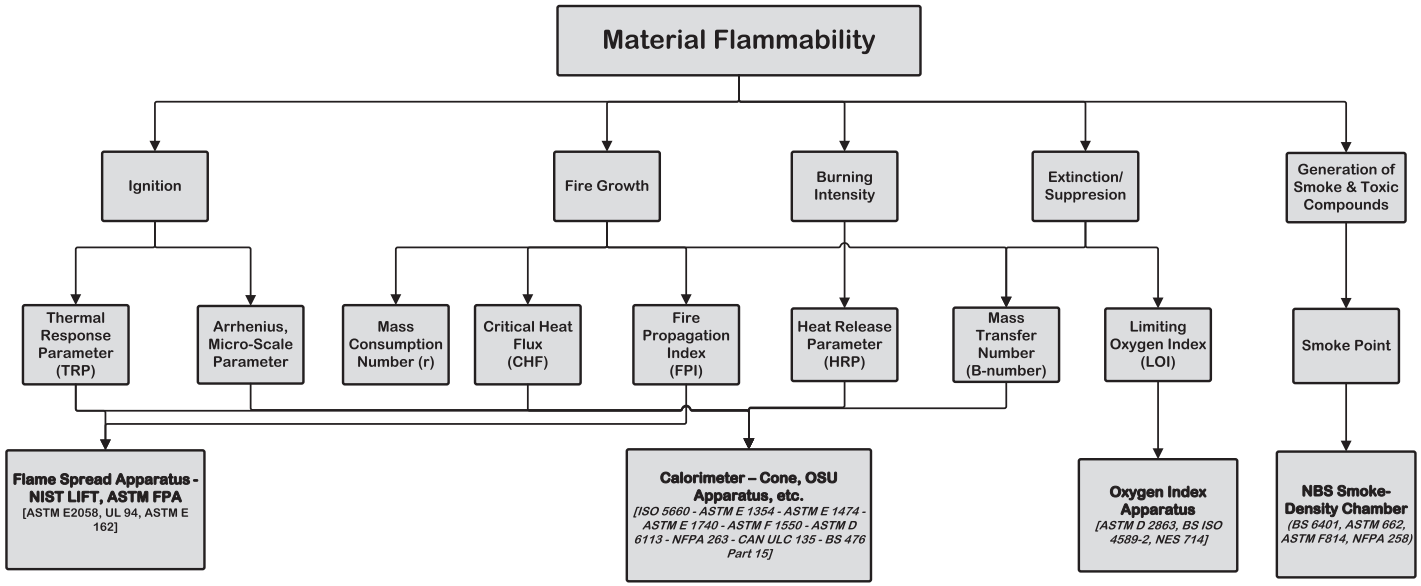

Figure 2.3: Material flammability flow chart. Tier two from the top describes five different aspects that describes a material's flammability. Tier three shows some of the many parameters that have been used or suggested to describe material flammability. Tier four shows four of the most common small-scale flammability test apparatus.

individual materials with the cone heater disabled [17]. The original OSU apparatus was the first developed and is also one of the best known bench-scale experiments closely related to the cone calorimeter. Its setup is very similar to the cone, except that it uses thermocouple temperature measurements to calculate heat-release rates from samples [28]. Some heat loss to the outside walls of the exhaust tube can occur, skewing thermocouple measurements. Most modern OSU experiments have been modified to take measurements by the oxygen-consumption method as well, as in the cone calorimeter. Various forms of the OSU apparatus have been used by the Federal Aviation Administration (FAA), National Research Council of Canada, Lund University, the Forest Products Laboratory, and the National Institute of Standards and Technology (NIST) [28]. Other bench-scale calorimeter-type devices include the FMRC combustibility apparatus, which can be modified to hold a tall sample and measure upward fire propagation on a sample. HRR measurements vary between different bench-scale calorimeters based on differences in geometry, test conditions, and mounting methods. Large-scale heat-release rate calorimeters have also been developed for furniture tests, tests of larger building materials not represented well by bench-scale testing, and room-scale testing mostly to calibrate computer models.

The LIFT fire propagation apparatus, developed by NIST, provides ignitability and flame-spread information for vertically oriented samples [30]. The apparatus consists of a radiant panel mounted at a 15 degree angle from a vertically oriented sample that provides a varying external heat flux along the length of a sample. A small pilot flame above the sample ignites the sample once a flammable mixture is achieved. Measurements by this device can provide the rates at which a flame propagates across a sample from a known, varying external heat flux.

Despite several previous studies, there does not currently exist a good method to correlate or compare small-scale test data to large-scale fire tests [31, 32]. Attempts to develop a large-scale model have also not addressed the fact that commodities and their packages involve several mixed materials, and the joint influence of these different materials together must be accounted for.

The FM Global Datasheet 8-1 on Commodity Classification outlines several tests used to evaluate the hazard classification of a commodity [25]. Bench-scale laboratory tests such as the heat-of-combustion test, percentage-inert-material test,

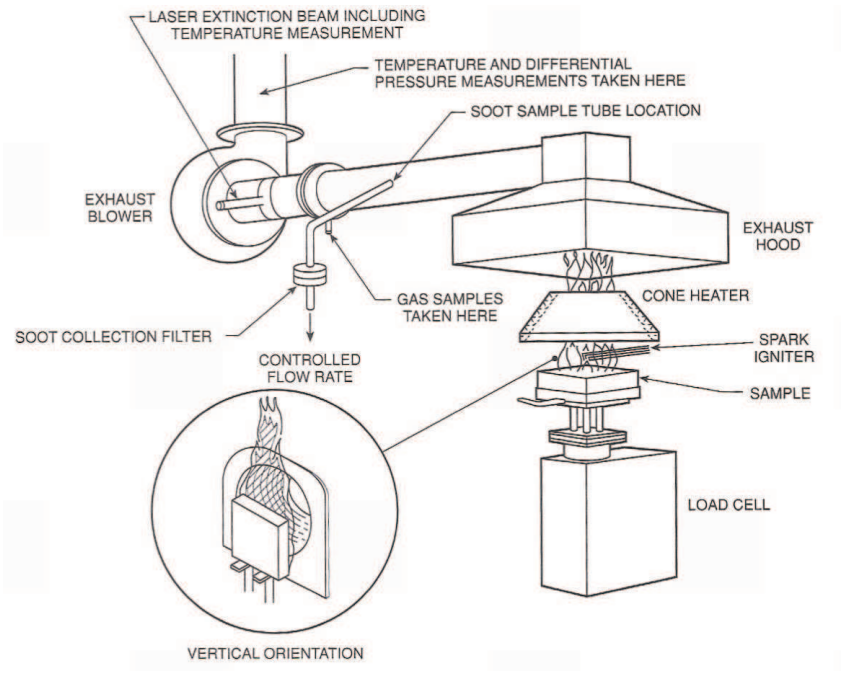

Figure 2.4: The Cone Calorimeter [24]

parallel-panel test, and random-burn test are all designed to aid in the classification of commodities. However, these tests only provide limited quantitative information and cannot simulate full-scale burning behavior of the product being tested. In order to fully evaluate the hazard classification of a commodity FM Global uses the Fire Products Collector (FPC) Commodity Classification Test. The FPC test is essentially a large-scale calorimeter which measures the heat-release, products of combustion, and burning rate of an 8 pallet array (4 standard commodities per pallet) [25]. Water is sprayed on the array to simulate sprinkler intervention during the burning process, and tested commodities are qualitatively evaluated against a known database of benchmark commodities to determine classification. A few fundamental problems with the FPC approach include an arbitrary configuration whose results are extended to taller arrays, and the addition of sprinkler suppression adding complexity before fundamentals can be understood. Although bench-scale testing would be highly desirable financially, at the current time FM Global's bench-scale tests cannot accurately predict large-scale behavior, although research to that end is continuing.

Other flammability tests are outlined in the United States by the American

Society for Testing and Materials (ASTM), Underwriters Laboratories (UL), and the International Conference of Building Officials (ICBO) [19]. The majority of these tests and standards focus on specific building products, materials, etc. Examples of these include tests for mattress flammability, airplane paneling, tire storage, etc. Each test is highly specific to the application, and the minimum requirements for materials differ widely depending on the test and application. Test equipment is available to measure a wide range of material flammability parameters, but isolating important parameters that may be useful in scaling a fire scenario requires a renewed focus on fundamental theory.

2.6 Diffusion Flame Theory and Development of the B-number

An ideal diffusion flame consists of an infinitesimally thin exothermic reaction zone which separates fuel diffusing from the burning material and oxygen from the air that diffuses in the opposite direction [33]. Burke and Schumann [34] were the first to develop an ideal description of a diffusion flame where fuel and oxygen meet in stoichiometric proportions in this thin burning layer to react and produce intense heat, supporting further combustion. An example of a diffusion flame is the combination of a liquid fuel droplet in an oxidizing gaseous atmosphere.

Spalding first introduced the B-number in 1950 to develop an expression for the burning rate of a liquid fuel droplet in a gas stream [35]. The B-number is a property of pyrolyzing material, and it appears in boundary conditions of energy conservation at the fuel surface. Physically, it relates the heat release from combustion (the numerator) to the energy required to generate fuel gases (the denominator) [33]. In 1956 Emmons provided a solution for the burning rate of a diffusion flame over a planar liquid fuel surface subjected to a forced flow parallel to the surface [36]. Emmons also used Spalding's B-number in a boundary condition at the fuel surface. The closed-form solution developed by Emmons shows that the local burning rate, or mass-loss rate varies inversley with the square root of distance from the leading edge and varies directly with the square root of air velocity. Using the Shvab-Zel'dovich

formulation [21] the highly non-linear reaction-rate term from energy and species equations could be eliminated. Due to the simplicity of this solution, Emmons's "classical solution" is widely used as a starting point for further studies.

Kosdon *et al.* developed a solution similar to Emmons for a buoyancy-driven flow [37]. A similarity theory for laminar natural convection along a wall was developed and compared to experiments conducted on cellulose cylinders. Results from experimentation show an over-prediction by theory by a factor of approximately two. The authors explain these discrepancies mostly due to radiant heat exchange. A similar study by Hedge *et al.* tried to resolve these discrepancies between theory and prediction by numerically introducing varying viscosity, specific heat, and conductivity constants [38]. Accuracy was increased by only 8% with tests on PMMA cylinders burning in air. Kim *et al.* numerically computed a solution of a laminar pyrolysis zone of a freely burning fuel surface similar to Kosdon *et al.* for a wide variety of fuels [39]. Their theoretical predictions of burning rate agree reasonably well for fuels with low molecular weights [40].

In all of the previously mentioned studies there are two important disadvantages that limit their use towards accurately characterizing flame spread. First, they do not include radiation effects, which become increasingly important as the flame height is increased [41]. Second, these studies only provide an empirical means of predicting flame height.

Pagni and Shih introduced the concept of *"excess pyrolyzate"* in 1978 to predict flame heights above the pyrolysis region [15]. According to this concept, fuel that does not burn in the pyrolysis region escapes downstream, forming a combusting plume where the fuel burns higher than earlier predicted. Both free and forced laminar convection burning were included by imposing initial conditions on the pyrolysis zone and using an integral scheme proposed by Yang [42] to solve for the combustion plume region (above the pyrolysis zone). Pagni and Shih's theory predicts nondimensional flame heights to be dependent only on B, the mass transfer number, and r, a mass consumption number. They do not address upward flame spread.

In work addressing upward spread, Annamalai and Sibulkin test Pagni and Shih's theory by replacing surface boundary conditions by a simplified polynomial fit [43, 14]. They plot experimentally determined pyrolysis lengths versus theory and still

find an over-prediction of the data by almost a factor of 2. Pagni's introduction of the concept of excess pyrolyzate brings some closure to the problem of buoyancy-driven vertical combustion, but mismatches between experimentation and theory still need to be addressed [44]. Work determining a variable B-number using flame standoff distance by Rangwala improves the accuracy of flame height predictions from Annamalai and Sibulkin in laminar regimes, but more work remains [40]. More recent work develops additional spread models by Saito *et al.* [45, 46], Delichatsios [47, 48], Quintiere *et al.* [49], Kulkarni and Sibulkin [50], Grant and Drysdale [51], Karlsson [52] and Hasemi *et al.* [53] that address upward and wind-driven flame spread. Additional reviews are given by Joulian [54] and Brehob *et al.* [55].

2.7 Use of the B-number in Fire Safety

Pagni applied his analysis of excess pyrolyzate in a later paper to fire-safety applications by comparing predicted flame heights of varying fuels as an assessment of flammability [56]. Pagni suggests the use of a mass consumption number, r, as an index of fire. Later work showed the mass consumption number, and thus the flame height, to be mostly dependent on the B-number, allowing the B-number to become a general ranking criterion for flammability classification [14]. Kanury also evaluated flammability (or burning intensity) of materials using the B-number, in this case for pool fires with a variety of polymers [33]. Kanury used a modified B-number that took into account flame radiation effects by using a radiative fraction of feedback, although radiation played a smaller roll in pool fires than say, for upward burning on a wall. Kanury proposed that a B-number serves as the best representation of flammability classification for these pool fires.

Recent work has been performed analyzing the B-number for its use as a universal flammability criterion for microgravity applications by Torero *et al.* [57]. The form for the B-number of a material used by Torero *et al.* takes into account complex modes of heat transfer, including excess pyrolyzate and an estimate for radiation. This experimentally determined B-number can be used to rank materials based on their propensity to sustain concurrent flame spread. Rangwala shows through experimental data that the B-number is not a constant, but rather changes from the leading

edge to the trailing edge of a flame [58]. A relationship between the B-number and flame standoff-distance was found, of the form $y_f = A(B)x^{1/4}$ and data supporting the increased accuracy of a flame-spread model thanks to this result was presented. Rangwala also suggested using the B-number as a material flammability criterion because a large B-number implies a highly exothermic fuel relative to heat required for gasification, thus the thermodynamic/thermochemical part of the flame spread problem is implicit in the B-number. The procedure for calculating a time-averaged B-number for material flammability ranking was suggested by the author.

Rasbash [59] has indicated that a critical B-number may be defined below which extinction occurs by water application. Recently Torero *et al.* presented additional methods of experimentally determining a critical B-number for extinction [57]. Thus, irrespective of whether extinction or delaying spread is the criterion, the B-number arises as a relevant parameter. Use of a critical B-number also allows exploration of extinction and suppression by means other than sprinklers.

Chapter 3

Theory

3.1 Definition of the B-number

It has been shown by Pagni and Shih [15] that upward laminar flame propagation can be described well by the B-number (also called Spalding's mass transfer number) [57]. The B-number appears in a boundary condition at the fuel surface in the classical Emmons solution for forced-flow flames over a condensed fuel [36]. This dimensionless parameter is quite simply a ratio that compares a summation of the various impetuses (e.g. heat of combustion) for burning to a summation of the various resistances (e.g. heat of vaporization) to the process. Originally [36] a purely thermodynamic quantity, its definition can be extended to encompass effects of different heat-transfer processes [40]. A useful definition that can be selected is [40]

$$B = \frac{(1-\chi)(\Delta H_c Y_{O_{2,\infty}})/\nu_s - C_{p,\infty}(T_p - T_\infty)}{\Delta H_g + Q} \tag{3.1}$$

where χ is the fraction of the total energy released by the flame that is radiated to the environment, ΔH_g denotes the heat of gasification of the condensed fuel and ΔH_c represents the heat of combustion. Here ν_s denotes the oxygen-fuel mass stoichiometric ratio, $Y_{O_2,\infty}$ is the mass fraction of oxygen in ambient air, $C_{p,\infty}$ represents the specific heat of air at an ambient temperature of T_∞, and T_p equals the pyrolysis temperature of the fuel. The parameter Q represents the normalized non-convective heat transfer at the surface, given by

$$Q = \frac{\dot{q}''_{s,c} + \dot{q}''_{s,r} - \dot{q}''_{f,r}}{\dot{m}''_f} \tag{3.2}$$

where $\dot{m}''_f$ is the burning rate per unit area, $\dot{q}''_{s,c}$ represents the rate of conduction of energy into the solid per unit area, $\dot{q}''_{s,r}$ represents the rate of surface re-radiation of energy per unit area, and $\dot{q}''_{f,r}$ denotes the radiative energy feedback from the flame to the surface per unit area. Thus, a large B-number basically implies a highly exothermic fuel relative to the heat required for gasification.

3.2 General Expected Evolution of the Combustion

Figures 3.1 and 3.2 show a theoretical picture of the burning observed in a standard warehouse commodity. The heat flux to unignited material from the fire plume that extends upwards over the distance $(X_f - X_p)$ is responsible for the rapid upward spread of the flame. In figures 3.1 and 3.2 the length of the fire plume, $(X_f - X_p)$ is a function of the B-number and pyrolysis height [58].

During the early stages of the fire (figure 3.1), the flame is small, and the burning rate is a function only of the material properties of the corrugated board. This is later described as stage I of burning for a standard warehouse commodity. Heat flux from combustion pyrolyzes the board and packing material, releasing gaseous fuel adjacent to the combustion surface. Some of this fuel burns in the boundary layer in front of the fuel surface, but some is carried above its originating height and burns above, creating much larger flames. This fuel carried above its originating surface is called *excess pyrolyzate* [15]. The pyrolysis height increases with time in the early stage represented by figure 3.1. In the later stages of figures 3.1 and 3.2 it has reached the top of the commodity.

Heat flux via in-depth conduction through the corrugated board can pyrolyze the packing material and commodity, releasing combustible vapors. As the outer corrugated board layers break down, these combustible vapors diffuse through the remaining board, enhancing the flame spread rate. At this stage, the B-number is a function of the material properties of the corrugated board as well as the pyrolysis

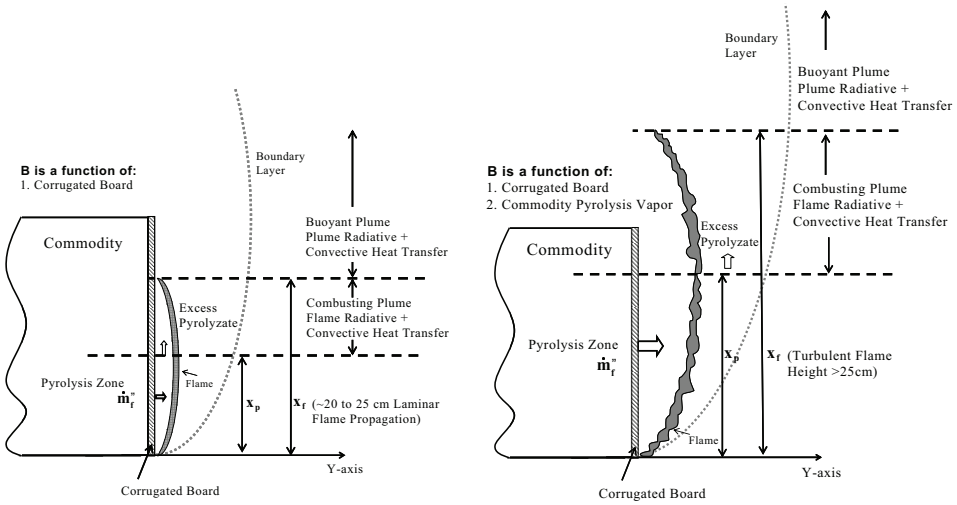

Figure 3.1: (Left) Flame propagation up the surface a warehouse commodity during the early stages of fire, where the flame height is below the height of the commodity. (Right) Flame height reaches above the height of the commodity. Both images are representative of Stage I burning of a standard plastic warehouse commodity.

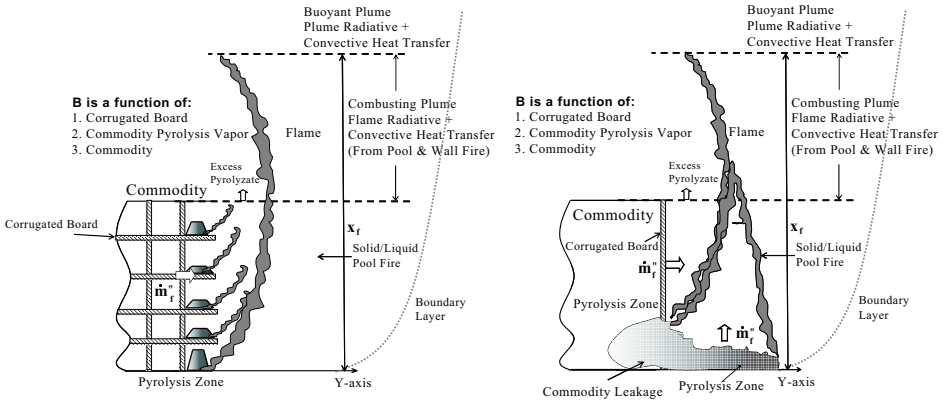

Figure 3.2: Turbulent upward flame propagation at later stages of the fire, where the commodity within the box either burns from within the box (left) or has spilled out into a pool fire (right). The commodity is now in stage III of burning where plastic dominates the burning rate.

vapor from the heated commodity that penetrates the corrugated board. As time advances, the corrugated board can disintegrate, thereby exposing the commodity inside to direct flame impingement.

After the outer covering and inner packaging burn off, they smolder significantly, slowing the burning rate as the inner plastic product heats towards its ignition temperature. This is described as stage II of burning. The plastic product (depending on its material properties) can then burn from inside or spill out as solid chunks or a viscous liquid pool once it reaches its ignition temperature, illustrated in figure 3.2. At this later stage, the B-number is a function of the material properties of the corrugated cardboard, the commodity pyrolysis vapor (diffusing outwards) and the commodity and packing material that have either spilled out or are burning within. This is later referred to as stage III of burning for a standard plastic warehouse commodity.

3.3 Calculation of the B-number from Experiments

One approach to correlating the vaporization and combustion rates of a warehouse commodity is to follow the procedure presented by Kanury [33], which expresses the average burning rate per unit area $\dot{m}''_f$ as

$$\dot{m}''_f = \frac{\overline{h}}{c_g} \ln(B+1) \tag{3.3}$$

where $\bar{h}$ is the heat-transfer coefficient and c_g may be approximated as the specific heat of air at a temperature equal to an average of flame temperature and ambient [60]. This equation links the burning rate, $\dot{m}''_f$ to the heat-transfer conditions $\overline{h}/c_g$ and material/thermodynamic $\ln(B+1)$controlling parameters. To estimate the rate of convective heat transfer and thus the influence of the flow field during upward turbulent burning, a relation with the Nusselt number, Nu_x may be used [61], namely

$$\frac{\bar{h}}{c_g} = \frac{\rho_g \alpha_g}{X_p} \overline{\mathrm{Nu}}_x \tag{3.4}$$

where ρ_g and α_g are the density and thermal conductivity of air, respectively. From this an average heat-transfer coefficient, $\bar{h}$ is determined. The Nusselt number is

determined from a standard correlation for turbulent heat transfer to a vertical surface [62]

$$\overline{\mathrm{Nu}}_x = 0.13(\mathrm{Gr}_x\mathrm{Pr})^{1/3} \tag{3.5}$$

where Gr_x is the Grashof number of the flow, and Pr is the Prandtl number of the gas, $\mathrm{Pr} = \nu_g/\alpha_g$. With the Grashof number defined as

$$\mathrm{Gr}_x = \frac{gX_p^3\Delta T}{\nu_g^2 T_g} \tag{3.6}$$

where $\Delta T = T_f - T_\infty$ equations 3.3–3.5 can be combined to yield the expression

$$B = \exp\left(\frac{\dot{m}_f{}''}{\rho_g\alpha_g 0.13[g\Delta T/\nu_g\alpha_g T_g]^{1/3}}\right) - 1 \tag{3.7}$$

which can be used to calculate a B-number from experimental measurements. Note that this expression for the B-number is dependent only on properties of the gas phase and the mass-loss rate; no fuel properties appear. This approach is useful for experiments in which turbulent convective heat transfer dominates radiative feedback, as is estimated to occur in the present experiments. The absence of the length X_p in equation 3.7 is a special characteristic of natural convective heat transfer to vertical surfaces being dominant in the experiments.

3.4 Thin-Skin Calorimeters

Heat flux above the commodity is measured using thin-skin calorimeters which are described in detail in ASTM E 459-97 [63]. A thin sheet of metal (Inconel) is coated in a thin layer of flat, black paint and a type-K thermocouple is spot-welded onto the back of the thin metal as shown in figure 3.3 [64]. The calculation of the flux is based on an assumption of one dimensional heat flow arriving on the exposed face of the thin-skin calorimeter.

The equation for planar heat flux across the thin-skin calorimeter is

$$\dot{q}'' = \rho C_p \delta \frac{dT}{dt} \tag{3.8}$$

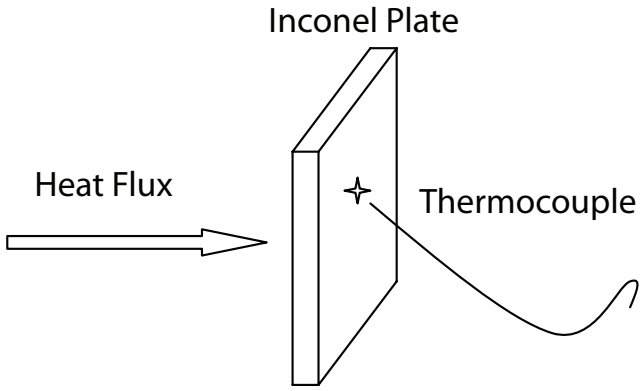

Figure 3.3: Diagram of thin-skin calorimeter with heat applied from the left and a thermocouple mounted to the back.

where ρ is the density of the metal, C_p is the metal's specific heat, δ the metal's thickness, and $\frac{dT}{dt}$ is the rate of rise in temperature of the back surface over time, in this experiment calculated numerically with a finite-difference code.

The combined heat flux from the thin skin calorimeter then becomes

$$\dot{q}_i'' = \dot{q}_c'' + \dot{q}_r'' + \dot{q}_{sto}'' - \dot{q}_{c,st}''. \tag{3.9}$$

as displayed graphically in figure 3.4. The heated plate will transfer heat to the cooler surrounding air by convective heat transfer expressed by

$$\dot{q}_c'' = \overline{h}(T_s - T_\infty) \tag{3.10}$$

where $\overline{h}$ is the convection heat transfer coefficient, T_s is the surface temperature of the Inconel plate, and T_∞ is the ambient temperature. The heated steel plate will radiate energy to the environment by the Stefan-Boltzmann law,

$$\dot{q}_r'' = \sigma\varepsilon(T_s^4 - T_\infty^4) \tag{3.11}$$

where σ is the Stefan Boltzmann constant and ε is the emissivity of the inconel plate. Conduction heat transfer within the plate will occur at a rate defined by Fourier's law,

$$\dot{q}_{c,st}'' = -k\frac{dT_s}{dt} \tag{3.12}$$

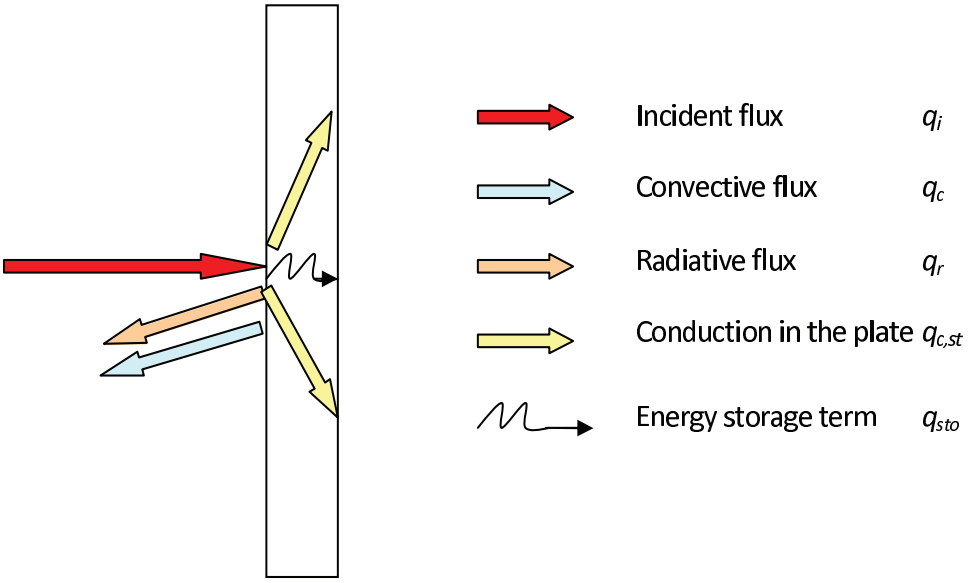

Figure 3.4: Total heat flux on a thin-skin calorimeter.

where k is the thermal conductivity of the plate. Storage of heat into the plate occurs at a rate defined by

$$\dot{q}''_{sto} = \rho C_p \delta \frac{dT}{dt}. \tag{3.13}$$

For a chosen metal with a low conductivity such as Inconel, losses from the plate can be ignored, and the combined equation for heat flux measured by a thin-skin calorimeter accounting for losses becomes

$$\dot{q}'' = h(T_s - T_\infty) + \sigma\varepsilon(T_s^4 - T_\infty^4) - k\frac{dT_s}{dt} + \rho C_p \delta \frac{dT}{dt}. \tag{3.14}$$

3.5 Flame Height Theory

Two methods are presented here to calculate a predicted flame height based upon experimental data. The first method of calculation is based upon on a theory for upward flame spread developed by Annamalai and Sibulkin, following the method Pagni and Shih used for their calculations [14, 15]. For vertical flame growth in a

naturally convected flame, the ratio of pyrolysis heights (flame height over pyrolysis front height) is given by a correlation [14]

$$\Phi = \frac{X_f}{X_p} = 0.64(r/B)^{-2/3}. \tag{3.15}$$

r is referred to as the mass consumption number or stoichiometric parameter, and is defined as the ratio of the mass fraction of ambient oxygen to the mass fraction of fuel in the transferred phase times the stoichiometric oxygen-fuel mass ratio [43]. To calculate the theoretical length of the pyrolysis front for a naturally convective flame, X_p is solved for using

$$(X_p^{1/2} - X_{p,0}^{1/2}) = \left(\frac{4(1 - 1.25(r/B)^{1/3}))}{\pi}\right) * \left(\frac{a_0^2}{\rho_s c_{p,s} k_s (T_g - T_\infty)}\right) * (t - t_0). \tag{3.16}$$

The term a_0 is a constant dependent on various fuel and gas properties and is given by [14]

$$a_0 = 0.27 \frac{B^{7/4}}{(B+1)^{1/4}} r^{0.19} \frac{\Delta H_c/\nu_s (g \Delta H_c/\nu_s^2 c_{p,g} T_\infty)^{1/4}}{\mathrm{Pr}^{1/2}} \ln(B+1) \tag{3.17}$$

where ΔH_g is the heat of gasification, ν_s is the stoichiometric oxygen-fuel mass ratio, and ΔH_c is the heat of combustion. Using equations 3.15 and 3.16, along with a value for r given by Annamalai and Sibulkin the flame height, X_f is solved for [43]. The resulting formulation represents a power-law dependence of the flame height on B and r.

An alternative method to predict flame heights, representing an exponential limit was developed by Saito *et al.* [45]. They present a rough formulation for the rate of pyrolysis spread assuming $X_f - X_p$ remains approximately constant during steady-state burning, which for a non-charring fuel yields

$$V_p = (X_f - X_p)/\tau. \tag{3.18}$$

V_p is the rate of spread of the pyrolysis front (dX_p/dt) and X_f and X_p are the flame and pyrolysis heights, respectively. τ is a material property, the characteristic ignition time for spread,

$$\tau = [\kappa\rho c_p(T_p - T_a)^2]/\dot{q}_0'' \tag{3.19}$$

where the numerator is often referred to as the Thermal Response Parameter (TRP), for which many experimentally-measured values exist [18]. In their paper, Saito *et al.* applies a flame height correlation of the form

$$x_f = K[\dot{Q}' + \dot{q}_0'' \int_0^{X_p} (\dot{m}_f'' dX)]^n \tag{3.20}$$

where K and n are constants, $\dot{q}_0''$ is the heat flux from the flame, $\dot{Q}'$ is the external heat flux to the surface, and $\dot{m}_f''$ is the fuel mass-loss rate. In the pyrolysis region, $0 < X < X_p$, $\dot{m}_f''$ can be assumed to be independent of x, and therefore combining equations 3.18 and 3.19 yields

$$\frac{dX_p}{dt} = (K[\dot{Q}' + \dot{m}_f''\dot{q}_0''X_p]^n - X_p)\tau. \tag{3.21}$$

For $n = 1$, this equation is easily solved. It can be further assumed that K and n are approximately equal to unity, and in the case of no applied heat flux ($\dot{Q}' = 0$)

$$X_f = A\exp(\alpha t) \tag{3.22}$$

where

$$\alpha = (X_f/X_p - 1)/\tau^2, \tag{3.23}$$

A is a constant determined by initial conditions, and X_f/X_p is determined by equation 3.15.

3.6 Acknowledgement

This chapter has partially included the following publication: "Controlling Parameters Involved in the Burning of Standard Storage Commodities: A Fundamental Approach Towards Fire Hazard Classification," at the *6th U.S. National Combustion Meeting*, (Ann Arbor, Michigan), 2009. M. J. Gollner, T. Hetrick, A. S. Rangwala, J. Perricone, and F. A. Williams. The thesis author is the primary researcher in this publication.

Chapter 4

Experimental Setup

4.1 Commodity

All testing reported herein was conducted at the Worcester Polytechnic Institute Fire Sciences Laboratory in Worcester, Massachusetts, USA, with no significant modifications to the apparatus or instrumentation made between test sessions. The Group A plastic commodity was burned with one exposed face, and the measured burning rates were employed to calculate the B-number of the mixed commodity by use of equation 3.7.

Table 4.1: Composition of standard commodities used in large-scale testing [2].

Commodity	**NFPA Class**	**Cardboard/ paper(kg)**	**Plastic (kg)**	**Total (kg)**
Polystyrene Cups	Group A Plastic	2.375	3.875	6.25
Paper Cups	Class III	4.25	0	4.25

Figures 4.1(a) and 4.1(b) shows the Group A plastic commodity. This commodity is often used by the fire-protection industry to test the effectiveness of fire sprinklers and other fire-protection devices [25]. The fuel consists of a corrugated cardboard carton subdivided into 125 compartments. The mass of each constituent

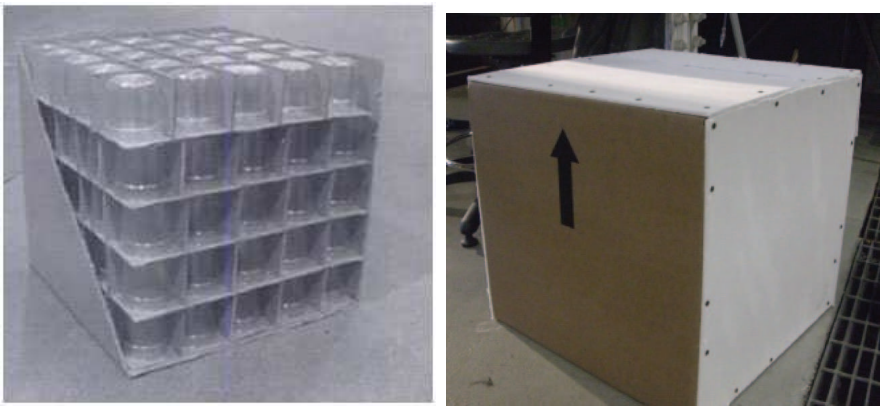

(a) Group A commodity with half of its exterior corrugated cardboard removed

(b) Commodity insulated on all but one side with Kaowool glass fiberboard

Figure 4.1: Standard Group A Plastic Commodity consisting of a 1-ply corrugated cardboard box continuing 125 polystyrene (PS) cups within segregated corrugated cardboard cells.

in the standard commodity is listed in table 5.1. The outer dimensions of each cardboard carton are 530mm wide by 530mm deep by 530mm high. The 125 cells are created by cardboard dividers subdividing the box in a $5 \times 5 \times 5$ matrix of cells. Each cell contains a 0.45L, 36g unexpanded PS cup. Each cup is 9cm in height, with the opening face down, a top radius of 4.5cm and a bottom radius of 3.75cm. The corrugated cardboard is 1-ply, with a thickness of approximately 4mm, but can be compressed to as little as 1mm in some places where handling damage has occurred. In all experiments where the cardboard is oriented vertically, the corrugations in the board are also oriented vertically. All measurements of the cardboard are approximate, and small variations exist between each commodity burned due to the adaptability of the cardboard. The commodity is wrapped in Kaowool insulating boards approximately 0.65cm (0.25in) thick on all except one vertical side, on which measurements were taken. This arrangement, limiting the burning of the box, allows for a closer investigation of the fundamental physics governing the combustion of the plastic commodity. The experimental setup consisted of the Group A plastic commodity placed on top of a Setra, Super II load cell that measured the mass loss of the plastic commodity to within an accuracy of ± 0.5 g.

4.2 Experimental Apparatus

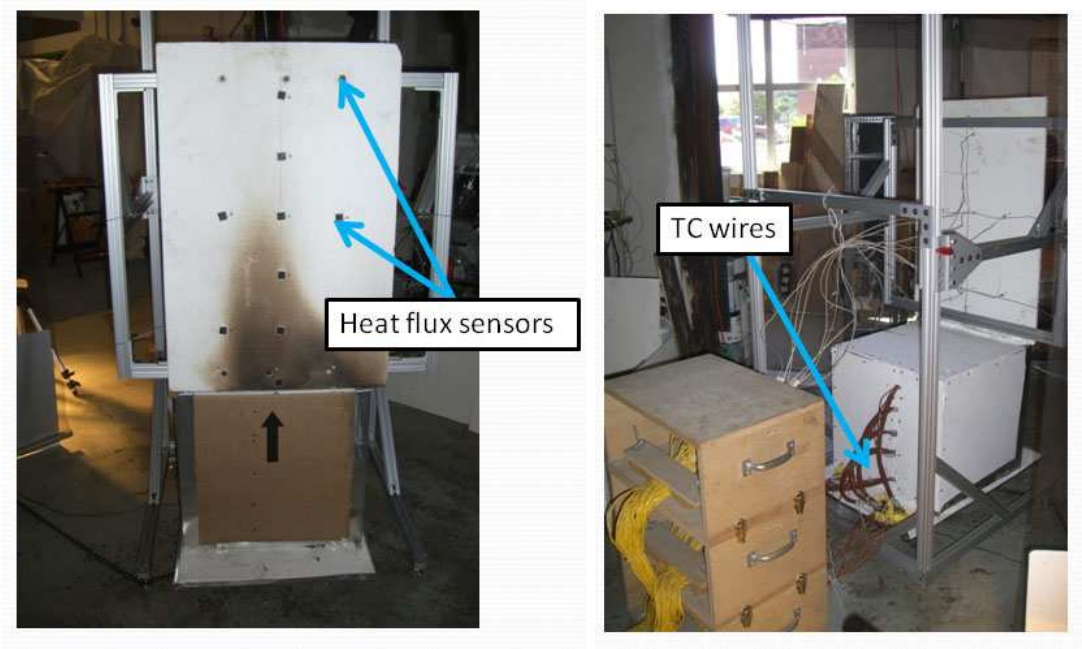

(a) Experimental setup at WPI front view (b) Experimental setup at WPI back view

Figure 4.2: The experimental setup used to evaluate a standard Group A plastic commodity is shown with accompanying thin-skin calorimeters to measure heat flux and thermocouple (TC) wires used to measure temperature inside the commodity.

Figure 4.3 shows the experimental setup and instrumentation configuration. Inside the box 3 Type-K Chromel-Alumel thermocouples are installed inside five cells on the front face of the box, as seen as in Figure 4.2. One set of thermocouples is placed on the front face of the cardboard to track the progression of the pyrolysis front along the face of the cardboard, one set is placed in the direct center of the PS cup to measure the temperature within the cup, nominally indicating the moment at which the cup ignites, and one set hangs to the side of the cup in the air space between the cup and cell wall, nominally indicating the cell's mean bulk temperature.

Cameras are setup on the sides of the apparatus to measure the flame standoff distance and in front of the setup to measure flame heights.

Nine thin-skin calorimeters were mounted on a 1.3cm thick (0.5in), vertically oriented glass fiber board oriented above- and flush to the front combusted face of the

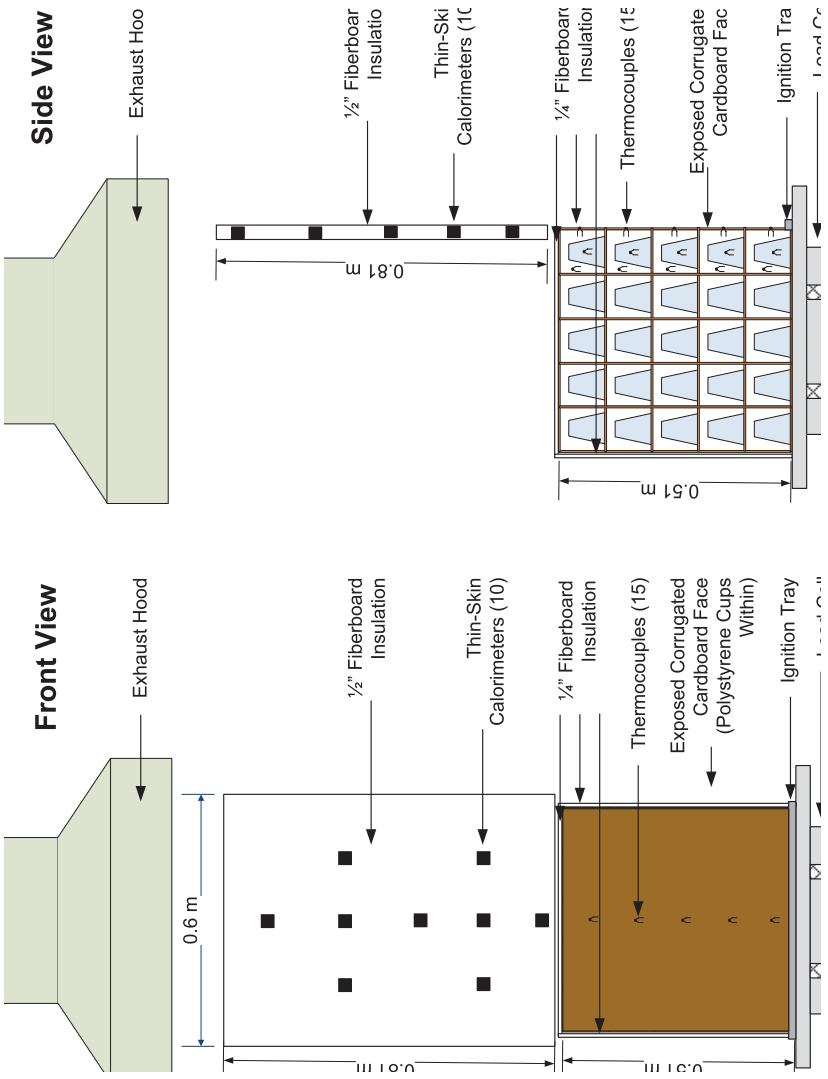

Figure 4.3: The experimental setup used to conduct tests on a standard Group A plastic commodity.

test commodity. This configuration allows for spatial measurements of the combined radiative and convective heat flux that the combusting plume of excess pyrolyzate will exert on stored commodities of higher elevation.

The setup was placed under a 4MW hood to eject burning fumes and embers. A controlled ignition was achieved by adding 4mL of n-heptane to a strip of glass fiber board approximately 1cm tall, 0.35m wide by 3mm in depth. The wetted wick igniter was held by an aluminum u-channel that was positioned adjacent to and below the lower front edge of the commodity. Experimental time begins when the strip is piloted at the centerline of the commodity's front face.

4.3 Acknowledgement

This chapter has partially included the following publication: "Controlling Parameters Involved in the Burning of Standard Storage Commodities: A Fundamental Approach Towards Fire Hazard Classification," at the *6th U.S. National Combustion Meeting*, (Ann Arbor, Michigan), 2009. M. J. Gollner, T. Hetrick, A. S. Rangwala, J. Perricone, and F. A. Williams. The thesis author is the primary researcher in this publication.

Chapter 5

Experimental Data and Results

Four tests were conducted on Group A Plastic commodities (see experimental setup, chapter 4). All tests, with the exception of test 1, measured flame height, pyrolysis height, mass-loss rate and temperatures within cells along the first layer of the commodity. Test 1 used thermocouple rods to collect temperature and pyrolysis height information that proved to be inaccurate, so that data has not been included. In tests 2-4, individually placed K-type thermocouples were used in the setup as described in detail in chapter 4. A summary of Group A commodity tests performed is provided in table 5.1

5.1 Detailed Observations during each Test

All tests were ignited by a wick soaked in 4mL of n-heptane. In each test the heptane in the wick burned off and a small pyrolyzing region began to develop at the bottom face of the exposed region of cardboard within 30 seconds of ignition. In test 1, 53 seconds after ignition the first layer of the front face of cardboard had begun to peel away. After 75 seconds the cardboard in the first rows of cells had ignited, and the flames began to extend above the top of the commodity. After 89 seconds the cups in the bottom row began to deform, and at 113 seconds all cardboard in the first layer of cells had ignited. Flame heights reached between 1.5–2 times the height of the commodity. The fire was manually extinguished 125 seconds after ignition. In

Table 5.1: Summary of Group A commodity tests.

Test	**Setup**	**Result**
Test 1	Front and side cameras, load cell, thin skins, thermocouple rods	Burned evenly across front face. Load-cell, thin-skin and camera data were complete. Thermocouple rods were inaccurate and needed to be replaced. First layer of cells burned.
Test 2	Front and side cameras, load cell, thin skins, thermocouples mounted in/on front face	Burned evenly. Load-cell, thin-skin, camera, and thermocouples data were complete. During first layer burning, PS cups melted onto front face of cardboard and prevented front face from burning off for extended burning "plateau" period. Hence, behavior was atypical from other tests.
Test 3	Front & side cameras, load cell, Thin Skins, Thermocouples mounted in/on front face one inside plastic cup	Burned evenly. Load-cell, thin-skin, camera, and thermocouples data were complete. Second layer PS cups ignited. Test was shut down before fully igniting second layer.
Test 4	Front and Side Cameras, Load Cell, Thin Skins, Thermocouples mounted in/on front face	Burned evenly. Load-cell, thin-skin, camera, and thermocouples data were complete. Second, third layer PS cups ignited. Test was shut down before fully igniting third layer.

Figure 5.1: Test 1 Timeline: (a) 53 seconds, peeling front face of cardboard, (b) 75 seconds, 1st layer cells cardboard ignite, (c) 89 seconds, PS cups in bottom row of first layer begin to deform, (d) 113 seconds, all PS cups and cardboard in 1st layer engulfed in flame.

subsequent tests the commodity was allowed to burn into further layers of cells, but because it had not yet been determined whether the polystyrene would create a pool fire, and there was uncertainty concerning the stability of the box, this first test was ended earlier than subsequent ones. A visual timeline of test 1 is shown in figure 5.1.

In test 2 the commodity was ignited in the same fashion and developed a laminar region of burning along the front face within 21 seconds. The flame was observed to transition into turbulent burning 4 seconds later. The front of the other cardboard cover (which consisted of two layers, a front one and an inner) peeled up quickly, and at approximately 50 seconds post-ignition it burned off. At the same time the bottom two rows of cells were exposed and burning, and the back layer of this outer cardboard above row two ceased to peel away and seemed to form a solid barrier slowing the burning process. Polystyrene had melted onto the back of the cardboard on the front face, holding this layer in place. The bottom two rows smoldered until at 122 seconds three cups on the bottom of the box begin to ignite and continued to ignite fully the bottom two rows of polystyrene cups. These created a large enough plume to force the top flap of cardboard off the front face at 158 seconds from ignition and the entire front face of the box burned at a rapid rate thereafter. At 172 seconds from ignition polystyrene began to melt and drip down the front face, creating a “wall of fire” with the remaining cardboard and melted polystyrene burning at an increased

Figure 5.2: Test 2 Timeline: (a) 21 seconds, laminar burning on front face, (b) 50 seconds, front layer of cardboard burned off; cardboard in bottom two rows of cells ignited, (c) 70 seconds, PS cups melted earlier than other tests, melted to front face and created shield stalling burning rate, (d) 122 seconds, bottom row of cups ignited, forcing top layer of cardboard/melted PS off, (e) 172 seconds, entire front layer of PS cups and cardboard burning in wall. Second layer of cells beginning to ignite.

rate. The fire was then extinguished. Inspection of the burned commodity revealed only several cells in the second layer ignited, but most cups in the second layer began to deform. A visual timeline of test 2 is shown in figure 5.2.

In test 3 the atypical behavior experienced in test 2 where the front face of cardboard became a barrier slowing the initial burning rate did not occur. Much like the first test, after approximately 30 seconds from ignition the front face of cardboard developed a progressing pyrolysis front whose associated flame quickly transitioned to turbulent burning. Without the top flap delaying the initial burning rate, within 92 seconds the entire front face of cardboard was exposed, and all exposed cardboard was burning. By 100 seconds the front face remained exposed and began smoldering, and the burning rate plateaued. Polystyrene began to ignite at 120 seconds in the center of the front face, and then the burning progressed to engulf the entire front face by 132 seconds. By 150 seconds the second layer of cells had begun to burn as well, significantly increasing the burning rate. The fire was extinguished at 172 seconds when the stability of the box was no longer ensured. A visual timeline of test 3 is shown in figure 5.3.

Figure 5.3: Test 3 Timeline (a) 30 seconds, front layer pyrolyzing and laminar burning along face, (b) 92 seconds, front face cells are exposed and burning, (c) 100 seconds, smoldering front face, second layer cells heating and PS cups deforming, (d) 132 seconds, all PS cups in the first layer ignited and burning, (e) 150 seconds, second layer of cells also burning.

The initial stages of test 4 had similar features to tests 1 and 3. After 30 seconds the first layer of cardboard was significantly pulled away and the second layer of cardboard began burning. After burning up approximately 10cm, the fire began to burn up the front face in two branches, left and right, with the right branch burning significantly faster than the left. By 110 seconds both fronts combined and the entire front face had burned away exposing all cells. The second layer of cells began to burn after 123 seconds in the center region of the second layer. Cups then began to ignite and by 150 seconds from ignition melted polystyrene began to drip down the front face creating a "wall of fire" in the front. By 180 seconds layer one and two of cells were fully involved, and both melted polystyrene and pieces of charred cardboard began to fall to the bottom of the commodity. The sides of the commodity began to bend and lose rigidity at which point the fire was extinguished 212 seconds after ignition. The first layer of cells was completely destroyed; only some melted plastic remained. The second layer was still distinguishable, but charred, with most polystyrene melted. The third layer was charred on the front of the layer due to the heat of the flames in front of it, and most of the cups had deformed, but the flames did not significantly penetrate layer 3 in the time the fire was permitted to burn. A visual timeline of test 4 is shown in figure 5.4.

Figure 5.4: Test 4 Timeline: (a) 30 seconds, first layer of cardboard burning, (b) 60 seconds, 2 fronts burning up front face of cardboard, (c) 123 seconds, second layer of box cells begin to ignite, (d) 150 seconds, PS cups ignited and dripping on front face, (e) 196 seconds, layer 1 and 2 of cells cardboard and PS fully enveloped.

5.2 General Observations from all Tests

Observations from all four tests have established a general pattern of the burning of a Group A plastic commodity. Ignition of a cardboard commodity may occur by piloted ignition with a wick, as in this experiment, or by radiant heating in the case of aisle-jumping in large-scale rack storage configurations. The outer face of the commodity is made of two-layer corrugated cardboard. On the face where ignition occurs, the first layer of cardboard will ignite and burn, eventually peeling away and igniting the second layer of corrugated cardboard, which will then experience a similar combustion process. The fire at this stage is comparable to that of a single doubly-ply sheet of cardboard burning upright. The arrangement of the commodity within the box has not yet influenced the burning. Figure 5.5 indicates that the stored plastic product is not yet involved in the burning. In a small percentage of commodities tested the polystyrene was observed to melt onto the second layer of corrugated cardboard which delays this layer from peeling away, reducing the initial burning rate.

For this typical commodity, the contents of the boxes burn sequentially as individual cells. Each cell is contained by corrugated cardboard on six sides with a polystyrene cup in the center as indicated in figure 5.5. While the front face of

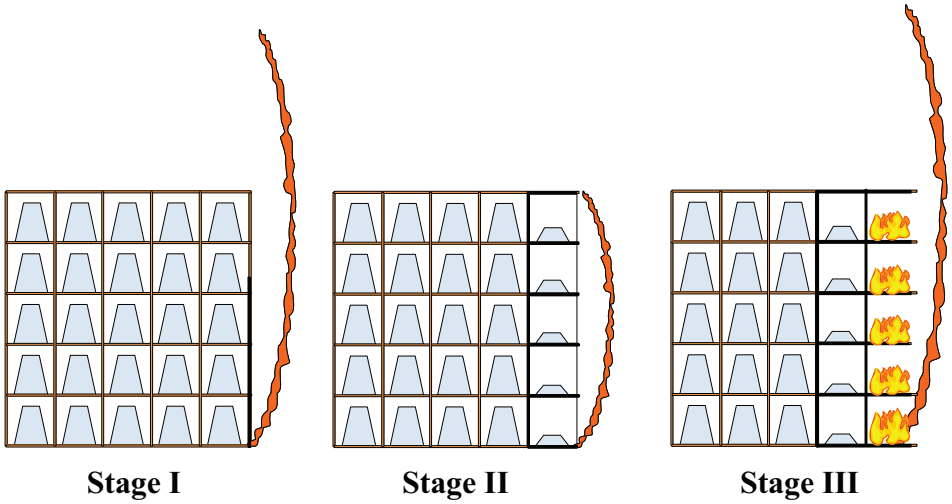

Figure 5.5: Side-view of the representative stages of burning for a Group A plastic commodity. Stage I on the far left consists only of upward flame spread along the outer cardboard face with no involvement of the inner packing commodity. Stage II in the center is the plateau region, where the inner packing material burns off and polystyrene heats before ignition, and Stage III on the far right involves combustion of polystyrene and remaining cardboard from within the commodity.

corrugated cardboard is burning, the first layer of cells begins to be heated, and the corrugated cardboard within the cells close to the front face begins to pyrolyze. As soon as the corrugated cardboard front face peels away, oxygen can reach the smoldering corrugated cardboard in the cell, causing it to ignite quickly. Adjacent cells heat one another, and in this manner the entire front layer of cells ignites, although the polystyrene is not yet affected significantly. Once the flaming combustion of corrugated cardboard within each cell in the first layer nearly ceases the commodity reaches the plateau stage of burning, shown in figure 5.5 labeled as stage II. During this plateau region cardboard smolders, cups absorb heat and are deformed until reaching the ignition temperature of polystyrene. Once the polystyrene reaches this temperature it ignites and begins to melt vigorously. The period of burning of the polystyrene cups is labeled in figure 5.5 as stage III. The melting and dripping of the polystyrene cups after their ignition, and the associated increased rate of heat flux from combustion of volatile polystyrene causes the second layer of cells to ignite and to repeat the process. As further layers of cells ignite, they add to a “wall” of

flame formed by the dripping polystyrene and charred cardboard that moves inwards sequentially through layers of cells in the package.

Although no tests conducted were able to continue past the third layer of cells, it is expected that burning through the remaining two layers of the commodity would continue in the same fashion until the structural stability of the commodity is compromised.

5.3 Quantitative Results

Measurements of the mass lost over time are shown in figure 5.6. Transitions between stages that are indicated in the figure were deduced with the help of the data from the thermocouples that were suspended within cardboard cells and polystyrene cups. Air currents resulting from the turbulent combustion process create fluctuations in the mass-loss readings on the order of 1–3 grams. These small fluctuations, which are not representative of the actual mass loss, are smoothed over by applying an nth-order polynomial fit to mass-loss data, resulting in the curves that are shown in figure 5.6 along with the raw data. Two test periods were not fit due to test inconsistencies. A ten-second section of test 2 in stage III was neglected because a piece of cardboard fell off the test sample then back onto the load cell, and all of stage II in test 4 was neglected due to behavior inconsistent with all other tests, probably because of large air-current fluctuations during this irregular burning period causing erratic load-cell readings. The transition between stages I and II, chosen as the point where inner packing material starts to burn and upward flame spread has reached the top of the front face of the package, or is close to the top, occurs around 77 seconds for three of the four tests. The inclusion of test 4, which displays an earlier transition between stages I and II, is useful for indicating the range of deviations that may occasionally occur in complex tests such as these.

The mass-loss rate was calculated from the derivatives of polynomial fits of recorded mass lost over time. Fluctuations in the mass-loss rate occur because of both time-dependent changes in the material burning and changes in the mixture of constituents burning throughout the box over time. The mass-loss rate shown in figure 5.7 steadily increases during most of stage I as the flame front progresses over

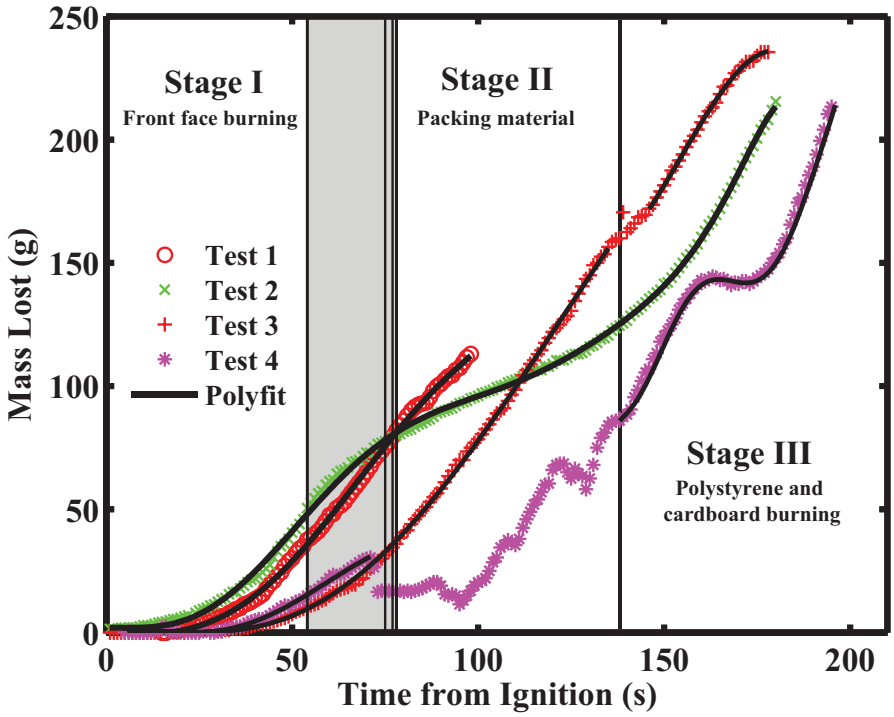

Figure 5.6: Mass lost from the commodity as a function of time, measured by a load cell at the base of the commodity. Polynomials are fit to the mass-loss measurements to smooth 2–3g fluctuations caused by air currents, but the smoothed data still captures the mixed commodity burning behavior. Relative stages of burning are indicated in the figure, with vertical lines denoting transitions between stages. The timeline for each test was shifted so that the transition betwen stages II and III occured at 138 seconds. The deviations in time for the transition between stage I and II for the four different tests is indicated by the vertical grey band between those stages.

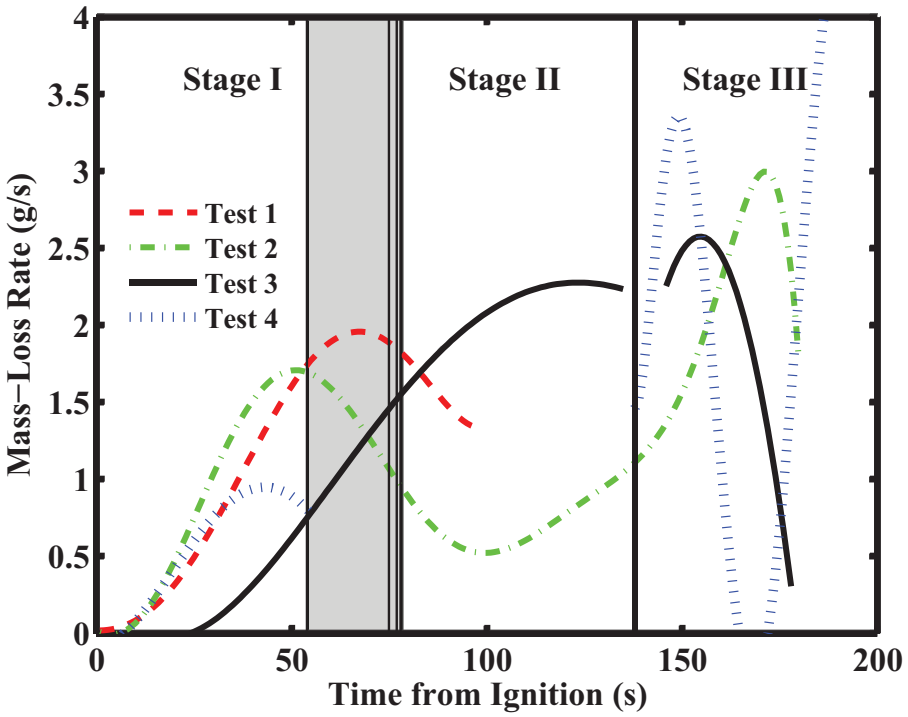

Figure 5.7: Mass-loss rates, calculated from the derivative of polynomial fits to the mass-lost data. Relative stages of burning are indicated in the figure as described in the caption of figure 5.6.

the front face. The mass-loss rate then reaches a plateau in stage II while corrugated cardboard packing material burns and polystyrene melts and gasifies. The mass-loss rate then typically decreases as all remaining corrugated cardboard burns out. Once polystyrene reaches its ignition temperature at the beginning of stage III, the mass-loss rate sharply increases, until water spray is applied to extinguish the flames.

The heat flux reaching a vertically oriented surface above the tested commodity, measured by thin-skin calorimeters, is shown in figure 5.8. The heat flux was determined by applying a 7-point moving average to temperature histories of the sensor element of the thin-skin calorimeters measured at 10 Hz. This serves to smooth the data while still giving a time resolution better than 1 second, much finer than that of the load cell and appropriate because this is nearly a point measurement, rather than being integrated over the entire volume of the fire. A finite-difference formula was applied to this data to determine its derivative. The heat flux was calculated

accounting for radiative, convective, and storage losses using a method outlined in section 3.4. The heat fluxes displayed in figure 5.8 represent a combined radiative and convective heat flux at this higher elevation. They cannot be equated to the heat flux directly in front of the commodity, but they can be used for analysis of upward spread rates. These heat fluxes sharply increase towards the end of stage I of burning, unlike the mass-loss rate which steadily increases throughout the first part of stage I. The high peak heat flux observed after approximately 1 minute of burning, due to increased amounts of excess pyrolyzate burning above the commodity, is likely to contribute to the rapid upward flame spread rates seen in large warehouse fires. The heat flux then steadily declines throughout the burning- rate plateau of stage II, and it increases again with the involvement of polystyrene in stage III. Heat fluxes measured over a large spatial region above the commodity are given in Appendix A.

Ranges of flame heights, determined from high-definition camcorder recordings of images of the front of the commodity are shown in figure 5.9. The flame height was defined as the highest peak of an attached yellow flame determined by running an edge-detection algorithm on the video output. The flame and pyrolysis heights measured are both shown in figure 5.9, with grey bands between curves indicating experimental scatter. In obtaining the pyrolysis height, thermocouples mounted along a column of cells in the front face of the commodity provided data on the position of the pyrolysis front along the front face of the box during stage I as shown in figure 5.10 (Thermocouple A). Recorded thermocouple temperatures of 380 °C, the ignition temperature of cellulose reported in literature [43], were chosen to mark the locations of the pyrolysis front as shown in figure 5.11. Approach to a temperature plateau is also indicative of reaching the pyrolysis front, and this was found to occur within 5 °C of 380 °C, the recorded temperatures sometimes being below the literature value, possibly due to heat loss from the junction or the instrument heating time. The results were consistent with charring that could be seen from the front-view cameras. Thermocouple temperature measurements used to calculated pyrolysis rates, as well as those located within the commodity are provided in Appendix B.

In figure 5.9, the pyrolysis height pertains only to stage I because at the end of that stage, the pyrolysis front has reached the top of the package, but the flame heights exhibit the same three stages as the mass-loss rate and heat flux shown in

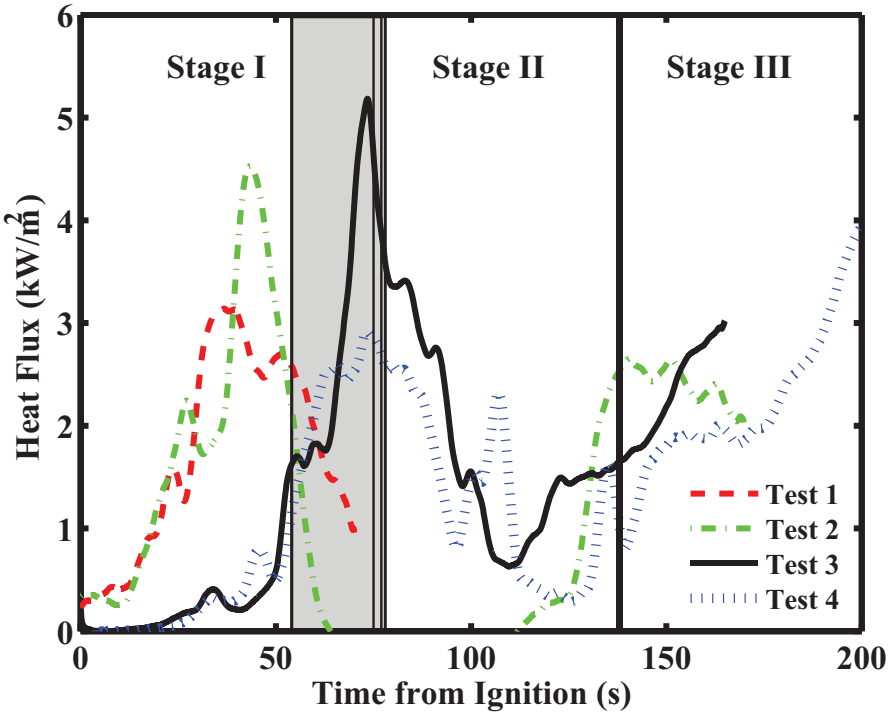

Figure 5.8: The heat flux measured by a vertically oriented thin-skin calorimeter approximately 3 cm directly above the top center of the face of the tested commodity, representing a combined convective plus radiative heat flux exerted on commodities at higher elevations. Relative stages of burning are indicated in the figure, as described in the caption of figure 5.6. Additional heat flux measurements are provided in Appendix A.

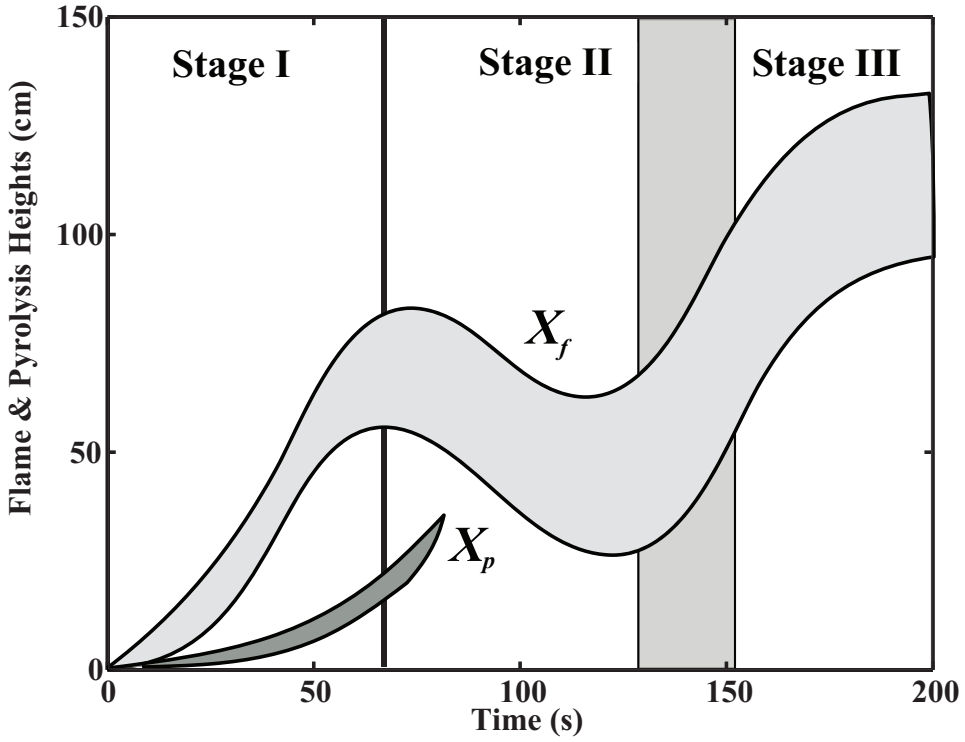

Figure 5.9: Ranges of flame (X_f) and pyrolysis (X_p) heights from four tests, with grey bands between the curves indicating experimental scatter. Relative stages of burning are indicated in the figure, with vertical lines denoting transitions between stages, as described in the caption of figure 5.6

figures 5.7 and 5.8. Flame heights rapidly increase during initial burning, reflecting the high fire hazard of outer corrugated cardboard covering. They then taper off as the cardboard begins to smolder. The decrease in flame heights corresponds to smoldering of packing material and to a decrease in the excess pyrolyzate burning above the tested commodity. A steady increase in flame height is observed once volatile polystyrene reaches its ignition temperature and dominates the burning process in stage III. The fact that the burning is more vigorous in stage III than in stage I is due to the involvement of more volatile plastic fuel, reflected in the higher mass-loss rate in stage III seen in figure 5.7, increases the excess pyrolyzate and causes more of the heat release to occur at higher elevations, moving the flames away from the thin-skin gauges, thereby tending to decrease their readings, as seen in figure 5.8.

All fire processes exhibit some random behavior inherent in their turbulent and

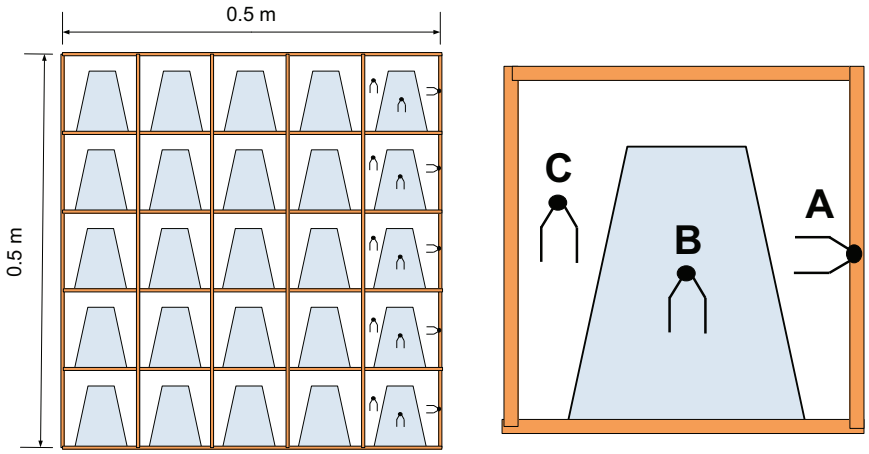

Figure 5.10: Locations of thermocouples placed within the grouped commodity. A closeup of one cell is shown on the right. Thermocouple 'A' is mounted on the front face of the cell to track the progression of the pyrolysis front, thermocouple 'B' is suspended in the air inside the polystyrene cup to detect ignition of the polystyrene, and thermocouple 'C' is suspended in the air between inside the cell to detect flashover within the cell.

complicated nature, but because this standard commodity is segregated into small cells it exhibits roughly repeatable behavior. When a large number of individual identical elements are measured, results on a large scale can become roughly repeatable, even with the random nature of events taking place on a small scale. The layers and dividers within the box also provide structural stability to the test commodity so that it takes a longer period of time for the commodity to disintegrate and thereby lead to burning behavior that is more unpredictable.

5.4 Extraction of B-number Values

Equation 3.7 was used to determine a B-number as a function of time using the experimentally determined mass-loss rates shown in figure 5.7. Time-dependent B-numbers have been addressed by Pizzo *et al.* [65] for laminar upward flame spread over small polymethylmethacrylate slabs. In the present work, larger fluctuations are experienced due to turbulence, the mixed nature of the commodity and its more

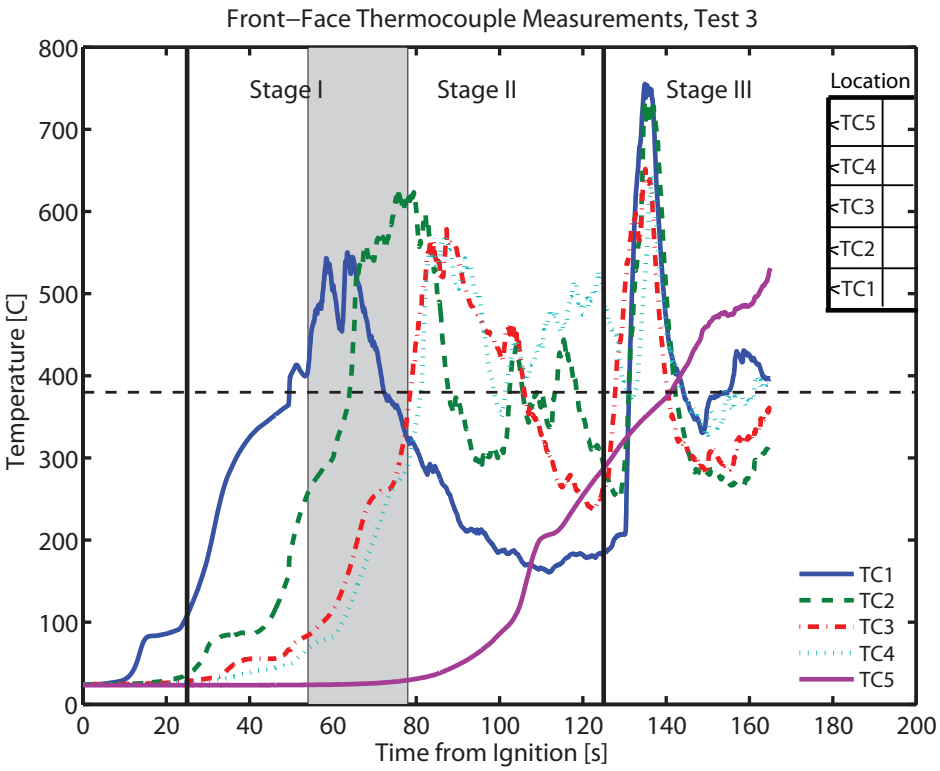

Figure 5.11: Temperatures readings by thermocouples located on the front cardboard face of the commodity in test 3. Temperatures measured determine the advancement of the pyrolysis front over the face of the commodity, with 380 ^{o}C representing the approximate ignition temperature of cardboard. Thermocouple 1 represents the lowest thermocouple location, and 5 the highest. Relative stages of burning are indicated in the figure, as described in the caption of figure 5.6.

complex geometry. In calculating B, the values [61] ρ_g =0.50 kg/m^3, $\alpha_g = 9.8 \times 10^{-5}$ m^2/s and $\nu_g = 6.8 \times 10^{-5}$ m^2/s were used. A mean gas temperature, T_g for use in the calculation was found by averaging the temperature of ambient gas, $T_\infty = 20\,^\circ$C and an approximate flame temperature for cellulosic materials, $T_f = 800\,^\circ$C [60, 23].

The area of burning during stage I was calculated from visual video measurements of the blackened pyrolysis region on the front face. The thermocouple measurements of X_p cannot be used accurately to obtain the area because of the irregular nature of the upward propagation along the imperfect wide surface of the front of the package; the X_p results pertain only to progress along one vertical thermocouple line. A second-order polynomial was fit to the area seen in the video for each test, for

the purpose of calculating $\dot{m}''_f$ in equation 3.7 for stage I. This area increases steadily over time, reaching a maximum value between 54 to 77 seconds (the end of stage I for the respective test). A constant area equal to the total area of the front face of the package was assumed for calculating $\dot{m}''_f$ during stages II and III. During stages II and III there are variations in the exposed burning surface areas of the packing material and of the commodity, but these areas cannot be estimated well, and on the average the total burning surface area in these stages is approximately the total front-face area. Because the initial burning area cannot be determined in stages II and III, uncertainties in B at any given time on the order of a factor of two must be accepted so that the resulting time dependence of B is at best qualitatively indicative of its variations during these later stages. The first 15-20 seconds of all measurements are neglected to remove effects of the ignition source. The resulting time-dependent B-numbers of the four tests are shown in figure 5.12, in which the most reliable time dependencies pertain to stage I.

With these procedures, in stages II and III the calculated variations of B are proportional to the variations of the mass-loss rate seen in figure 5.7. In stage I, however, the increasing area causes the variations in B to exceed those of the mass-loss rate. Comparisons of figures 5.7 and 5.12 shows that the result is that the values of B tend to vary over roughly the same range in all three stages, while the mass-loss rate is clearly much smaller during the early part of stage I than during the later stages. While significant deviations in the time-dependent B-number exist, just as for the mass-loss rate, the subsequent average values of B for each stage vary much less, as can be inferred from figure 5.12.

The time-dependent B-number in stage I reaches a peak towards the end of the stage as the pyrolysis front accelerates upward, consistent with the increasing heat flux from the flame, shown in figure 5.8. The B-number then decreases as the cardboard smolders in stage II, where the pyrolysis front has reached the top of the front face, reducing the amount of excess pyrolyzate and thus the applied heat flux. In some cases this is different from the mass-loss rate in figure 5.7 for stage I, where it is seen that for test 3 the mass-loss rate nearly constantly increases throughout stage I and into stage II, underscoring the general variability of the fire development. Stage III presents even more varied behavior as the ignition of polystyrene cups in each test

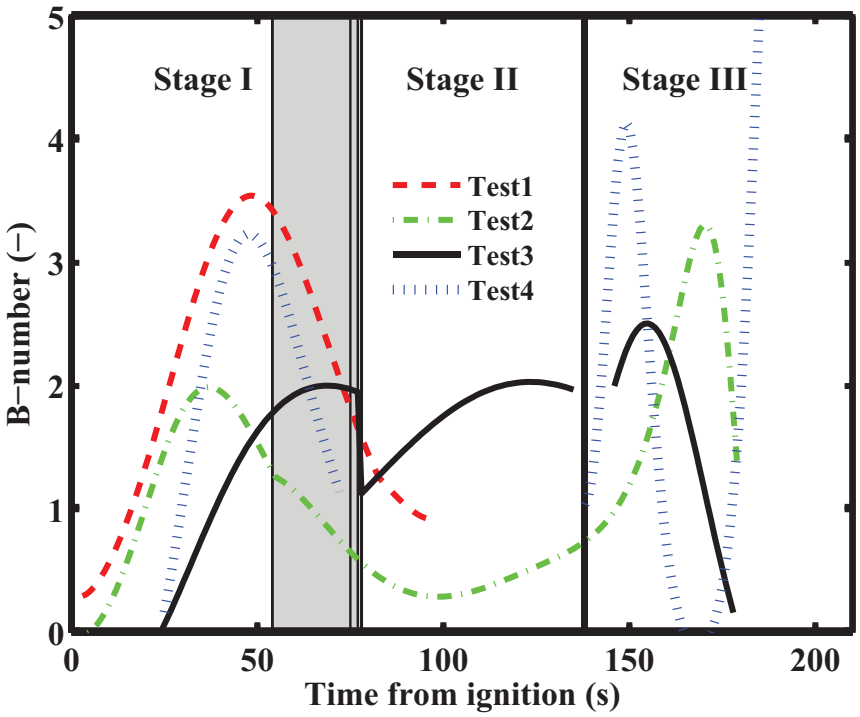

Figure 5.12: Time-dependent B-numbers calculated from the mass-loss rate using equation 3.7. The B-numbers in stage I were calculated using a varying area of burning, while the area was taken constant in stages II and III. Relative stages of burning are indicated in the figure, with vertical lines denoting transitions between stages, as described in the caption of figure 5.6.

Table 5.2: Summary of burning behavior over 3 representative stages for a standard plastic commodity. Note that values are taken as either the indicated maximum or average in the denoted region for each test, and then averaged for all four tests. The average and peak heat fluxes given here were measured by a thin-skin calorimeter 3 cm directly above the test commodity, indicating the heat flux applied to material directly above the commodity.

Summary of Stages			
Stage I	Outer layer of commodity is ignited, producing rapid upward turbulent flame spread over the front face of a commodity. B is independent of polystyrene.	$\boldsymbol{B_{avg}}$ $\dot{m}_{f,avg}$ $X_{f,max}$ $\dot{q}_{f,avg}$	**1.8** 0.83 g/s 0.51 m 1.2 kW/m^2
Stage II	Front layer of corrugated cardboard has burned to top, exposing inner region, which burns and then smolders. Polystyrene does not burn because of its higher ignition temperature.	$\boldsymbol{B_{avg}}$ $\dot{m}_{f,avg}$ $X_{f,max}$ $\dot{q}_{f,avg}$	**1.4** 1.7 g/s 0.48 m 0.38 kW/m^2
Stage III	Polystyrene ignites and a rapid increase in the burning rate occurs.	$\boldsymbol{B_{avg}}$ $\dot{m}_{f,avg}$ $X_{f,max}$ $\dot{q}_{f,avg}$	**1.9** 2.2 g/s 0.65 m 2.4 kW/m^2

occurs in a different pattern, but all show very steep increases in the B-number, just as in the mass-loss rate. Stage III introduces additional uncertainties associated with using a constant area of burning because polystyrene melts and drips, increasing its burning surface area, and it is difficult to accurately determine the processes involved during such a dynamic stage.

Rangwala *et al.* [58] found that an experimentally determined B-number changes over time for a material, and they suggested a method of averaging the B-number over time. Applying their method, a time-averaged B-number for each of three stages was found by time-averaging the mass-loss rate per unit area in each stage, and using this value to calculate an average B-number of the stage. Values of B averaged for each relative stage of burning, reflecting the average burning rate for that stage are given in table 5.2. While a number of other averaging methods can be defined, such as averaging directly over time in figure 5.12, the results are not substantially different.

Average burning rates, $\dot{m}_{f,avg}$ in table 5.2 were determined by averaging mass-loss rates from figure 5.7 for each stage, and taking the average of these values for

all four tests. The mass-loss rates, independent of burning area, increase from stages I-III, growing as the amount of material burning increases, and in stage III they increase as volatile polystyrene becomes the primary material burning.

The B-number for stage I is markedly higher than it would have been if it were calculated using a non-varying area, because the small area of burning during the initial stages of upward spread dramatically increases the value in that calculation, as shown in figure 5.12. The average B-number of each stage of burning is influenced by the mixture of constituent materials involved in combustion during that stage. In stage I, the burning rate is solely dependent on corrugated cardboard combustion, resulting in a B-number of 1.8. Next, during stage II, the plateau in the burning rate due to smoldering of cardboard and gasification of polystyrene results in a decreased B-number of 1.4. The B-number for stage III, 1.9, is similar to that of stage I even though it is influenced by the combustion of polystyrene and cardboard together.

Maximum flame heights observed from the videos were averaged from all four tests to give the values of $X_{f,max}$ for each stage listed in table 5.2. The highest flame heights were observed during stage III, where volatile polystyrene burns at the highest B-number, producing additional excess pyrolyzate lifting the flames higher above the test apparatus. The flame height is noticably shorter in Stage II, on average, because the smoldering of cardboard packing material slows down the burning process. Maximum flame heights observed in test I are greater than those observed in stage II, although earlier in stage I flame heights are smaller.

Peak heat fluxes above the commodity for each stage, averaged from all four tests, achieve their highest values in stages I and III, similar to the flame heights as seen in table 5.2. Heat fluxes above the commodity peak substantially higher in stage III than in stage I, at double the value, and are significantly lower in stage II than in stage I, one third the value. These sharp deviations occur because smaller increases in the burning rate significantly increase the amount of excess pyrolyzate burning above the front face of the commodity, thereby increasing the rate of heat release and thus the heat flux to think-skin calorimeters mounted above the commodity.

Table 5.3: B-numbers of polystyrene, cellulose, and fir wood from previous literature.

Polystyrene	**Cellulose**	**Fir Wood**
0.48 [15]	0.86 [15]	0.58 [15]
1.55 [43]	6.96 [43]	1.75 [43]
1.3 [56]	0.45 [67]	0.35^2 [67]
	0.8 [56]	

5.5 Discussion of Results

The "practical," experimentally measured average values of B given in table 5.2 can be compared to theoretically calculated thermodynamic values for both corrugated cardboard and polystyrene by using equation 3.1 and assuming χ and Q equal zero [57] to obtain an ideal value, assuming there are no losses. For a representative picture of previously-measured B-numbers of polystyrene and cellulosic materials[1] they are displayed in 5.3. Annamalai and Sibulkin [43] report values of heats of combustion and heats of vaporization which when used provide B-numbers of 6.4 and 1.6 for cellulose and polystyrene, respectively. The value for cellulose is, however, not representative of cellulosic materials; it is much too high because the heat of gasification is too low. Tewarson [66] reports a heat of gasification for corrugated cardboard, which results in $B = 1.1$ instead, a more reasonable value. The calculated ideal value of 1.6 for polystyrene is consistent with results obtained from other literature [66, 56]. It may be concluded that the thermodynamic values of B for these two materials do not differ greatly, both lying between 1 and 2, with the values for polystyrene somewhat higher than the other. The values in table 5.2 are also in this range, although a little higher, especially for stage I, since 1.8 solely represents corrugated cardboard. The difference between the thermodynamic and experimental values reflect real-world heat-transfer processes, notably radiative feedback, which can cause Q to be negative in equation 3.1.

The determination of a B-number of mixed materials would be useful for warehouse commodity classification. The B-number of stage III would be expected to be

[1]Cellulose and fir wood are displayed in the table as representative of cardboard because previous measurements of the B-number for cardboard have not been recorded.

some combination of corrugated cardboard and polystyrene, creating a "composite" B-number for the stage. One approach would be to combine the influence of material constituents by weight percent. Combining the B-numbers of corrugated cardboard and polystyrene by weight percent results in a composite B of 1.4[3] if thermodynamic values are used. Another possible combination could be by exposed burning surface area, which results in a combined thermodynamic B-number of 1.2[4]. Both of these approaches produce values of B lower than the experimentally measured value for stage III. The value of B for corrugated cardboard measured experimentally is the same as the theoretical value for polystyrene, within experimental error, so any combination using this value and the thermodynamic value of B for polystyrene would be the same, and thus inconclusive for testing how best to estimate a value for mixed materials. It would be of interest to perform experiments on mixed materials that have very different values of B.

While the "predicted" values of B in table 5.2 lie between 1 and 2, fluctuation in values between 0 and 5 are seen to occur in figure 5.12. Only by averaging over these large fluctuations can values be obtained that are potentially useful for commodity classification. The relatively small range of the averaged values suggest the possibility of selecting values representative of mixed materials that can be helpful in hazard assessments.

It is to be noted that this test setup presents many obstacles to determine an accurate B-number. The surface is wide which allows horizontal flame spread as well as buoyancy-induced vertical spread. Deviations in the front face of corrugated cardboard as well as varying influences of materials within the commodity during upward flame spread present many difficulties in this test setup. Careful observations of the test results must be conducted in order to reject regions of non-upward flame spread during this test, as well as other deviations such as chunks of material falling off the test stand. Despite the difficulties of this test setup, it has yielded relevant information on general fire behavior, ranges of values of B to be expected and on

[3]Thermodynamic B-numbers for corrugated cardboard, $B = 1.1$ and polystyrene $B = 1.6$ were used. Product mass percent was calculated from total weight of Group A commodity: 2.38 kg corrugated cardboard and 3.88 kg polystyrene.

[4]Exposed surface area was defined as the area exposed in the first layer of cells, not including the front face which burned away. The area of exposed polystyrene was 0.296 m^2, and corrugated cardboard 0.944 m^2.

the incremental stages of burning which occur within the commodity. More accurate smaller-scale tests should be conducted as research continues.

Initial fire spread in warehouses, during the first 1–2 minutes of burning is typically restricted to spread over vertical corrugated cardboard surfaces. Prediction of fire spread during this initial stage of burning is important to predict sprinkler activation times, and may provide a link between fire behavior and a commodity ranking scale. Flame heights observed during the first stage of burning for a Group A plastic commodity tend to be restricted to a small range of fluctuations unlike later stages, suggesting a common behavior occurs for flame spread up vertical cardboard surfaces. A variety of flame-spread theories have been developed that may be used to predict flame heights, a summary of which was presented in section 2.6. Flame and pyrolysis heights observed in figure 5.9 suggest either a power-law or exponential increase in flame height over time. It will be of particular interest to compare theories that produce flame height predictions of this type. Two potential models are suggested here, one based upon a boundary-layer model by Annamalai and Sibulkin [43] and another flame-spread theory by Saito *et al* [45], is an extension of the model of Markstein and De Ris [68]. These two formulations will produce different dependencies of flame and pyrolysis heights on time to predicted flame spread behavior in the future, and analysis of the results may yield accurate prediction methods. Both also require readily-available input parameters, such as the B-number, TRP, etc.

5.6 Acknowledgement

This chapter has partially included the following publication: "Controlling Parameters Involved in the Burning of Standard Storage Commodities: A Fundamental Approach Towards Fire Hazard Classification," at the *6th U.S. National Combustion Meeting*, (Ann Arbor, Michigan), 2009. M. J. Gollner, T. Hetrick, A. S. Rangwala, J. Perricone, and F. A. Williams. The thesis author is the primary researcher in this publication.

Chapter 6

Conclusion

6.1 Summary

This work has laid a framework to experimentally measure the B-numbers of a mixed commodity for use as a fire-hazard ranking criterion in warehouses. Small-scale tests performed on a Group A plastic commodity were used to calculate time-dependent as well as time-averaged values of the B-number for three representative stages of burning. This commodity consisted of 125 polystyrene cups in segregated corrugated cardboard compartments within a corrugated cardboard container. Because a Group A plastic commodity is mixed, consisting of plastic and corrugated cardboard products, three representative stages of burning were outlined for the combustion of the commodity, each with unique burning behavior The influence of constituent materials varied depending on the stage of burning.

The significant hazards known to occur in warehouses due to upward flame spread have been addressed here, quantifying aspects of high heat fluxes, rapidly increasing flame heights, and large B-numbers immediately after ignition of the commodity and during the combustion of the plastic product, with a decrease in the burning rate between the two regions. The experimental B-numbers reported here contain inaccuracies, but they take into account more physical processes than analytically determined thermodynamic B-numbers.

6.2 Broader Impact

A history of warehouse fires and resulting damage was presented in chapter 1. Preventing these high-loss situations requires knowledge of the initial behavior of fire in rack-storage situations as well as the influence of the storage configuration and inner products on later stages of the fire. The research conducted in this project is the first to use the B-number as a single criterion to calculate the flame height during the initial burning region, approximately 1–1.5 minutes in most warehouse fires. Thus far a relation to later stages of burning in the warehouse has not been addressed by this research, but a link between small-scale testing and large-scale behavior using the same test methods in a related study has been established. With this, the B-number seems to be a likely candidate for use as a universal fire-hazard classification criterion in warehouses. Because upward spread is dominant in these fires, other influences can be approximately neglected for the use of classifying hazards of commodities.

6.3 Recommendations for Future Work

Predicting fire behavior is an important task associated with commodity classification, and future work to develop accurate predictions of flame and pyrolysis heights will aid the eventual goal of developing a fundamental method to classify commodities. Future work should compare flame and pyrolysis heights measured in this study with previous studies. Different flame height prediction methods should be applied, with particular attention paid to the input parameters required to generate predictions. A wide variety of parameters are currently used throughout a variety of ranking schemes and flame spread models (CHF, FPI, TRP, r, etc.), and it would be useful to study the relationships between these parameters and the B-number.

With sufficient additional research, B-numbers may be used in the future in approaches to classifying the flammability of a given warehouse commodity and designing a suppression system to protect the commodity. Experimentally obtaining the B-number in a repeatable manner for a mixed commodity is of prime importance, and studies using devices such as a cone calorimeter to calculate the B-number on smaller-scale cells and individual materials should be continued [17]. The influence

of material and volume density of materials within a commodity should be closely studied to determine a relationship between these parameters and a composite B-number that could be used to calculate the B-number of a grouped commodity. A critical B-number used as an extinction criterion may also be determined to lay a groundwork for a warehouse fire model. These combined ignition, fire spread, and extinction/suppression characteristics may be used by fire protection engineers to determine a general prediction of warehouse fire behavior in the future, aiding safer design of these storage occupancies. The use of a B-number and similar nondimensional parameters in computational fluid dynamics (CFD) models of fire-driven fluid flow in the future present a huge potential to simplify the parameters necessary to model fires, and should also be investigated in the future.

Appendix A

Additional Heat Flux Data

Measurements of heat flux from the combusting plume above the burning commodity to a vertically-oriented surface above are provided here to supplement the material given in chapter 5, Experimental Results. The heat flux displayed in figures A.2–A.23 represents a combined radiative and convective heat flux from the flame to a surface of a higher elevation. Ten thin-skin calorimeters were instrumented above the 0.5 meter high commodity, measuring the variation of heat flux at increasing heights above the commodity and between the centerline and sides of the commodity. This spatial information provides a picture of the heat flux that potentially would be provided to commodities of higher elevations stored in racks, and may be useful in the future analyses to quantify upward flame spread rates.

The heat flux, much like the burning rate varies over the three stages of burning for a Group A plastic commodity. Figures A.2–A.11 show the variation of heat flux for each of the three stages of burning for all ten thin-skin calorimeters. Although the relative magnitude of heat flux decreases at increasing heights, the behavior of increasing heat flux rates during stage I, decreased heat flux rates rates during stage II, and peak heat fluxes during stage III are observed at all elevations. The increasing heat flux observed during the first stage occurs because of increasing excess pyrolyzate with increased pyrolysis heights, and thus a higher and larger combusting plume. In the second stage, corrugated cardboard smoulders, dramatically reducing the height of the combusting plume and observable flame heights, thus the observed heat flux significantly decreases during this burning plateau. During the third stage,

polystyrene ignites and the combustion of the dripping, sooty polystyrene increases the observed heat flux above the commodity.

Figures A.12–A.15 show that the magnitude of heat fluxes over time is much greater at lower elevations closer to the top surface of the burning commodity, and drastically decays as elevation increases. A comparison of heat fluxes across the bottom width of the thin-skin calorimeter setup is shown in figures A.16–A.19 and across the top width of the think-skin setup in figures A.20–A.20. Typically, the heat fluxes observed along the centerline are greater than those 16 cm to the sides of the centerline. This value is not usually significantly greater than the measurements taken to the sides of the centerline, and in some cases is the same or actually lower than heat flux measurements to the side (e.g. figure A.21). Heat flux measurements along the centerline are generally expected to be slightly greater than those on the side because of additional heat losses at the sides of the vertical combusting plume. In cases where this is not the case the cause is most likely uneven burning of the commodity below. The wide base of the sample does not always burn evenly, and for some short time periods greater pyrolysis heights and burning rates may be observed on one side or the other below the thin-skin calorimeters.

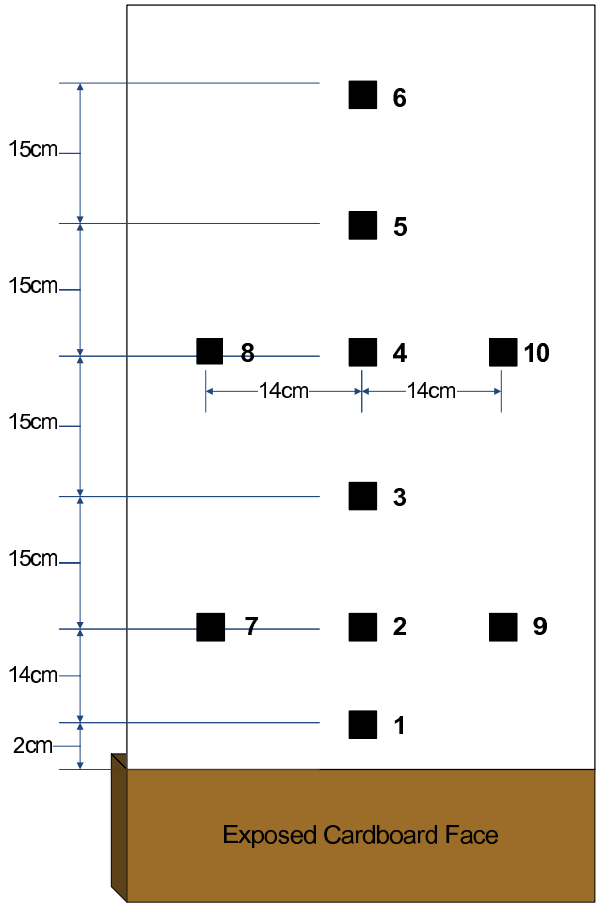

Figure A.1: Location of thin-skin calorimeters 1-10 used to measure heat flux above the tested commodity.

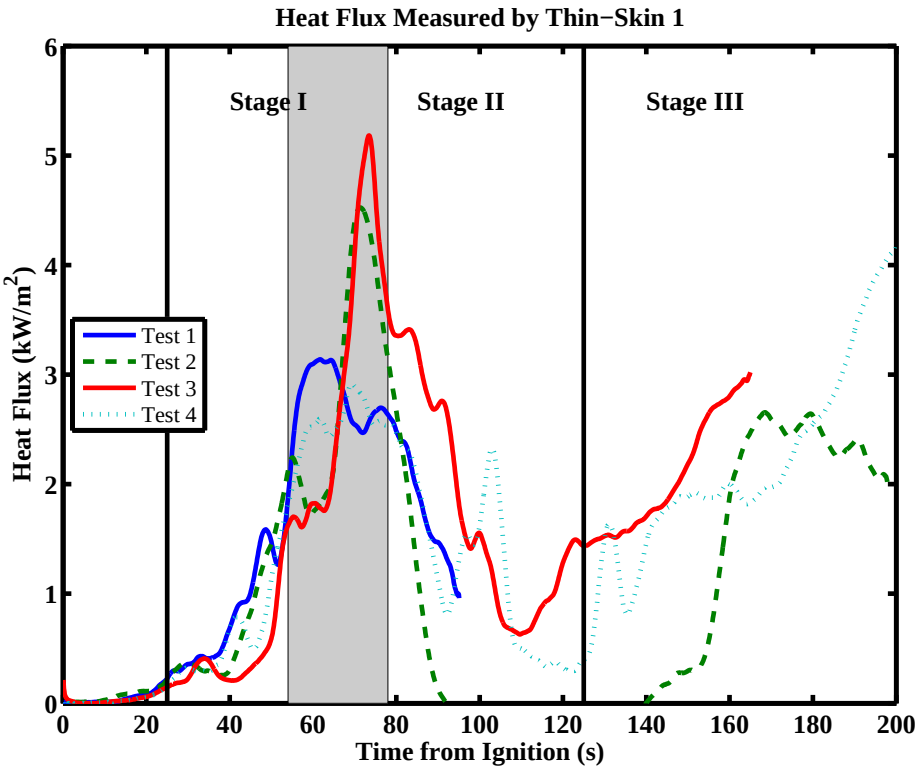

Figure A.2: The heat flux measured by a vertically oriented thin-skin calorimeter approximately 2 cm directly above the top center of the face of the tested commodity, representing a combined convective plus radiative heat flux exerted on commodities at higher elevations. Relative stages of burning are indicated in the figure, as described in the caption of figure 5.6. Results for all four tests are displayed.

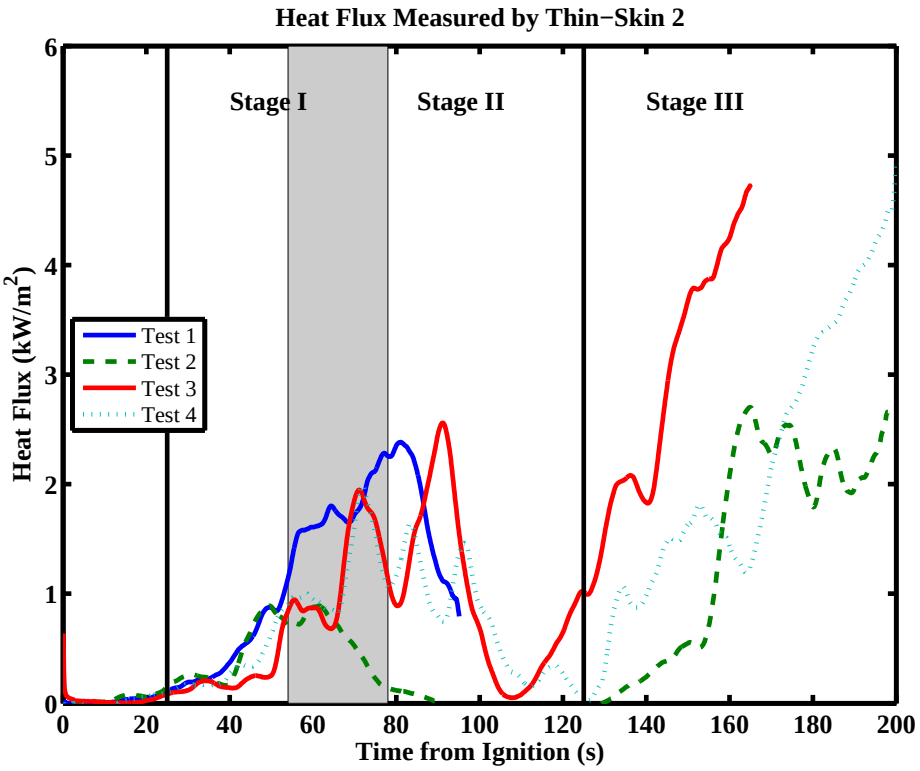

Figure A.3: The heat flux measured by a vertically oriented thin-skin calorimeter approximately 16 cm directly above the top center of the face of the tested commodity, representing a combined convective plus radiative heat flux exerted on commodities at higher elevations. Relative stages of burning are indicated in the figure, as described in the caption of figure 5.6. Results for all four tests are displayed.

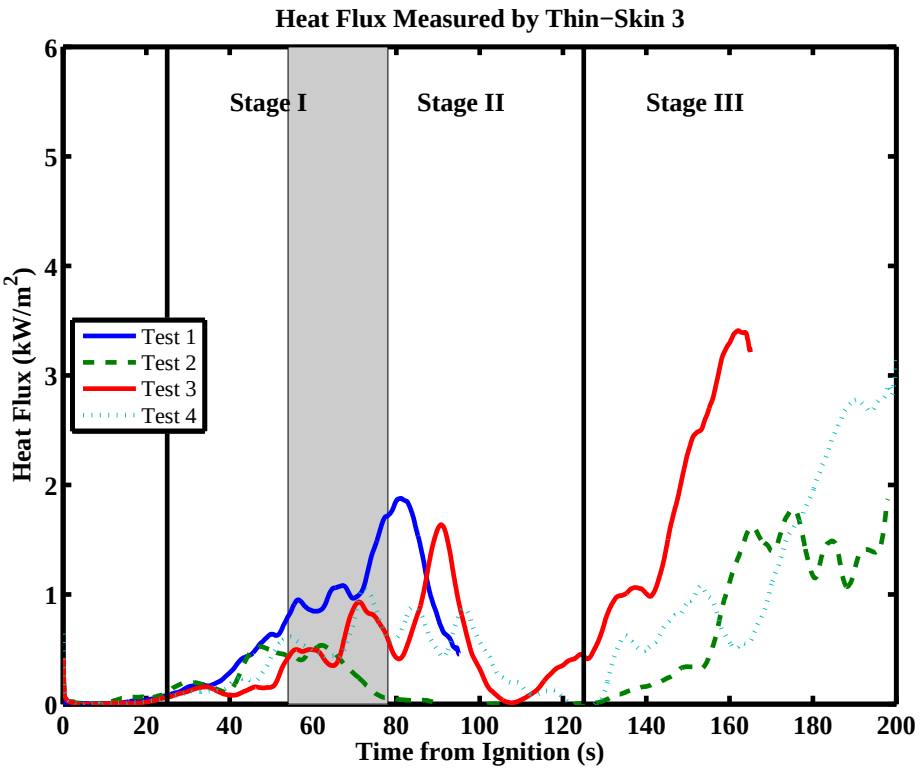

Figure A.4: The heat flux measured by a vertically oriented thin-skin calorimeter approximately 31 cm directly above the top center of the face of the tested commodity, representing a combined convective plus radiative heat flux exerted on commodities at higher elevations. Relative stages of burning are indicated in the figure, as described in the caption of figure 5.6. Results for all four tests are displayed.

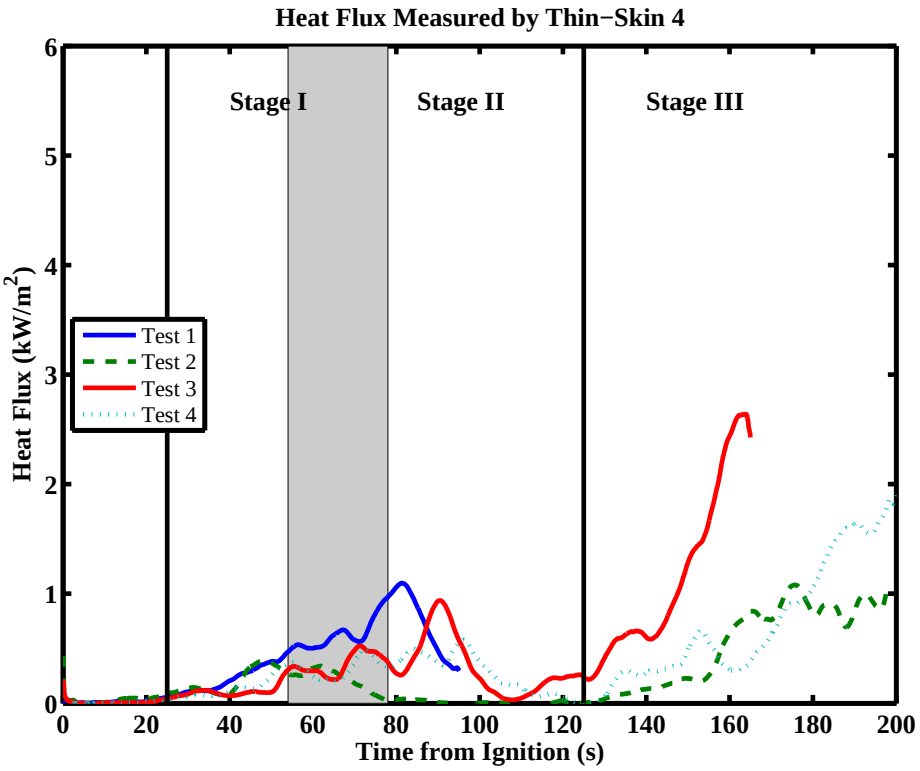

Figure A.5: The heat flux measured by a vertically oriented thin-skin calorimeter approximately 46 cm directly above the top center of the face of the tested commodity, representing a combined convective plus radiative heat flux exerted on commodities at higher elevations. Relative stages of burning are indicated in the figure, as described in the caption of figure 5.6. Results for all four tests are displayed.

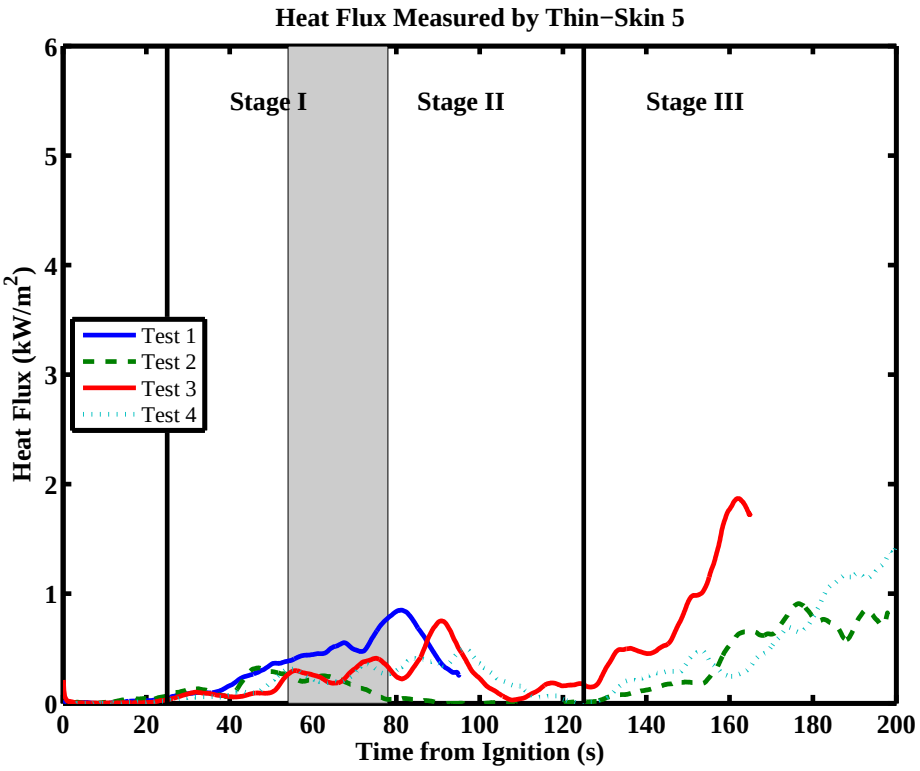

Figure A.6: The heat flux measured by a vertically oriented thin-skin calorimeter approximately 61 cm directly above the top center of the face of the tested commodity, representing a combined convective plus radiative heat flux exerted on commodities at higher elevations. Relative stages of burning are indicated in the figure, as described in the caption of figure 5.6. Results for all four tests are displayed.

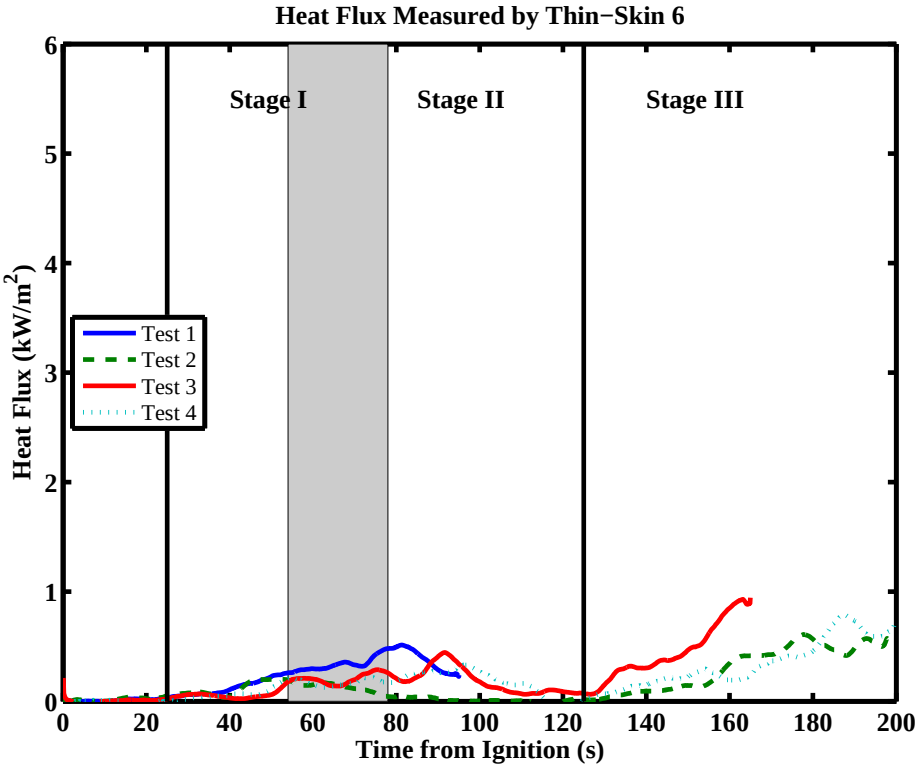

Figure A.7: The heat flux measured by a vertically oriented thin-skin calorimeter approximately 76 cm directly above the top center of the face of the tested commodity, representing a combined convective plus radiative heat flux exerted on commodities at higher elevations. Relative stages of burning are indicated in the figure, as described in the caption of figure 5.6. Results for all four tests are displayed.

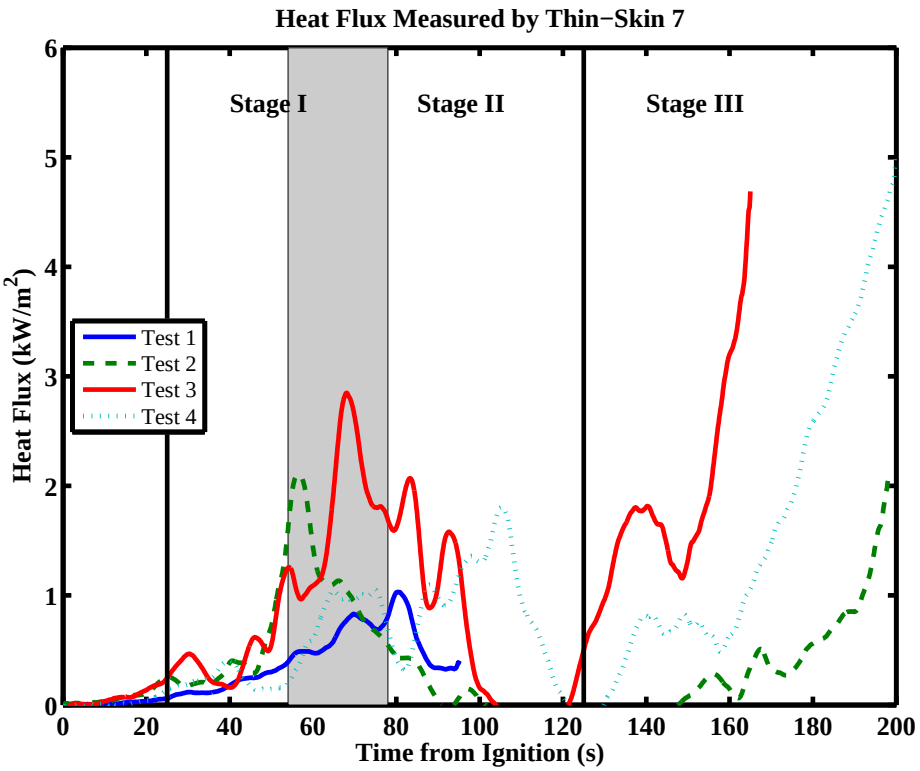

Figure A.8: The heat flux measured by a vertically oriented thin-skin calorimeter approximately 16 cm above and 14 cm to the left of the top center of the face of the tested commodity, representing a combined convective plus radiative heat flux exerted on commodities at higher elevations. Relative stages of burning are indicated in the figure, as described in the caption of figure 5.6. Results for all four tests are displayed.

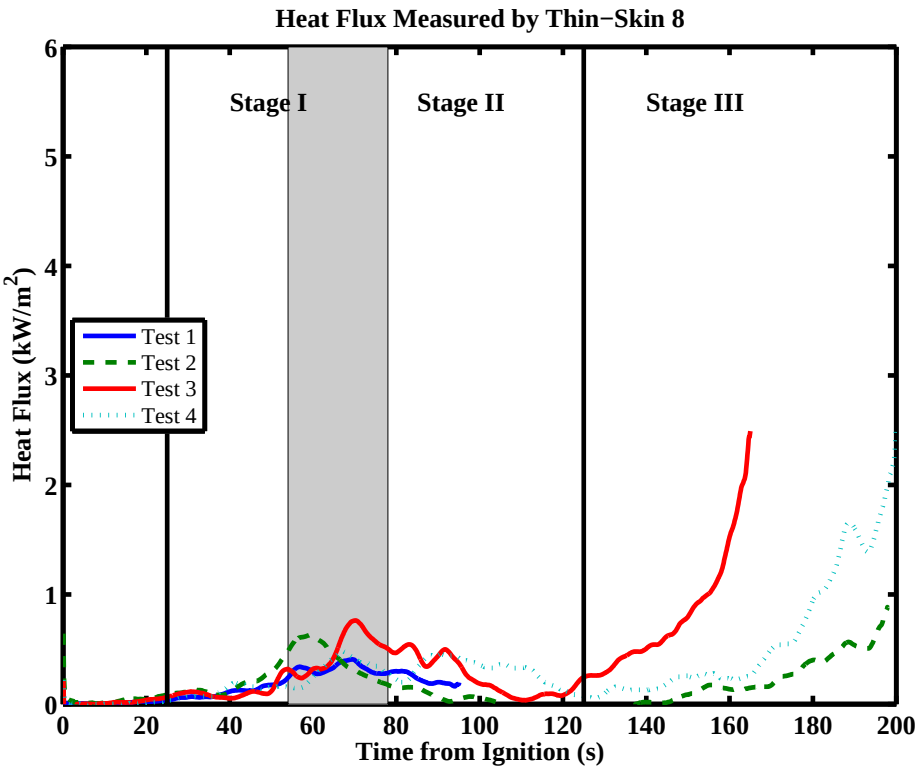

Figure A.9: The heat flux measured by a vertically oriented thin-skin calorimeter approximately 46 cm above and 14 cm to the left of the top center of the face of the tested commodity, representing a combined convective plus radiative heat flux exerted on commodities at higher elevations. Relative stages of burning are indicated in the figure, as described in the caption of figure 5.6.

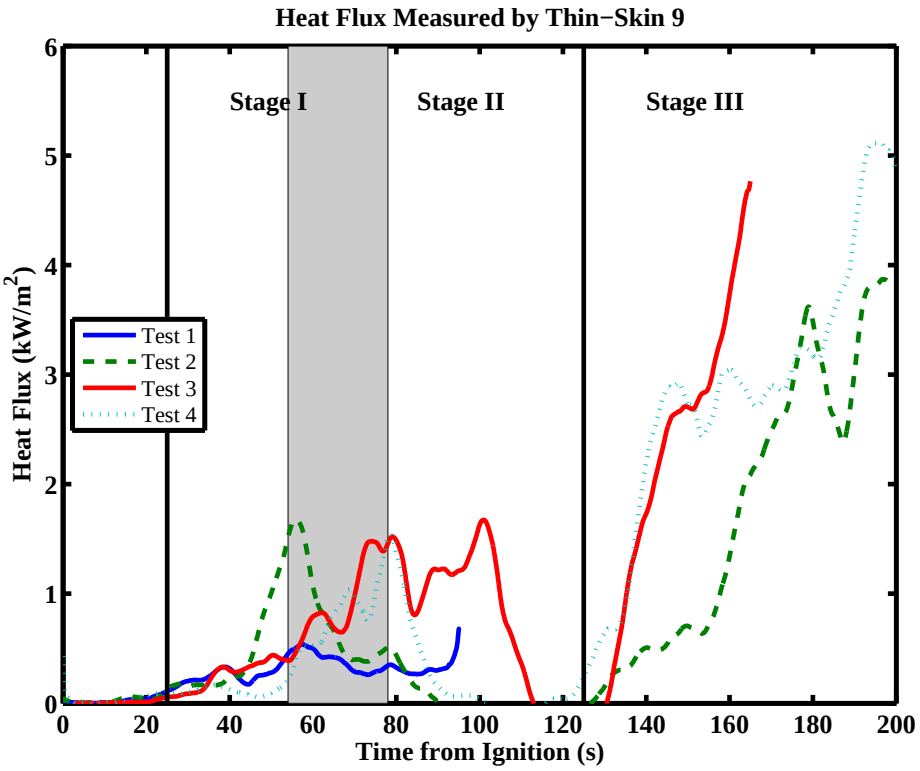

Figure A.10: The heat flux measured by a vertically oriented thin-skin calorimeter approximately 16 cm above and 14 cm to the right of the top center of the face of the tested commodity, representing a combined convective plus radiative heat flux exerted on commodities at higher elevations. Relative stages of burning are indicated in the figure, as described in the caption of figure 5.6.

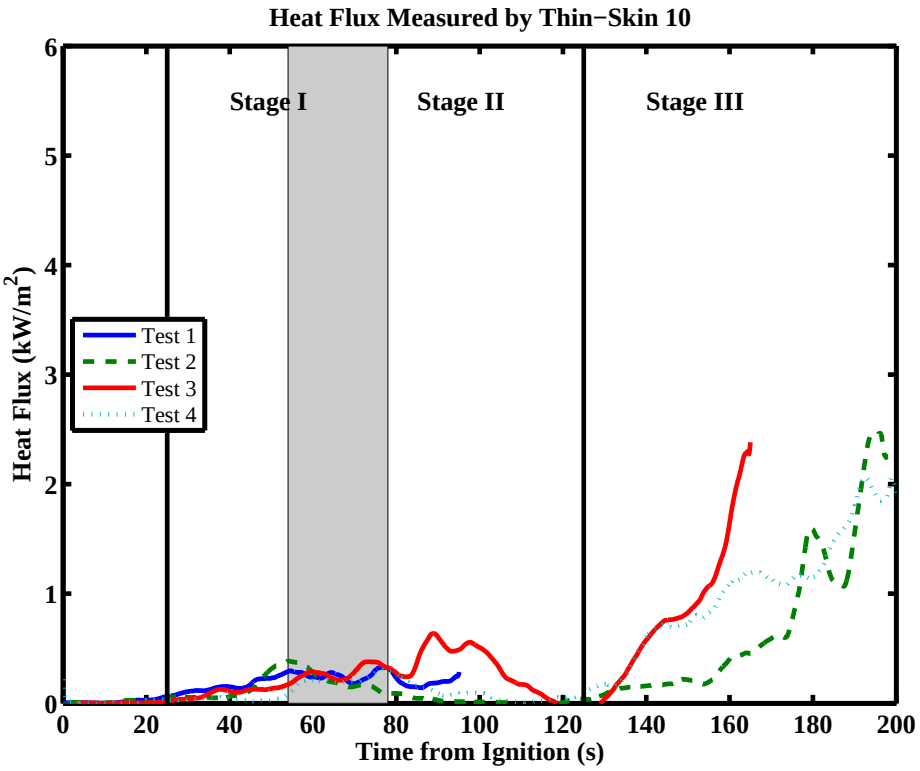

Figure A.11: The heat flux measured by a vertically oriented thin-skin calorimeter approximately 46 cm above and 14 cm to the right of the top center of the face of the tested commodity, representing a combined convective plus radiative heat flux exerted on commodities at higher elevations. Relative stages of burning are indicated in the figure, as described in the caption of figure 5.6.

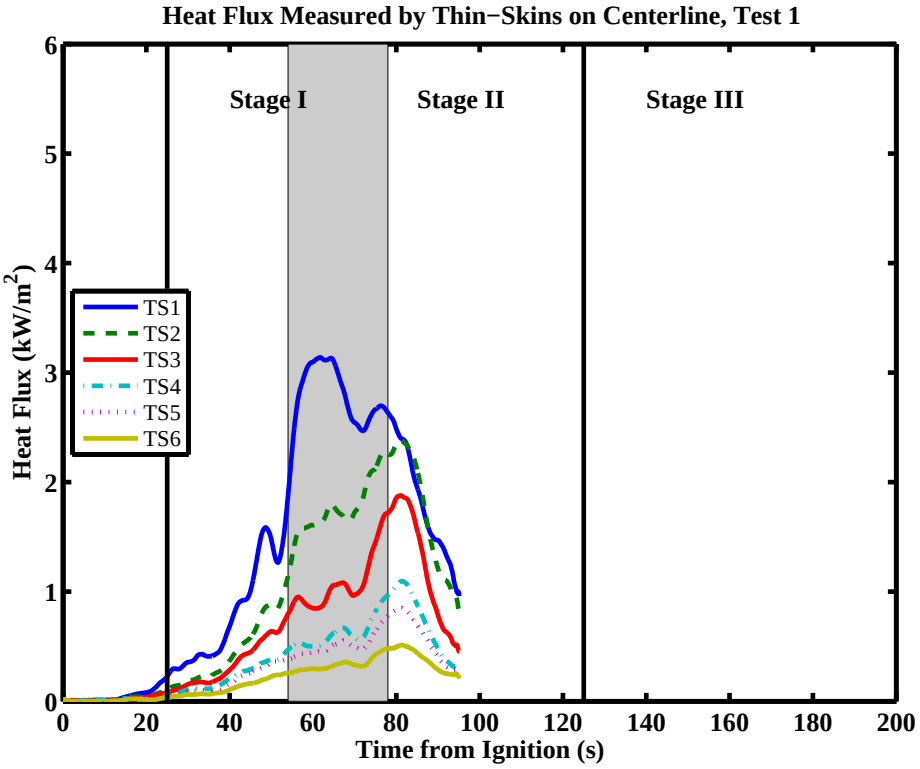

Figure A.12: The heat flux measured by 5 vertically oriented thin-skin calorimeters approximately 16 cm directly above the top center of the face of the tested commodity representing a combined convective plus radiative heat flux exerted on commodities at higher elevations in test 1. Relative stages of burning are indicated in the figure, as described in the caption of figure 5.6.

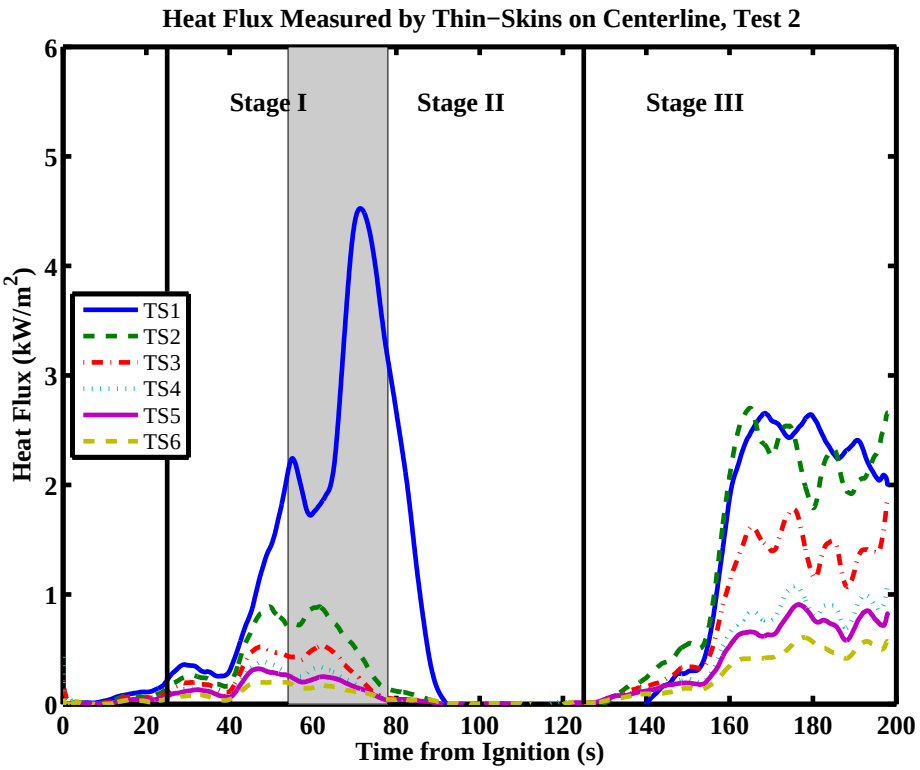

Figure A.13: The heat flux measured by 5 vertically oriented thin-skin calorimeters approximately 16 cm directly above the top center of the face of the tested commodity representing a combined convective plus radiative heat flux exerted on commodities at higher elevations in test 2. Relative stages of burning are indicated in the figure, as described in the caption of figure 5.6.

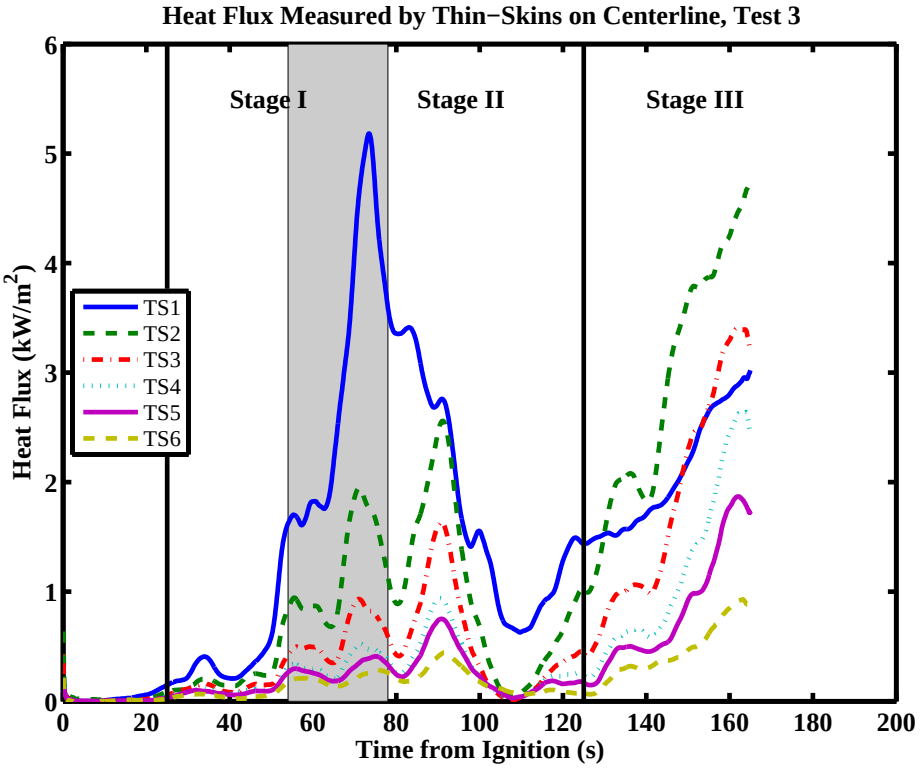

Figure A.14: The heat flux measured by 5 vertically oriented thin-skin calorimeters approximately 16 cm directly above the top center of the face of the tested commodity representing a combined convective plus radiative heat flux exerted on commodities at higher elevations in test 3. Relative stages of burning are indicated in the figure, as described in the caption of figure 5.6.

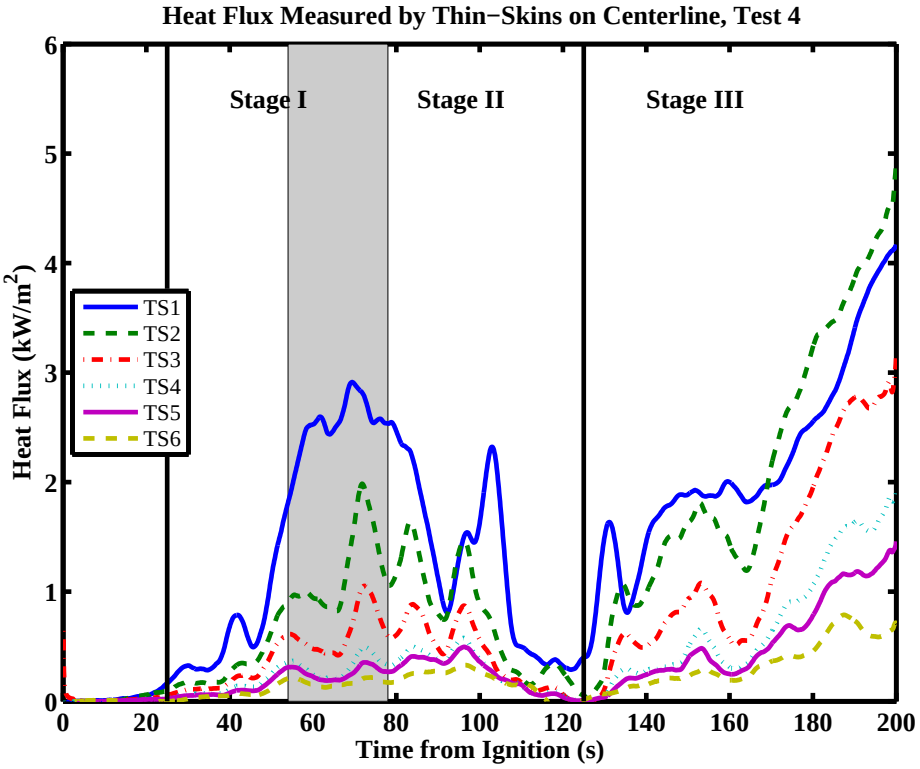

Figure A.15: The heat flux measured by 5 vertically oriented thin-skin calorimeters approximately 16 cm directly above the top center of the face of the tested commodity representing a combined convective plus radiative heat flux exerted on commodities at higher elevations in test 4. Relative stages of burning are indicated in the figure, as described in the caption of figure 5.6.

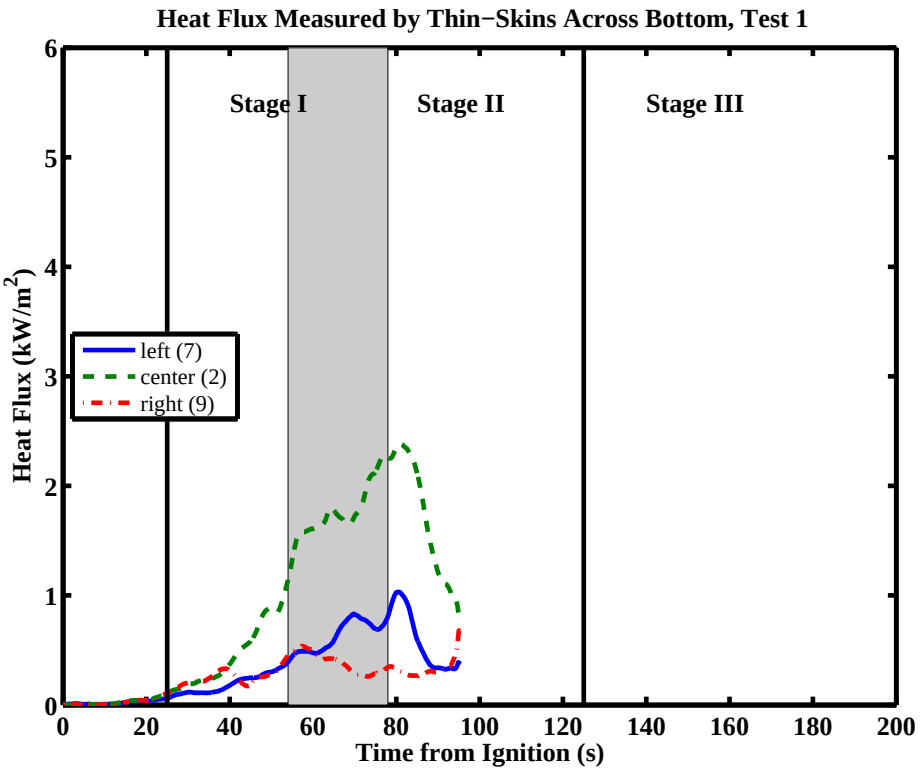

Figure A.16: The heat flux measured by 3 vertically oriented thin-skin calorimeters approximately 16 cm directly above and at center, 14 cm to the left and 14 cm to the right of the top of the face of the tested commodity representing a combined convective plus radiative heat flux exerted on commodities at higher elevations in test 1. Relative stages of burning are indicated in the figure, as described in the caption of figure 5.6.

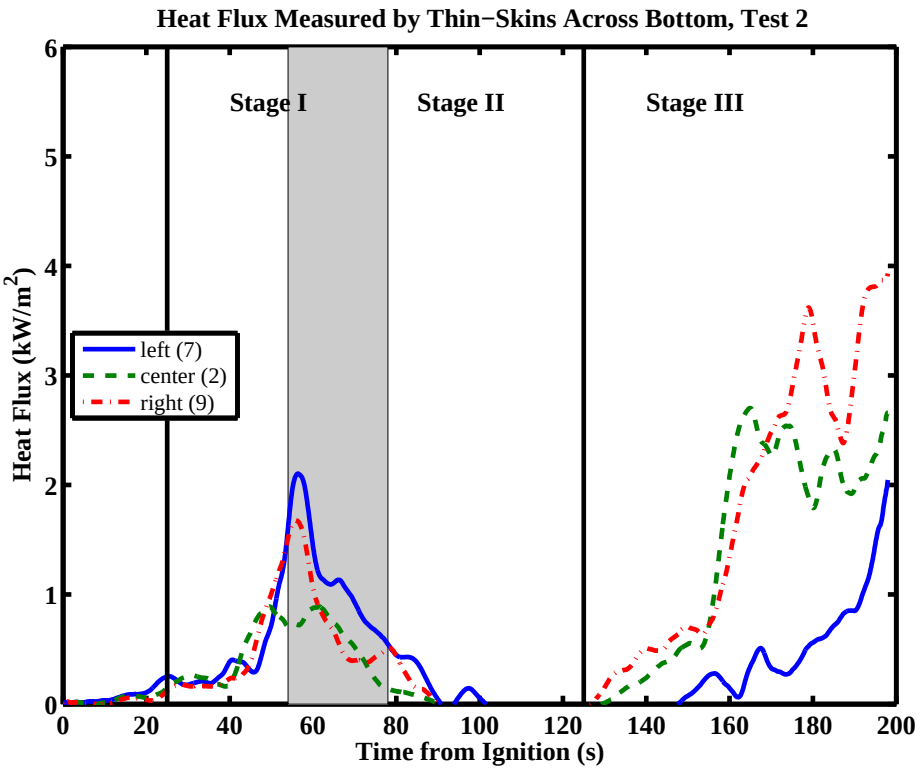

Figure A.17: The heat flux measured by 3 vertically oriented thin-skin calorimeters approximately 16 cm directly above and at center, 14 cm to the left and 14 cm to the right of the top of the face of the tested commodity representing a combined convective plus radiative heat flux exerted on commodities at higher elevations in test 2. Relative stages of burning are indicated in the figure, as described in the caption of figure 5.6.

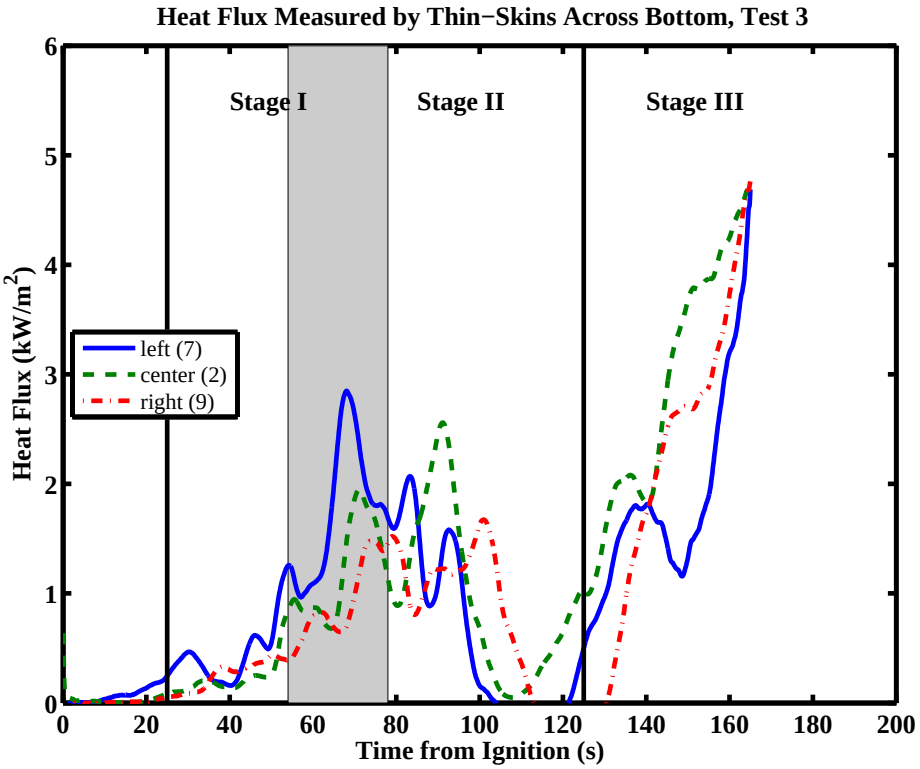

Figure A.18: The heat flux measured by 3 vertically oriented thin-skin calorimeters approximately 16 cm directly above and at center, 14 cm to the left and 14 cm to the right of the top of the face of the tested commodity representing a combined convective plus radiative heat flux exerted on commodities at higher elevations in test 3. Relative stages of burning are indicated in the figure, as described in the caption of figure 5.6.

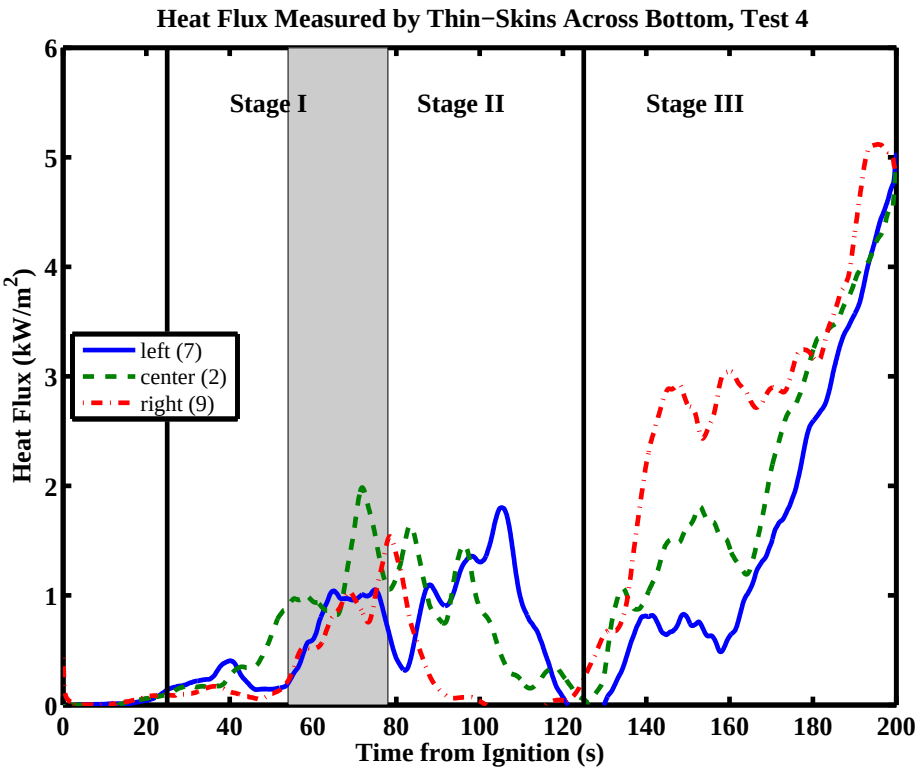

Figure A.19: The heat flux measured by 3 vertically oriented thin-skin calorimeters approximately 16 cm directly above and at center, 14 cm to the left and 14 cm to the right of the top of the face of the tested commodity representing a combined convective plus radiative heat flux exerted on commodities at higher elevations in test 4. Relative stages of burning are indicated in the figure, as described in the caption of figure 5.6.

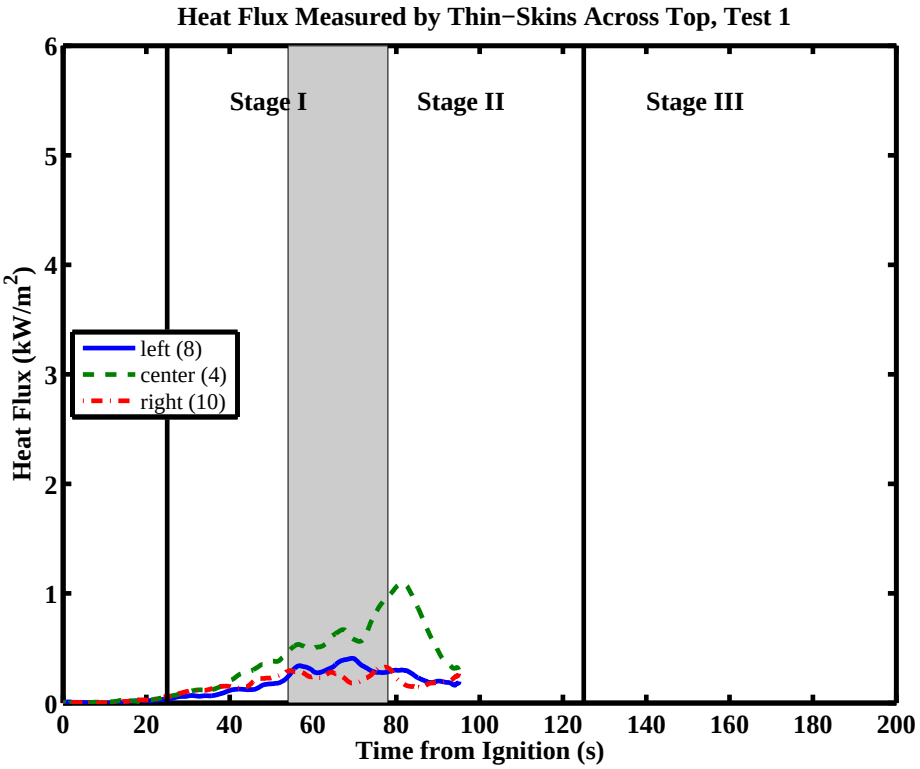

Figure A.20: The heat flux measured by 3 vertically oriented thin-skin calorimeters approximately 46 cm directly above and at center, 14 cm to the left and 14 cm to the right of the top of the face of the tested commodity representing a combined convective plus radiative heat flux exerted on commodities at higher elevations in test 1. Relative stages of burning are indicated in the figure, as described in the caption of figure 5.6.

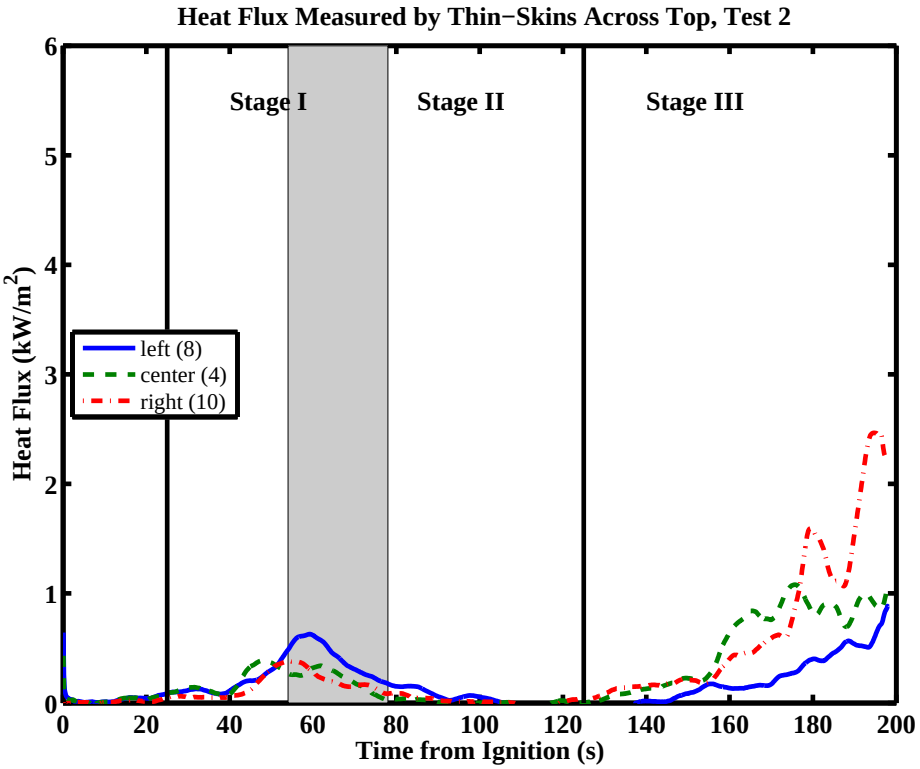

Figure A.21: The heat flux measured by 3 vertically oriented thin-skin calorimeters approximately 46 cm directly above and at center, 14 cm to the left and 14 cm to the right of the top of the face of the tested commodity representing a combined convective plus radiative heat flux exerted on commodities at higher elevations in test 2. Relative stages of burning are indicated in the figure, as described in the caption of figure 5.6.

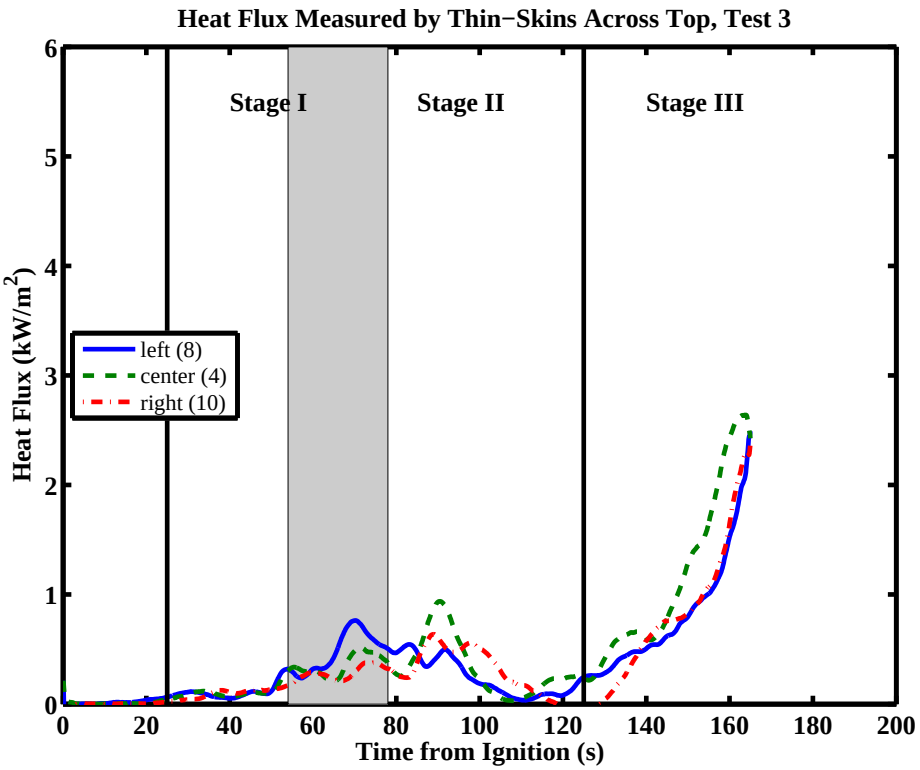

Figure A.22: The heat flux measured by 3 vertically oriented thin-skin calorimeters approximately 46 cm directly above and at center, 14 cm to the left and 14 cm to the right of the top of the face of the tested commodity representing a combined convective plus radiative heat flux exerted on commodities at higher elevations in test 3. Relative stages of burning are indicated in the figure, as described in the caption of figure 5.6.

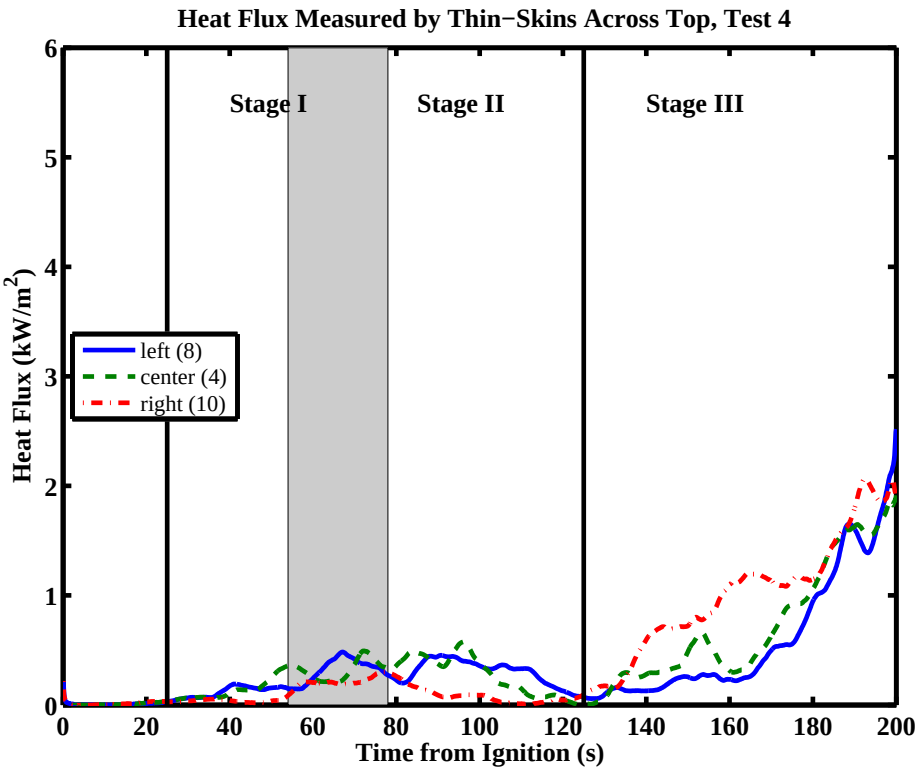

Figure A.23: The heat flux measured by 3 vertically oriented thin-skin calorimeters approximately 46 cm directly above and at center, 14 cm to the left and 14 cm to the right of the top of the face of the tested commodity representing a combined convective plus radiative heat flux exerted on commodities at higher elevations in test 4. Relative stages of burning are indicated in the figure, as described in the caption of figure 5.6.

Appendix B

Additional Thermocouple Data

Thermocouples were installed on the face of and within the tested commodity along its centerline, shown in figure 5.10. Thermocouples in figure 5.10 labeled 'A' were located along the front face of the commodity and were embedded within the corrugated cardboard to measure the effective location of the pyrolysis front. Figures B.1–B.3 show the temperature measurements along the front face used to track the progression of the pyrolysis front for the three tests in which this information is available. At approximately 100°C a small plateau in temperatures indicates vaporization of water moisture that was present in the corrugated cardboard. 380°C is marked by a horizontal dotted line in figures B.1–B.3 and indicates the approximate ignition temperature of cardboard used to determine the pyrolysis location. Therefore, where thermocouple measurements intersect this dotted line the pyrolysis front was assumed to have reached that point. In some cases thermocouple measurements provided inconsistent data, such as TC 5 in B.2, and those measurements were not used in calculating the location of the pyrolysis front. Most likely these errors, typically from the top thermocouple, were caused by changes in the sample geometry during burning that disturbed the mounted thermocouple.

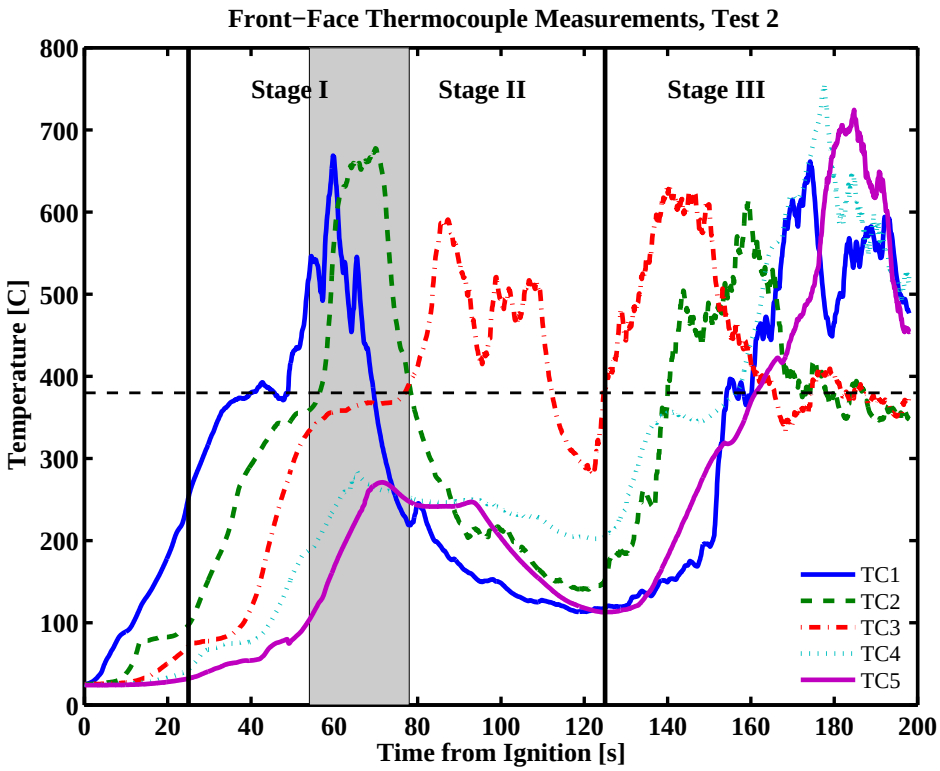

Figure B.1: Temperatures readings by thermocouples located on the front cardboard face of the commodity in test 2. Temperatures measured determine the advancement of the pyrolysis front over the face of the commodity, with 380 ^{o}C representing the approximate ignition temperature of cardboard. Thermocouple 1 represents the lowest thermocouple location, and 5 the highest. Relative stages of burning are indicated in the figure, as described in the caption of figure 5.6.

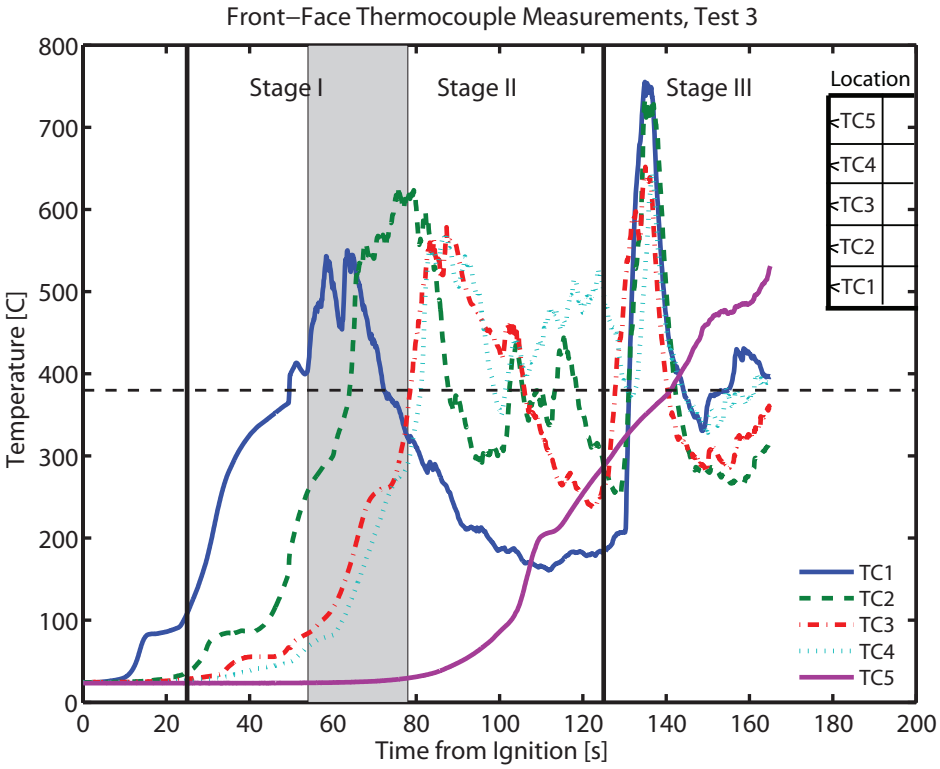

Figure B.2: Temperatures readings by thermocouples located on the front cardboard face of the commodity in test 3. Temperatures measured determine the advancement of the pyrolysis front over the face of the commodity, with 380 ^{o}C representing the approximate ignition temperature of cardboard. Thermocouple 1 represents the lowest thermocouple location, and 5 the highest. Relative stages of burning are indicated in the figure, as described in the caption of figure 5.6.

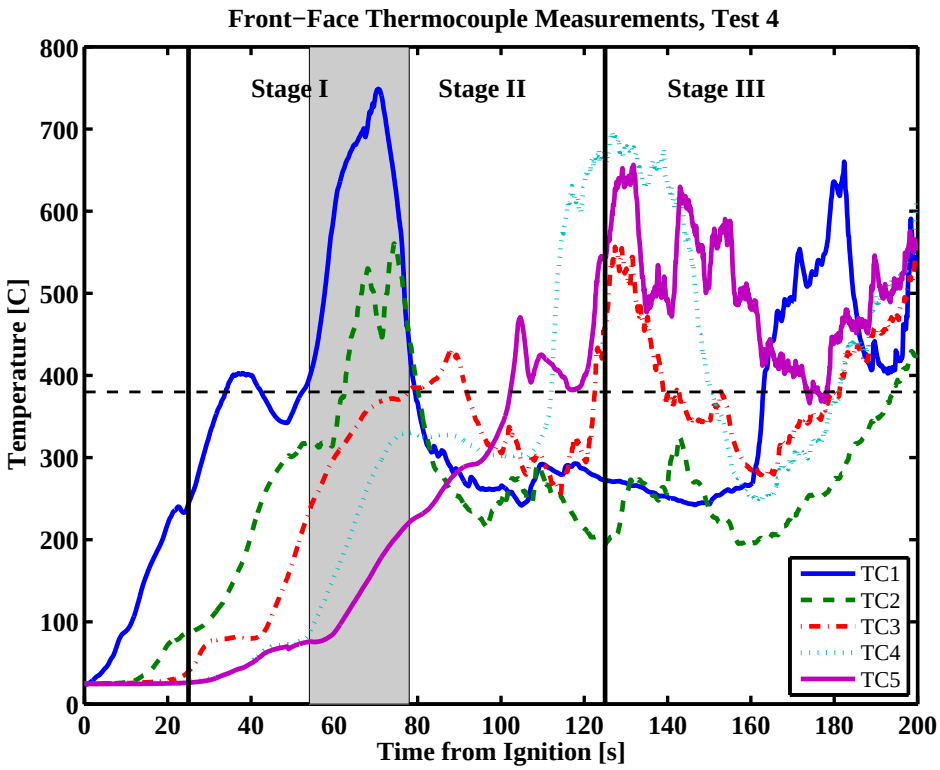

Figure B.3: Temperatures readings by thermocouples located on the front cardboard face of the commodity in test 4. Temperatures measured determine the advancement of the pyrolysis front over the face of the commodity, with 380 ^{o}C representing the approximate ignition temperature of cardboard. Thermocouple 1 represents the lowest thermocouple location, and 5 the highest. Relative stages of burning are indicated in the figure, as described in the caption of figure 5.6.

Thermocouples were also mounted inside a vertical column of cells along the centerline, shown in figure 5.10 as thermocouple 'B'. Because the thermocouple was suspended in the center of the polystyrene cups and not in contact with the burning material, the temperatures measured do not actually indicate the actual burning temperature of polystyrene. Video footage along with temperatures within the cups shown in figures B.7–B.9 was used to determine transition times to stage III of burning (i.e. ignition of the polystyrene cups). It was difficult to use these temperatures alone to determine ignition times of the polystyrene cups due to the staggered ignition of the cups, but this data was useful to determine stage transitions when used alongside associated video footage.

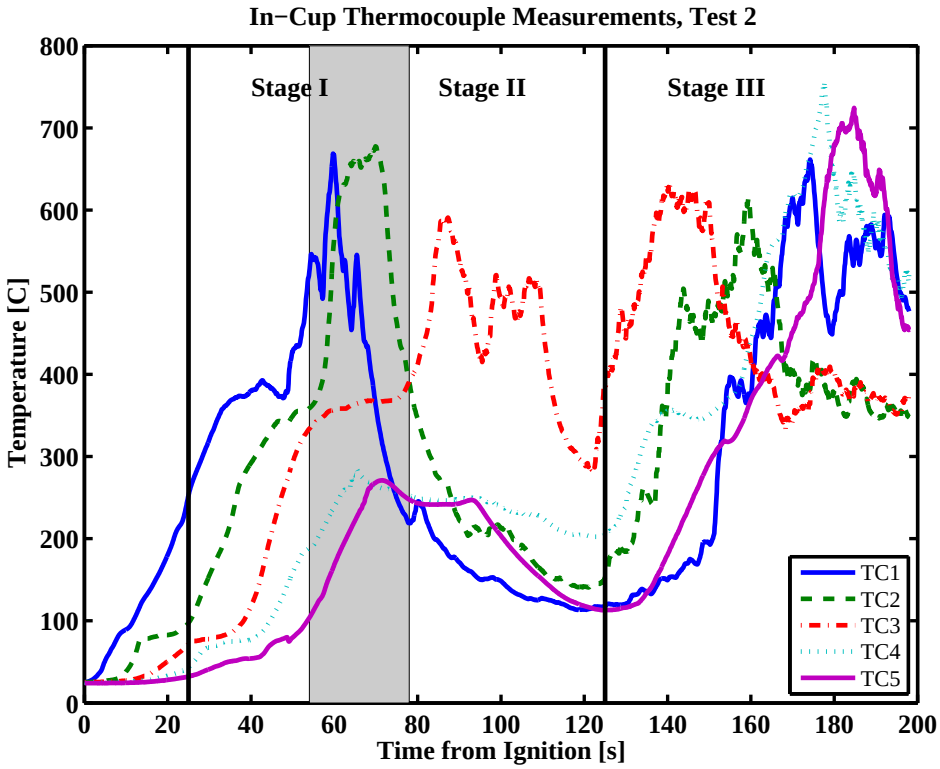

Figure B.4: Temperatures readings by thermocouples located inside the polystyrene cup in test 2. Temperatures measured determine the time the polystyrene cup ignites. The temperature does not directly relate to an ignition temperature of polystyrene. Thermocouple 1 represents the lowest thermocouple location, and 5 the highest. Relative stages of burning are indicated in the figure, as described in the caption of figure 5.6.

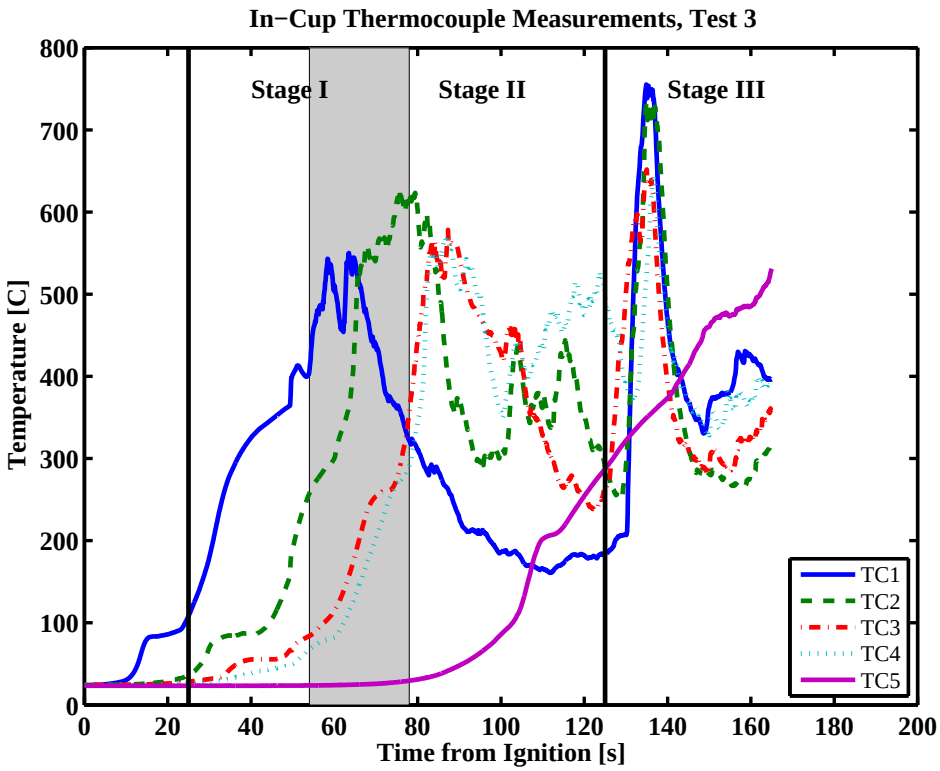

Figure B.5: Temperatures readings by thermocouples located inside the polystyrene cup in test 3. Temperatures measured determine the time the polystyrene cup ignites. The temperature does not directly relate to an ignition temperature of polystyrene. Thermocouple 1 represents the lowest thermocouple location, and 5 the highest. Relative stages of burning are indicated in the figure, as described in the caption of figure 5.6.

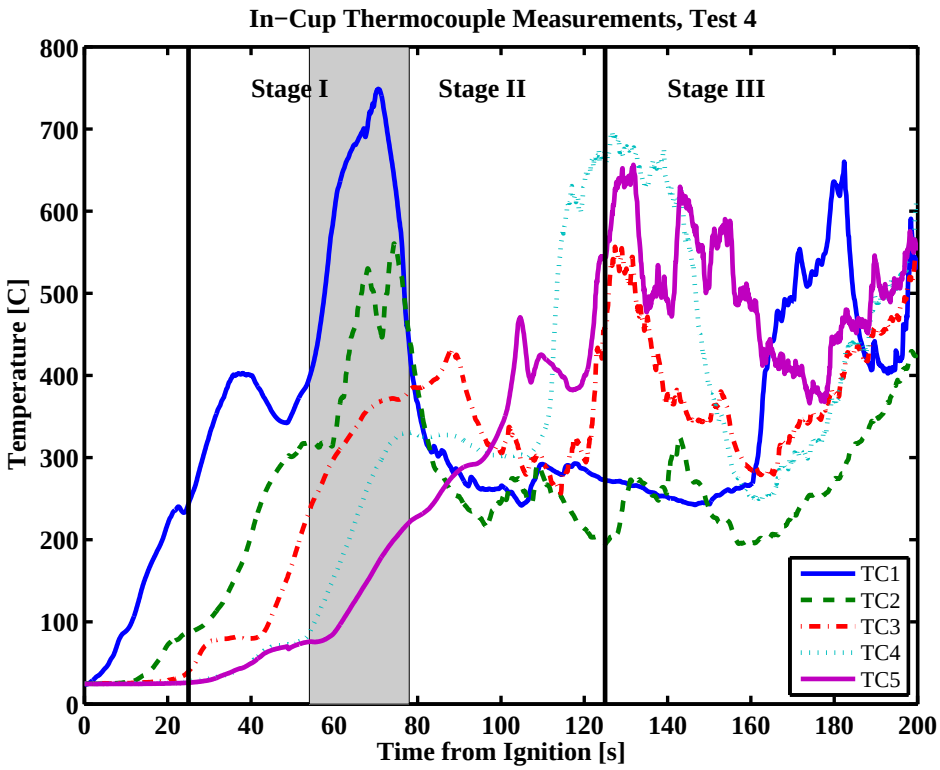

Figure B.6: Temperatures readings by thermocouples located inside the polystyrene cup in test 4. Temperatures measured determine the time the polystyrene cup ignites. The temperature does not directly relate to an ignition temperature of polystyrene. Thermocouple 1 represents the lowest thermocouple location, and 5 the highest. Relative stages of burning are indicated in the figure, as described in the caption of figure 5.6.

Thermocouples were also suspended in the air within five cells of corrugated cardboard, shown in figure 5.10, labeled as thermocouple 'B'. Again, thermocouples were not in direct contact with the burning material, and deducing actual temperatures of burning materials or specific ignition times was too difficult and unreliable to be performed. Evidence of the evolution of the burning process, such as higher temperatures in stage III were observed and provide another qualitative picture of the progression of burning internally within the commodity.

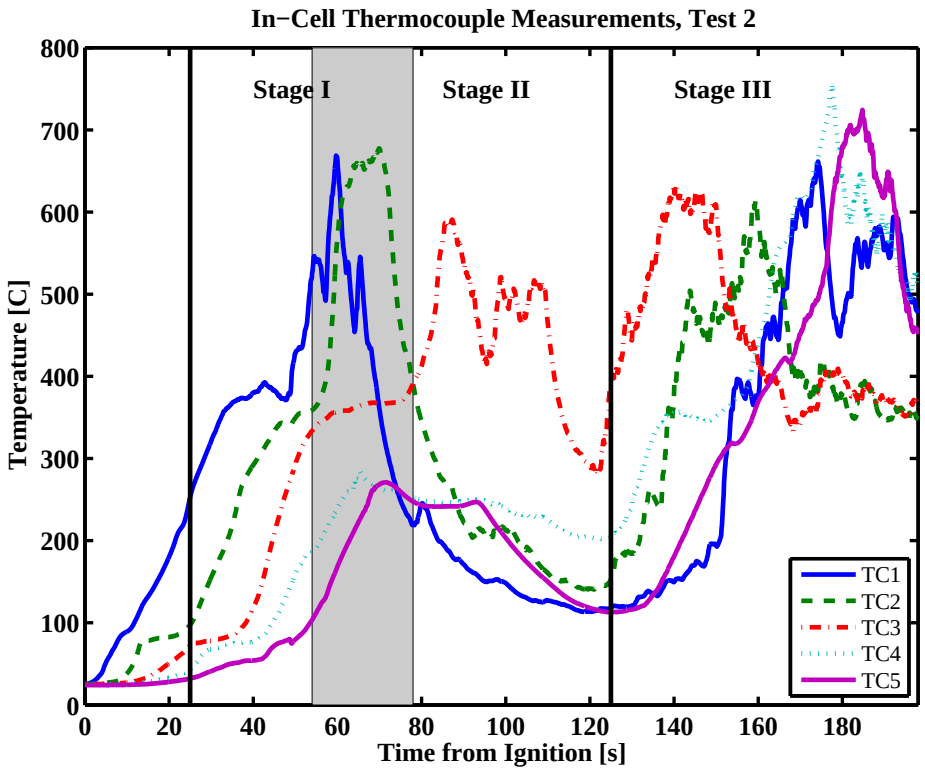

Figure B.7: Temperatures readings by thermocouples located inside the cardboard cell in test 2. Temperatures measured determine the time the cardboard cell reaches flashover. The temperature does not directly relate to an ignition temperature of cardboard. Thermocouple 1 represents the lowest thermocouple location, and 5 the highest. Relative stages of burning are indicated in the figure, as described in the caption of figure 5.6.

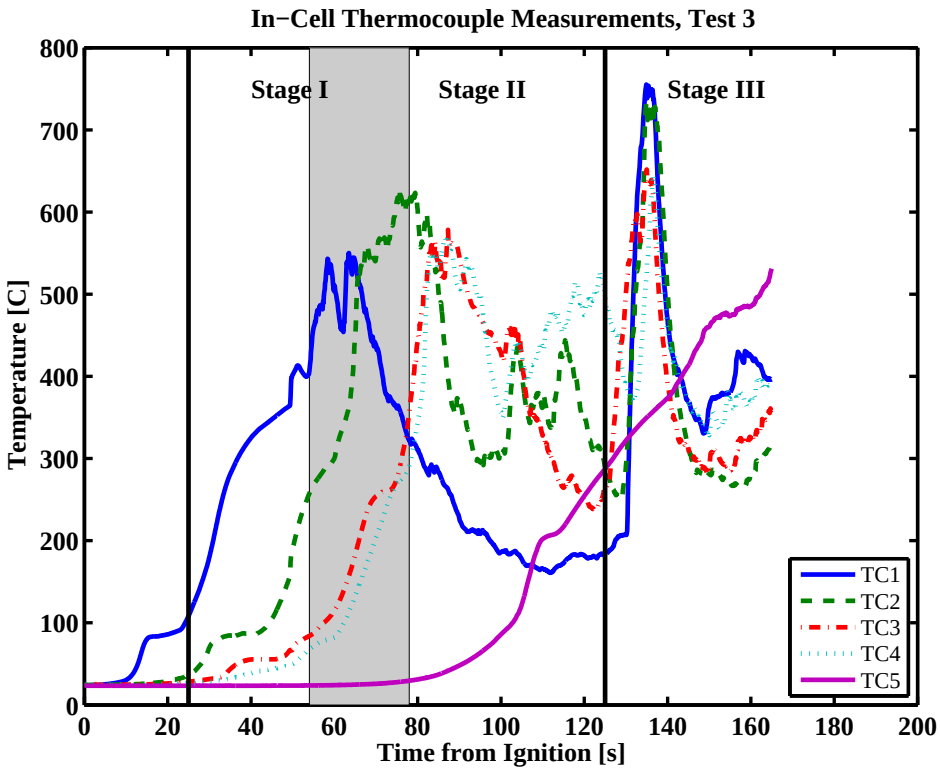

Figure B.8: Temperatures readings by thermocouples located inside the cardboard cell in test 3. Temperatures measured determine the time the cardboard cell reaches flashover. The temperature does not directly relate to an ignition temperature of cardboard. Thermocouple 1 represents the lowest thermocouple location, and 5 the highest. Relative stages of burning are indicated in the figure, as described in the caption of figure 5.6.

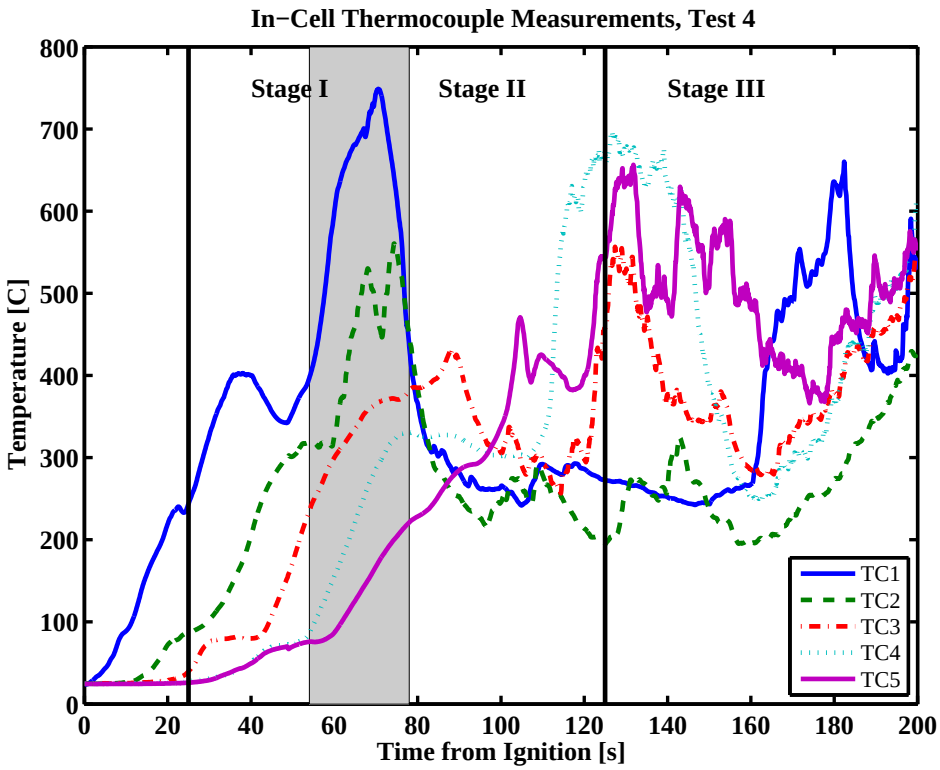

Figure B.9: Temperatures readings by thermocouples located inside the cardboard cell in test 4. Temperatures measured determine the time the cardboard cell reaches flashover. The temperature does not directly relate to an ignition temperature of cardboard. Thermocouple 1 represents the lowest thermocouple location, and 5 the highest. Relative stages of burning are indicated in the figure, as described in the caption of figure 5.6.

Appendix C

Test of Possibility of Ventilation Control

The Group A commodity tested is segregated into individual cardboard cells which ignite one by one, and a baseline analysis was performed to determine if combustion in each cell occured as separate enclosure fires, and if so if they were oxygen or fuel-controlled. If it was found that combustion in the cells was oxygen-controlled, it might be possible to estimate the expected rates of burning from the size of openings into the cells. Using a calculation for the burning rate of an enclosure fire from P.H. Thomas [69]

$$-\frac{dM}{dt} \simeq 91.67 * A_w \sqrt{H_w} \tag{C.1}$$

where A_w is the window area and H_w is the window height. The formula gives the mass-loss rate in grams per second. A burning rate of approximately 20 g/s is predicted assuming the interior of the box is burning post-flashover and is ventilation-controlled.

During peak burning, when all exposed surfaces in the interior of the box are combusting, a peak mass-loss rate of 5–8 g/s is observed, less than half the predicted value if the box was ventilation controlled. This suggests that the box is not ventilation controlled, but rather fuel controlled.

Another method of determining whether an opening is ventilation or fuel controlled is provided by Thomas and Heselden [70] and shows regimes of fuel and ven-

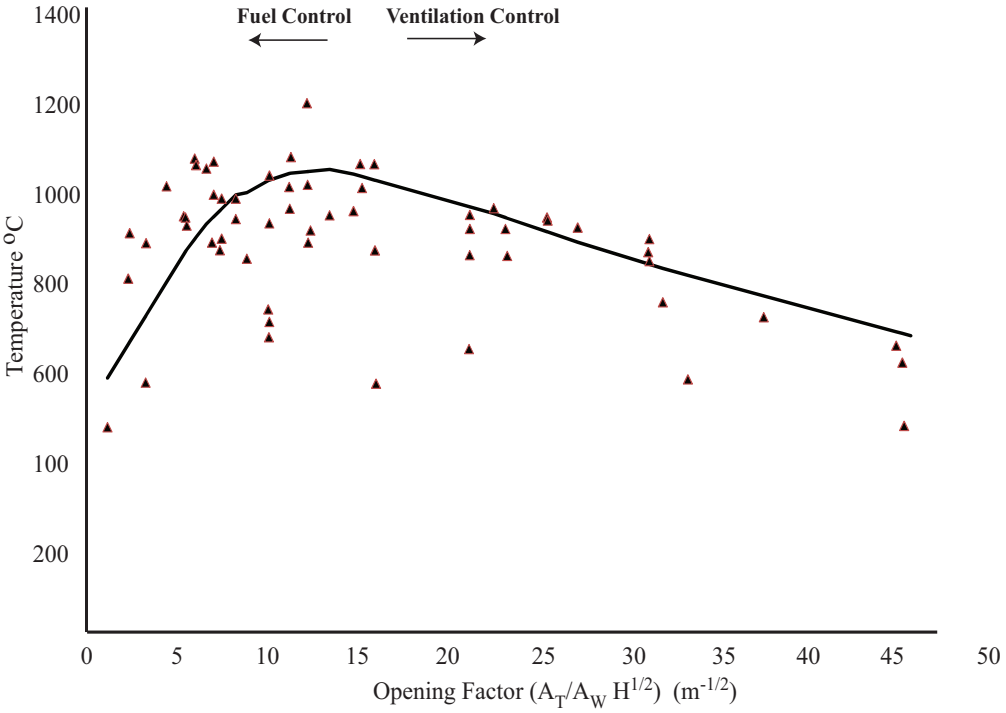

Figure C.1: Opening factor and predicted temperature for compartment fires of various geometries. Regimes of fuel and ventilation controlled burning are also displayed on the graph.

tilation controlled fires with the temperatures measured within sorted between fuel and ventilation controlled fires based on an opening factor $A_T/A_w H^{1/2}$. A_T here is the total area of walls, ceiling, and floor of the compartment not including A_w. For this experiment, where the front face of the burning commodity has burned away, the opening factor is calculated to be approximately 2.5. A diagram given by Thomas and Heselden showing this relationship between opening factor and fuel/ventilation control is shown in figure C.1 [22]. Based on this graph, this test fits clearly within the fuel-controlled regime, and burning rates cannot be determined from the amount of oxygen available to the system.

References

[1] National Fire Protection Association, *NFPA 13: Standard for the Installation of Sprinkler Systems*. National Fire Protection Association, 2007.

[2] R. Zalosh, *Industrial Fire Protection Engineering*. John Wiley & Sons, New York, 2003.

[3] Palenske, G. and O'Connor, D., "Single point sprinkler design criteria vs. traditional density-area curves," NFPA automatic sprinkler committee research project, National Fire Protection Association, Fire Protection Research Foundation, 2007.

[4] clicktohouston.com, "Fire destroys Houston furniture warehouse." May 22, 2009.

[5] Nadile, L., "The problem with big," *NFPA Journal*, March/April 2009.

[6] Merinar, T. R., "Nine career fire fighters die in rapid fire progression at commercial furniture showroom - South Carolina," Fatality assessment and control evaluation (FACE) investigation report. No. F2007-18, National Institute for Occupational Safety and Health, 2009.

[7] Frederick, L., Tarley, J. L., Guglielmo, C. and Merinar, T. R., "Career fire fighter dies of carbon monoxide poisoning after becoming lost while searching for the seat of a fire in warehouse - New York," Fatality assessment and control evaluation (FACE) investigative report. No. F2004-04, National Institute for Occupational Safety and Health.

[8] National Fire Protection Association, "Fire investigation report: supermarket - Phoenix, Arizona (March 14, 2001)," tech. rep., National Fire Protection Association.

[9] Washenitz, F., Cortez, K., Mezzanotte, T., McFall, M., Merinar, T., McDowell, T. and Dunn, V., "Warehouse fire claims the life of a battalion chief - Missouri," fatality assessment and control evaluation (FACE) investigative report. No. 99-F48, National Institute for Occupational Safety and Health.

[10] Braddee, R. W., Merinar, T. R., Mezzanotte, T. P., Pettit, T., Romano, N. T., and Washenitz, F. C., "Six career fire fighters killed in cold-storage and warehouse building fire - massachusetts," Fatality assessment and control evaluation (FACE) investigative report. No. 99-F47, National Institute for Occupational Safety and Health, 2000.

[11] NFPA, "NFPA fire investigations report, bulk retail store fire, Albany, GA, April 16, 1996," tech. rep., National Fire Protection Association, Quincy, MA. 1997.

[12] Copeland, T. D., and Schaenman, P. S., "Sherwin-Williams paint warehouse fire: Dayton, Ohio (May 27, 1987) with supplemant on Sandoz chemical plant fire: Basle, Switzerland," tech. rep., United States Fire Administration Technical Report, Federal Emergency Management Agency, 1987.

[13] Carter, D. A., "Dispersion of toxic combustion products from large fires," *Fire Technology*, May 1992.

[14] Annamalai, K. and Sibulkin, M., "Flame spread over combustible surfaces for laminar flow systems part II: flame heights and fire spread rates," *Combustion Science and Technology*, vol. 19, no. 5, pp. 185–193, 1979.

[15] Pagni, P. J. and Shih, T. M., "Excess Pyrolyzate," in *Sixteenth Symposium (International) on Combustion*, vol. 16, pp. 1329–1343, 1977.

[16] Rangwala, A., Buckley, S., Torero, J. L., "Modeling and analysis of the upward burning of PMMA," in *3rd AIAA Aerospace Sciences Meeting and Exhibit*, (Reno, Nevada), 2005.

[17] Overholt, K. J., Gollner, M. J., and Rangwala, A. S., "Characterizing the flammability of corrugated cardboard using a cone calorimeter," in *6th U.S. National Combustion Meeting*, (Ann Arbor, Michigan), 2009.

[18] Tewarson, A., "Flammability parameters of materials: ignition, combustion, and fire propagation," *Journal of Fire Sciences*, vol. 12, no. 4, p. 329, 1994.

[19] C. J. Hilado, *Flammability Handbook for Plastics*. CRC Press, 1998.

[20] Tewarson, A. and Pion, R. F., "Flammability of plastics. I. Burning intensity," *Combustion & Flame*, vol. 26, pp. 85–103, 1976.

[21] Williams, F.A., *Combustion Theory, 2nd ed.* Addison-Wesley, Reading, MA, 1985.

[22] Drysdale, D., *An Introduction to Fire Dynamics*. John Wiley & Sons, New York, 1998.

[23] Quintiere, J.G., *Fundamentals of Fire Phenomena*. John Wiley & Sons, New York, 2006.

[24] Babrauskas, V., *SFPE Handbook of Fire Protection Engineering, Fourth Edition*, ch. The Cone Calorimeter, pp. 3–(90–108). National Fire Protection Association, 2008.

[25] Factory Mutual Insurance Company, *FM Global Property Loss Prevention Data Sheet 8-1*, 2004.

[26] Dean, R. K., "A final report on fire tests involving stored plastics," *Fire Technology*, vol. 12, no. 1, pp. 55–65, 1976.

[27] Golinveaux, J. and LeBlanc, D., "Is the code right? New warehouse fire test experience," *World Safety Conference & Exposition, (Duluth, GA)*, June 2008.

[28] Babrauskas, V., *SFPE Handbook of Fire Protection Engineering, Fourth Edition*, ch. Heat Release Rates, pp. 3–(1–59). National Fire Protection Association, 2008.

[29] Janssens, M., *SFPE Handbook of Fire Protection Engineering, Fourth Edition*, ch. Calorimetry, pp. 3–(60–89). National Fire Protection Association, 2008.

[30] Cleary, T.G., "Technical and marketing issues impacting the fire safety of building and construction and home furnishings applications," in *Fire Retardant Chemicals Association, Spring Conference*, pp. 99–115, Technomic Publishing Co, 1992.

[31] Ingason, H., *Experimental and Theoretical Study of Rack Storage Fires*. PhD thesis, Lund University, Institute of Technology, 1996.

[32] Foley, M., *The use of small scale fire test data for the hazard assessment of bulk materials*. PhD thesis, University of Edinburgh, 1995.

[33] Kanury, A. M., *Introduction to Combustion Phenomena*. Gordon and Breach Science Publishers, New York, 1975.

[34] Burke, S. P. and Schumann, T. E. W., "Diffusion flames," *Industrial & Engineering Chemistry*, vol. 20, no. 10, pp. 998–1004, 1928.

[35] Spalding, D. B., "Combustion of liquid fuel in gas stream," *Fuel*, vol. 29, pp. 2–7, 1950.

[36] Emmons, H.W., "The film combustion of liquid fuel," *ZAMM-Zeitschrift fur Angewandte Mathematik und Mechanik*, vol. 36, 1956.

[37] F. Kosdon, F. Williams, and C. Buman, "Combustion of vertical cellulosic cylinders," in *Twelfth Symposium (International) on Combustion*, pp. 253–64, 1969.

[38] Hedge, M., Paul, P.J. and Mukunda, H.S., "Free Convective Combustion with Variable Properties," *Proc. Combust. Instit.*, vol. 21, pp. 33–43, 1986.

[39] Kim, J.S., De Ris, J. and Kroesser, F.W., "Laminar free convective burning of fuel surfaces," in *Proc. 13th Symp. (Int.) on Combustion*, p. 949, 1971.

[40] Rangwala, A., *Flame spread Analysis using a Variable B-Number*. Phd thesis, University of California, San Diego, La Jolla, CA, 2006.

[41] Orloff, L., De Ris, J. and Markstein, G. H., "Upward turbulent fire spread and burning of fuel surface," *Fifteenth Symposium (International) on Combustion*, vol. 15, pp. 183–192, 1974.

[42] Yang, K. T., "Laminar free-convection wake above a heated vertical plate," *ASME Journal of Applied Mechanics*, vol. 86, pp. 131–138, 1964.

[43] Annamalai, K. and Sibulkin, M., "Flame spread over combustible surfaces for laminar flow systems part I: excess fuel and heat flux," *Combustion Science and Technology*, vol. 19, no. 5, pp. 167–183, 1979.

[44] Torero, J.L. and Bahr, N.J. and Carman, E.J., "Assessment of material flammability for microgravity environments," in *IAF, International Astronautical Congress, 48th, Turin, Italy*, 1997.

[45] Saito, K. and Quintiere, J. G. and Williams, F. A., "Upward turbulent flame spread," in *Fire Safety Science-Proceedings of the First International Symposium*, pp. 75–86, 1985.

[46] Saito, K., Williams, F. A., Wichman, L. and Quintiere, J. G., "Upward turbulent flame spread on wood under external radiation," *Journal of Heat Transfer (Transactions of the ASME)*, 1989.

[47] Delichatsios, M. M., and Delichatsios, M. A., "Effects of transient pyrolysis on wind-assisted and upward flame spread," *Combustion and Flame*, vol. 89, no. 1, 1992.

[48] Delichatsios, M.M., Mathews, M.K. and Delichatsios, M.A., "An upward fire spread and growth simulation," in *Fire Safety ScienceProceedings of the Third International Symposium*, pp. 207–216, 1991.

[49] Quintiere, J.G. and Harkleroad, M. and Hasemi, Y., "Wall flames and implications for upward flame spread," *Combustion Science and Technology*, vol. 48, no. 3, pp. 191–222, 1986.

[50] Kulkarni, A. K. and Sibulkin, M., "Burning rate measurements on vertical fuel surfaces," *Combustion and Flame*, vol. 44, 1982.

[51] Grant, G. and Drysdale, D., "Numerical modelling of early flame spread in warehouse fires," *Fire Safety Journal*, vol. 24, no. 3, pp. 247–278, 1995.

[52] Karlsson, B., "A mathematical model for calculating heat release rate in the room corner test," *Fire Safety Journal*, vol. 20, pp. 93–113, 1993.

[53] Y. Hasemi, M. Yoshida, A. Nohara, and T. Nakabayashi, "Unsteady-state upward flame spreading velocity along vertical combustible solid and influence of external radiation on the flame spread," in *Fire Safety ScienceProceedings of the Third International Symposium*, pp. 197–206, 1991.

[54] Joulain, P., "Convective and radiative transport in pool and wall fires: 20 years of research in Poitiers," *Fire Safety Journal*, vol. 26, no. 2, pp. 99–149, 1996.

[55] Brehob, E.G. and Kim, C.I. and Kulkarni, A.K., "Numerical model of upward flame spread on practical wall materials," *Fire Safety Journal*, vol. 36, no. 3, pp. 225–240, 2001.

[56] P. J. Pagni, "Diffusion flame analyses," *Fire Safety Journal*, vol. 3, no. 4, pp. 273–285, 1981.

[57] Torero, J.L., Vietoris, T., Legros, G. and Joulain, P., "Estimation of a total mass transfer number from the standoff distance of a spreading flame.," *Combustion Science and Technology*, vol. 174, no. 11, pp. 187–203, 2002.

[58] Rangwala, A.S. and Buckley, S.G. and Torero, J.L., "Analysis of the constant B-number assumption while modeling flame spread," *Combustion and Flame*, vol. 152, no. 3, pp. 401–414, 2008.

[59] Rasbash, D.J., "The extinction of fires by water sprays," *Fire Res. Abst. Rev.*, vol. 4(1), no. 28–53, 1962.

[60] Law, C. K. and Williams, F. A., "Kinetics and Convection in the Combustion of Alkane Droplets," *Combustion and Flame*, vol. 19, pp. 393–405, 1972.

[61] DiNenno, P.J., ed., *SFPE Handbook of Fire Protection Engineering, Fourth Edition.* National Fire Protection Association, 2008.

[62] F. P. Incropera and D. P. DeWitt, *Introduction to Heat Transfer.* John Wiley & Sons, New York, 1996.

[63] ASTM, *Standard Test Method for Measuring Heat Transfer Rate Using a Thin-Skin Calorimeter.* ASTM, West Conshohocken, PA, test standard ed.

[64] Florit, C., "Charateristics of a flame spreading on a corrugated cardboard." Internship Report, Worcester Polytechnic Institute, Department of Fire Protection Engineering, 2008.

[65] Pizzo, Y. and Consalvi, J.L. and Porterie, B., "A transient pyrolysis model based on the *b*-number for gravity-assisted flame spread over thick pmma slabs," *Combustion and Flame*, vol. In Press, Corrected Proof, 2009.

[66] Tewarson, A., *Generation of Heat and Gaseous, Liquid, and Solid Products*, pp. 3–(109–194). 2008.

[67] D. Holve and R. Sawyer, "Diffusion controlled combustion of polymers," in *Symposium (International) on Combustion*, vol. 15, pp. 351–361, Elsevier, 1975.

[68] Markstein, G. H., and De Ris, J., "Upward fire spread over textiles," *Fourteenth Symposium (International) on Combustion*, pp. 1085–1097, 1973.

[69] Thomas, P.H., *Heat Transfer in Fires: Thermophysics, Social Aspects, Economic Impact*. John Wiley & Sons, New York, 1974.

[70] Thomas, P.H., and Heselden, A.J., "Fully developed fires in single compartments. A cooperative research programme of the Conseil International du Batiment Report No. 20," tech. rep., Fire Research Note No. 923, 1972.